

12-2016

# Fabricating Suspended Carbon Structures Using SU-8 Photolithography

Emanuele Giogli  
*Clemson University*

Follow this and additional works at: [http://tigerprints.clemson.edu/all\\_theses](http://tigerprints.clemson.edu/all_theses)

---

## Recommended Citation

Giogli, Emanuele, "Fabricating Suspended Carbon Structures Using SU-8 Photolithography" (2016). *All Theses*. 2555.  
[http://tigerprints.clemson.edu/all\\_theses/2555](http://tigerprints.clemson.edu/all_theses/2555)

This Thesis is brought to you for free and open access by the Theses at TigerPrints. It has been accepted for inclusion in All Theses by an authorized administrator of TigerPrints. For more information, please contact [awesole@clemson.edu](mailto:awesole@clemson.edu).



# **FABRICATING SUSPENDED CARBON STRUCTURES USING SU-8 PHOTOLITHOGRAPHY**

---

A Thesis  
Presented to  
the Graduate School of  
Clemson University

---

In Partial Fulfillment  
of the Requirements for the Degree  
Master of Science  
Mechanical Engineering

---

by  
Emanuele Giogli  
December 2016

---

Accepted by:  
Professor Rodrigo Martinez-Duarte, Committee Chair  
Professor Mark A. Blenner  
Professor Xiangchun Xuan



# ABSTRACT OF THE MASTER OF SCIENCE THESIS

## Fabrication of Suspended Carbon Structures Using SU-8 Photolithography

By

Emanuele Giogli

Master of Science Student in Mechanical Engineering

Clemson University, Clemson 2016

Professor Rodrigo Martinez-Duarte, Chair

The phenomenon of T-topping has been deemed as an imperfection of the SU-8 photolithography process, due to light diffraction, overexposure of the SU-8, and other process parameters. The first objective of this work is to demonstrate that T-topping can be used as a microfabrication resource to produce suspended structures between photo-patterned high aspect ratio SU-8 posts, as precursors for carbon wires (width $>1\mu\text{m}$ ) and bridges (width $>1\mu\text{m}$ ). Such carbon structures could be used in a number of applications, such as the fabrication of nanowire based biosensors for the medical and food industry. The second objective is to develop a model able to predict what type of structures will be featured by an array of SU-8 posts, and in case of suspended structures, their length and width, in function of the particular choice of process parameters.

The parameters examined are: type of contact, exposure time, type of gap, nominal size and nominal gap. A variety of suspended structures are obtained, and repeatable carbon wires of diameter as low as 800nm can be fabricated with the right choice of parameters. Given a choice of the parameters, the model proposed succeeds



into predicting the presence and length of posts of hexagonal, squared and circular shape, but fails in calculating their width.

The model needs future work to reliably calculate the width of the suspended structures, and needs to be calibrated for triangles and diamonds. Also, the SU-8 thickness will have to be integrated in the model.



## ACKNOWLEDGMENTS

I would like to thank my advisor, Rodrigo Martinez-Duarte, for the opportunity of joining the Multiscale Manufacturing Laboratory and working on cutting-edge research along with an outstanding team of graduate and undergraduate students. During the two years of my graduate studies at Clemson, Dr. Martinez-Duarte has been a constant guidance for my research, and in turns a counselor and a friend.

Also, I would like to thank my American and International friends inside and outside the lab, to have contributed on making me live an unforgettable experience at Clemson.

Finally, I would like to thank my family for the uncountable support and love. Last but not least, a special thank goes to my brand new wife Dimitra Michalaka, which is the sweetest and loveliest army captain that I have ever met, and I love her from tip to toe.



## TABLE OF CONTENTS

|   | Page |
|---|------|
| TITLE PAGE .....  | i    |
| ABSTRACT.....   | ii   |
| ACKNOWLEDGMENTS .....   | iv   |
| LIST OF TABLES .....  | vii  |
| LIST OF FIGURES .....   | ix   |
| ACRONYMS .....  | xiii |
| CHAPTER   |      |
| I. INTRODUCTION .....   | 1    |
| II. BACKGROUND .....  | 7    |
| 2.1 Carbon-MEMS.....  | 7    |
| 2.2 SU-8 .....  | 9    |
| 2.3 Photolithography of SU-8 .....                            | 11   |
| 2.4 Importance of the Exposure in making suspended wires..... | 15   |
| 2.6 T-Topping .....   | 16   |
| 2.7 Turning T-Topping into an opportunity.....                | 19   |
| III. PARAMETERS OF INTEREST .....                             | 21   |
| 3.1 General assumptions: .....                                | 21   |
| 3.2 Type of Contact.....                                      | 27   |
| 3.3 Exposure Dose .....                                       | 29   |
| 3.4 Nominal Gap .....   | 30   |
| 3.5 Type of Gap .....   | 31   |
| 3.6 Nominal Size.....   | 33   |
| 3.7 SU-8 Thickness .....                                      | 34   |



|  |      |
|--|------|
| Table of Contents (Continued)  | Page |
| IV. MATERIALS AND METHODS.....   | 35   |
| 4.1 Microfabrication .....   | 35   |
| 4.2 Geometry and Dimensions.....   | 40   |
| 4.3 Methodology .....  | 41   |
| V. RESULTS .....   | 47   |
| 5.1 General Considerations .....   | 47   |
| 5.2 Type of Contact.....   | 50   |
| 5.3 Exposure dose .....  | 58   |
| 5.4 Nominal Size.....  | 65   |
| 5.5 Type of Gap .....  | 71   |
| 5.6 Nominal Gap.....   | 75   |
| 5.7 SU-8 Thickness .....   | 76   |
| 5.8 Carbonization.....   | 77   |
| 5.9 Discussion .....   | 88   |
| VI. CONCLUSIONS AND FUTURE WORK .....  | 109  |
| APPENDIX   |      |
| A: <u>Types of gap geometry: calculating the shape factor <math>c_s</math></u> ..... | 112  |
| REFERENCES .....   | 115  |



## LIST OF TABLES

| Table  | Page |
|--|------|
| 2.1 Photolithography process, step by step .....   | 12   |
| 4.1 Colors and codes used for the qualitative analysis .....   | 43   |
| 4.2 Sample qualitative analysis for hexagons STS, obtained with 30s exposure in soft contact.....  | 44   |
| 5.1 Maximum and minimum gaps with stable bridges for different types of gap and exposure times. The results are shown for the case of soft contact exposure, and nominal size of 160 $\mu$ m. All dimensions in $\mu$ m.....             | 60   |
| 5.2 Fabrication gaps for Hexagons STS and PTP in function of the exposure time. The results are shown for the case of soft contact exposure, nominal size of 160 $\mu$ m, and nominal gap of 25 $\mu$ m. All dimensions in $\mu$ m ..... | 61   |
| 5.3 Cross section in function of the time of exposure, for different shapes with characteristic dimension 160 $\mu$ m. All dimensions in $\mu$ m .....   | 64   |
| 5.4 Bridges length and width in function of the nominal size. The results are shown for hexagons STS, exposed in soft contact for 40s. All dimensions in $\mu$ m.....  | 69   |
| 5.5 Qualitative analysis for triangles PTB, exposed in soft contact for 20s in the case of 50 $\mu$ m (top chart), and 300 $\mu$ m (bottom chart) SU-8 thickness.....  | 77   |
| 5.6 Value of maximum and minimum gaps with stable bridges in function of the nominal size, for hexagons STS, exposed for 30s in soft contact .....   | 79   |
| 5.7 Optimum fabrication parameters for obtaining repeatable, reliable and continuous bridges and wires.....  | 89   |
| 5.8 Average values of $K_{b,NB}$ and $K_{b,SB}$ , and acceptable interval for $\overline{K_b}$ . All values are grouped by type of gap.....  | 93   |



| List of Tables (Continued)  | Page |
|---|------|
| 5.9 Shape factor $c_s$ grouped by type of gap .....   | 96   |
| 5.10 Equations to calculate $\Delta D_{n,e}$ , shape by shape .....   | 99   |
| 5.11 Equations to calculate $\Delta D_{n,Dn}$ , shape by shape.....   | 101  |
| 5.12 Equations to calculate $\Delta D_{n,Dn}$ , for each type of gap.....   | 102  |
| 5.13 Values of $K$ , for each type of gap .....   | 103  |
| 5.14 Absolute and relative error of the length calculated<br>respect to the measured value. The results have been<br>grouped by type of gap ..... | 104  |



## LIST OF FIGURES

| Figure  | Page |
|---|------|
| 1.1 Vertical and top view of a sample suspended structure in between two circular posts. Important dimensional parameters that will be used later on this work are shown .....      | 6    |
| 2.1 A) SEM picture of SU-8 feature overexposed by 100%; B) SEM picture of a carbon plate; C) SEM picture of a T-topped SU-8 ribbon, exposed with 100 $\mu$ m contact distance ..... | 17   |
| 3.1 Exposure of an SU-8 post in vertical view .....   | 21   |
| 3.2 SEM picture of an array of hexagonal posts, featuring suspended bridges .....   | 22   |
| 3.3 Shift from fully cross-linked to partially and not cross-linked areas, in function of the distance from the post center .....   | 24   |
| 3.4 Effect of light exposure on the interaction between two adjacent circular posts .....   | 25   |
| 3.5 SEM picture of the effect of overexposure on the width (w) and thickness (t) of a suspended bridge in between triangular posts BTB .....  | 26   |
| 4.1 Wafer #22641 (100 $\mu$ m-hard contact) .....   | 36   |
| 4.2 Spin coating cycle. ....  | 37   |
| 4.3 Soft baking cycle.....  | 38   |
| 4.4 Post Exposure Baking cycle.....   | 39   |
| 4.5 Carbonization cycle .....   | 46   |



|      |  |    |
|------|--|----|
| 5.1  | SEM images of: A) no bridges; B) broken bridge; C) suspended bridges (horizontal) and wires (vertical); D) merged, note that the wall extends throughout the height of the posts; E) irregular ..... | 48 |
| 5.2  | Fabricated gap against nominal gap for different types of contact. The results are shown for the case of exposure fixed to 40s, and nominal size of 160 $\mu$ m .....                                | 53 |
| 5.3  | Width against nominal gap for different types of contact. The results are shown for the case of exposure fixed to 40s, and nominal size of 160 $\mu$ m.....  | 55 |
| 5.4  | Gap reduction against nominal gap for different types of contact. The results are shown for the case of exposure fixed to 40s, and nominal size of 160 $\mu$ m .....                                 | 57 |
| 5.5  | Fabricated against nominal gap for different exposure times. The results are shown for the case of soft contact exposure, and nominal size of 160 $\mu$ m .....                                      | 59 |
| 5.6  | Width against nominal gap for different exposure times and types of gap. The results are shown for the case of soft contact, and nominal size of 160 $\mu$ m .....                                   | 62 |
| 5.7  | Gap reduction against nominal gap for different types of contact and exposure times. The results are shown for the case of hexagons STS of nominal size 160 $\mu$ m.....                             | 63 |
| 5.8  | Fabricated gap against nominal gap for different nominal sizes and types of gap. The results are shown for the case of exposure 40s in soft contact .....  | 66 |
| 5.9  | Width against nominal gap for different nominal sizes and types of gap. The results are shown for the case of exposure 40s in soft contact.....  | 68 |
| 5.10 | Gap reduction against nominal gap for different nominal sizes and exposure times. The results are shown for hexagons STS exposed in soft contact.....  | 70 |



| List of Figures (Continued)   | Page |
|---|------|
| 5.11 Fabrication gap against nominal gap for different types of gap and exposure times. The results are shown for nominal size 160 $\mu$ m exposed in soft contact .....                                  | 72   |
| 5.12 Width against nominal gap for different types of gap and exposure times. The results are shown for nominal size 160 $\mu$ m exposed in soft contact .....  | 74   |
| 5.13 Gap reduction against nominal gap for different types of gap and exposure times. The results are shown for nominal size 160 $\mu$ m exposed in soft contact .....                                    | 75   |
| 5.14 Circular shapes obtained for nominal size 160 $\mu$ m, nominal gap 30 $\mu$ m and exposure time 30s in soft contact. A) SU-8; B) carbonized.....   | 78   |
| 5.15 Fabrication gap in function of the nominal gap in the case of SU-8 and carbon structures, for different times of exposures. The results shown are for hexagons STS with nominal size 40 $\mu$ m..... | 80   |
| 5.16 Width in function of the nominal gap in the case of SU-8 and carbon structures, for different times of exposures .....   | 81   |
| 5.17 A, C) Fabrication gap and B, D) width, in function of the nominal gap, for nominal size 80 $\mu$ m, and exposure time 30s, with different types of contact. Post carbonization.....                  | 82   |
| 5.18 A, C) Fabrication gap and B, D) width, in function of the nominal gap, and time of exposure, for nominal size 80 $\mu$ m, exposed in soft contact. Post carbonization.....                           | 83   |
| 5.19 A, C) Fabrication gap and B, D) width, in function of the nominal gap and nominal size, for exposure time 30s in soft contact. Post carbonization.....   | 84   |
| 5.20 Different increase of fabrication gap in function of nominal size .....  | 85   |



| List of Figures (Continued)   | Page |
|---|------|
| 5.21 A) Fabrication gap and B) width, in function of the nominal gap, for different types of gap. The results are shown for nominal size of 80 $\mu$ m, exposed for 30s in soft contact ..... | 86   |
| 5.22 Effect of the thermal stress induced by carbonization on 2 arrays of squared posts.....  | 87   |
| 5.23 Examples of SU-8 structures obtained. A) Circular self-standing posts; B) Squared posts featuring suspended bridges; C) Triangular posts featuring suspended wires.....                  | 88   |
| 5.24 A) Hexagonal subset featuring optimal bridges and B) Triangular subset featuring optimal wires .....   | 90   |
| 5.25 Geometrical illustration of the shape factor $c_s$ for the case of squares .....   | 95   |
| 5.26 Linear approximation of the influence of the time exposure on the cross-section increment, for every shape .....   | 98   |
| 5.27 Linear approximation of the influence of the nominal size on the cross-section increment, for every shape.....   | 100  |
| 5.28 Width against length for 20 subsets of hexagons, circles, squares, diamonds and triangles .....  | 108  |
| A.1 Shape factor $c_s$ for: A) hexagons STS; B)hexagons PTP; C) circles; D) squares; E) triangles BTB_STS; F) triangles BTB_PTP; G) triangles PTB_PTS; H) triangles PTB_PTP; I) diamond.....  | 113  |



## ACRONYMS

|        |   |                                       |
|--------|---|---------------------------------------|
| GMO    | - | Genetically Modified Organism         |
| CNT    | - | Carbon Nanotube                       |
| CNF    | - | Carbon Nanofiber                      |
| C-MEMS | - | Carbon Microelectromechanical Systems |
| C-NEMS | - | Carbon Nanoelectromechanical Systems  |
| STS    | - | Side to side                          |
| PTP    | - | Point to point                        |
| PTS    | - | Point to side                         |
| CTC    | - | Circle to circle                      |
| BTB    | - | Base to base                          |
| PTB    | - | Point to base                         |
| HP     | - | Horizontal points                     |
| VP     | - | Vertical points                       |



## **CHAPTER ONE**

### **INTRODUCTION**

Biosensors are devices that sense the variation of a biological change and transduce it on a measurable signal [1]. A biosensor is constituted by a biological probe that selectively reacts to a specific molecule either trapping it or emitting a signal, and a transducer which can convert the probe signal to a measurable electric signal. Among the different sensor types, electrochemical sensors are a relative recent technology, which combines the high sensitivity of electrochemical transducers and the high selectivity of biological recognition probes. An extensive review of the different types of electrochemical biosensors has been written by Ronkainen et al. [2]. Electrochemical biosensors are largely used in many applications involving healthcare, such as medical diagnosis and food inspection. For medical purposes, biosensors are employed for the detection and quantification of a variety of dangerous biomolecules, including proteins, DNA mutagens, bacteria, viruses and cancerous cells. In the alimentary industry, they are primarily used as means to detect the presence of bacteria or GMO, which could compromise the freshness and salubrity of food [3].

Important properties that make a biosensor preferable include but are not limited to: selectivity, sensitivity, dynamic range and multiplexing. Selectivity is the capacity of selecting only the analyte of interest; sensitivity (or limit of detection) is the smallest concentration of analyte in the sample solution that can be reliably read; dynamic range is defined on the lower boundary by the limit of detection, and on the upper one by the



maximum flow sustainable by the sensor; multiplexing is the capacity of trapping different molecules at the same time.

The limits of classic biosensors conceptions have been pushed forward with the introduction of nanofabrication technologies. Nanobiosensors rely on their extremely small dimension, comparable to biomolecules size, to largely enhance the sensitivity. Nanoparticles, nanomembranes, nanowires, carbon nanofibers (CNFs) and nanotubes (CNTs), are all different working principles for nanobiosensors [4-5]. Above all, CNTs, CNFs and nanowires are the ones looking more promising, and extensive reviews can be found in: CNFs [6,7]; CNTs [8-10]; nanowires [11,12].

These structures are too thin to be considered as 1-D structures in the literature. Their strength point is the possibility of obtaining very long structures, which translates to high area to volume ratios, increasing the sensitivity and the response time. Although the highest ratios are obtained with CNFs and CNTs, some authors have found the nanowires biosensors preferable, due to the possibility of tailoring the material properties with doping techniques and because the natural oxide layer formed around the nanowires allows to use well developed probes [5,13].

Several key features of the nanowires biosensors are the label-free, real-time transduction of the signal, very high sensitivity and selectivity, and the possibility of being assembled in arrays for improving multiplexing [12]. In every case, the biggest problem does not come from the sensors performance, but from their fabrication. A number of methods to fabricate nanowires have been developed, including laser ablation



synthesis [14], solution phase synthesis [15], metal-assisted chemical etching [16], and electron beam lithography [17].

A common issue of the current technologies is that nanowires have to be fabricated by themselves, and then attached to the anchor posts. Therefore, attempts have been made to develop a bottom-up fabrication technology able to produce the whole sensor at once. The architecture of a typical nanowire biosensor is a series of biological probes attached to a nanowire connecting two anchor posts. A constant voltage is applied to the two posts, and the current flowing through the nanowire is recorded and transformed in an electric signal by a transducer. When the analytes in exam are captured by the probes, the resistivity of the nanowire changes, affecting the current in transit and thus the sensor reading. The variation of the current is proportional to the amount of biomolecules stack on the nanowires, which gives the quantity of the analytes in the sample solution.

It has been reported that carbon electrodes can be fabricated through pyrolysis in inert atmosphere of photolithographically patterned SU-8, in protocols known as carbon microelectromechanical systems (C-MEMS) and carbon nanoelectromechanical systems (C-NEMS) technologies [18-21]. SU-8 is an epoxy-based negative photoresist popular in the micromanufacturing industry because of its good chemical, thermal and mechanical properties [22]. SU-8 is commonly used in a large number of structural applications, including lab-on-a-chip, micromolding, and microfluidics [23-26].

SU-8 photolithography is commonly used to obtain self-standing posts, which can be used, upon characterization, for different applications, for example cell manipulation



using electric field gradients [27-28]. However, many authors have reported the joining of the top of the SU-8 posts, when too close to each other [29-31]. This effect has been defined T-topping by some authors and has been attributed to light diffraction. The combination of light diffraction and overexposure initiates crosslinking processes of the SU-8 in zones that should be shielded by the opaque part of the mask. The result is an increased dimension of the cross-section respect to the nominal value, and therefore, possible interaction between posts as the gap between them narrows.

Although T-topping is unanimously considered a fabrication defect, the possibility of exploiting the T-topping for producing suspended structures, nanowires in particular, has already been investigated by Wang and Madou [32]. The results found proved that suspended structures and nanowires can be obtained through pyrolysis of SU-8, but the features obtained were considered unpredictable. At the best of my knowledge, no results have been obtained so far on the control of the T-topping phenomenon, to obtain structures of the desired dimensions through pyrolysis of photolithographically patterned SU-8.

Therefore, the hypothesis of this work is that T-topping can be successfully used as a powerful microfabrication tool, by controlling the photolithography parameters, and a mathematical model can be defined to successfully predict the results of the process, in function of the relative parameters. More specifically, in this work, a large number of self-standing SU-8 posts arrays have been patterned through photolithography, while varying six parameters of the photolithography process: SU-8 thickness, type of contact, time of exposure, type of gap, nominal size and nominal gap. Because of the effect of T-



topping, not all the posts were produced as designed, but a number of different outcomes, such as SU-8 bridges, wires, or merged structures, were reported, depending on the particular combination of parameters used.

The goal of this work is to characterize the suspended structures obtained, with particular focus on the nanowires, in function of the photolithography parameters chosen. The results of the characterization are successively analyzed to find common trends which will lead to define a mathematical model, devoted to predict the microfabrication results in function of the parameters selected. A schematic illustration of the parameters is shown in Figure 1.1.



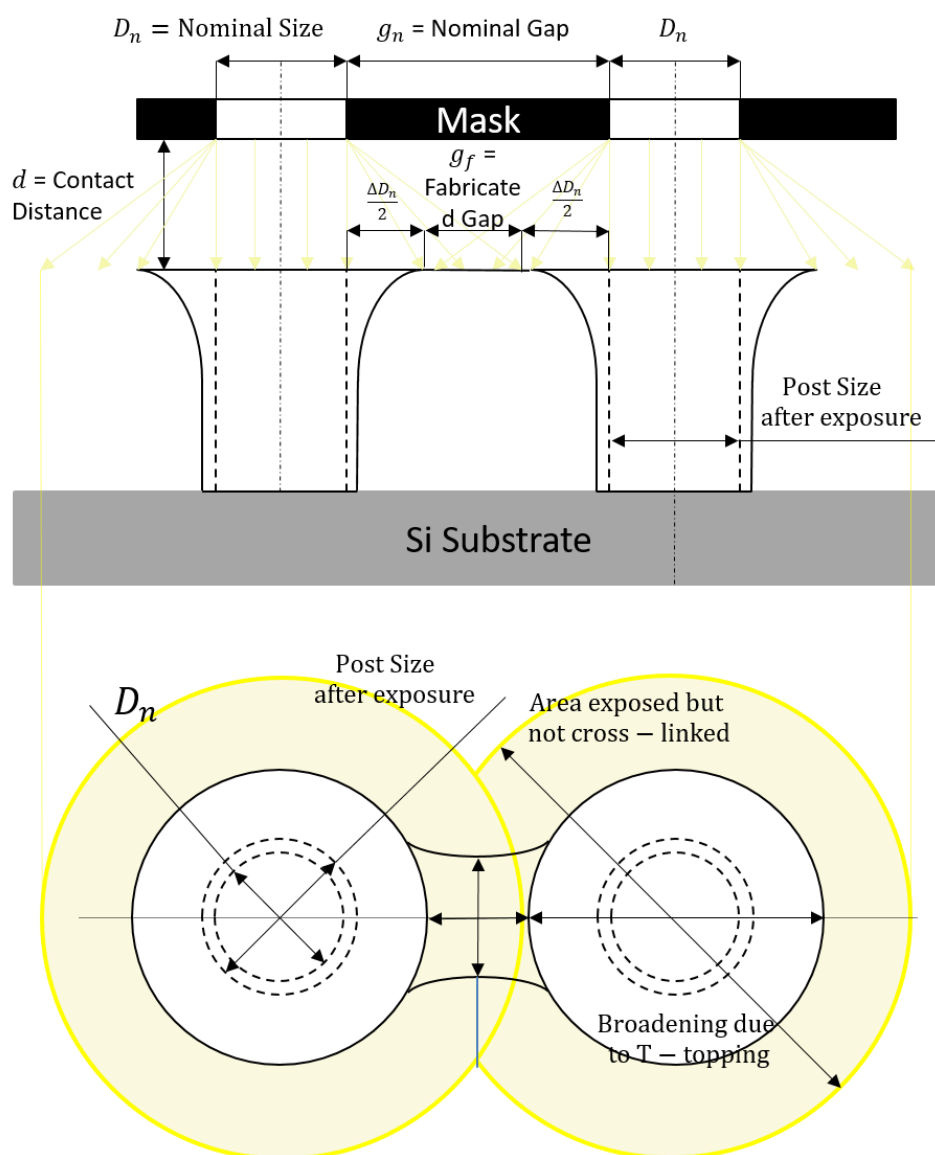


Figure 1.1: Vertical and top view of a sample suspended structure in between two circular posts. Important dimensional parameters that will be used later on this work are shown.



## **CHAPTER TWO**

### **BACKGROUND**

#### **2.1 Carbon MicroElectroMechanical Systems (C-MEMS)**

Carbon MEMS or C-MEMS are the ensemble of techniques devoted to obtain glass-like carbon structures by carbonization of organic polymers. Carbon derivation, or carbonization, is a heat treatment performed in inert atmosphere, which derives solid residues very rich in carbon from a variety of organic materials, such as resins, alcohols, polyimides and cellulose. The treatment is divided in three steps, depending on the temperature: pre-carbonization, carbonization and annealing. The pre-carbonization is for  $T < 300^{\circ}\text{C}$ , when the molecules of solvent and unreacted monomer are expelled from the material. The carbonization happens in two sub steps: for  $300 < T < 500^{\circ}\text{C}$ , when the material mass is quickly reduced because of the expulsion of oxygen and others heteroatoms; for  $500 < T < 1200^{\circ}\text{C}$ , when hydrogen oxygen and nitrogen are expelled. The last step is the annealing, for  $T > 1200^{\circ}\text{C}$ , used to eliminate structural defects. The final temperature reached during carbonization affects the degree of carbonization of the material obtained.

Glass-like carbon can be derived by pyrolysis of organic polymers. The name glass-like carbon is derived from its resemblance to the glass surface, and their common fracture mode. The surface of the glass-like carbon is smooth and shiny, and the fracture profile is characterized by concentric ripples, like those of seashells (conchoidal fracture). This material was introduced in the early second half of the 20<sup>th</sup> century. Almost simultaneously, studies from two material scientists, the English Bernard Redfern and the



Japanese Shigehiko Yamada, were published, promoting the atypical properties of a new glassy-carbon material [33-34]. Many studies and research about the microstructure and properties of glass-like carbon have followed, but there has not been a single microstructure model unanimously accepted. Some of the studies are openly contradicting each other such as the model of Jenkins and Kawamura (1971) [35] with the model of Oberlin (1989) [36], while other models are incomplete, for example Pesin and Baitinger (2015) [37]. The model given by Jenkins and Kawamura, is one of the oldest, but still largely accepted. It describes the glass-like carbon as a ball of tangled aromatic ribbons, randomly interconnected through covalent bonds in between carbon atoms. This structure is in accordance with some of the glass-like carbon properties, tested experimentally, such as the very low permeability for gases and liquids, the good conductivity, and the glass-like brittleness. Other interesting properties are the very high stability and corrosion resistance, even under the attack of very strong acids, the low oxidability compared to other carbon forms, and the very low thermal conductivity (compared to graphite). Although the structure of glass-like carbon is amorphous, and the material does not show propensity to recrystallize in graphitised structures at high temperatures, it is not an amorphous carbon, because it does not respect completely the definition of amorphous carbon, given by the International Union of Pure and Applied Chemistry (IUPAC).

Initially, most of the interest on the glass-like carbon was about its gas impermeability and chemical inertness, which made it a good material for laboratory equipment. The fact of not reacting with molten metals, made it popular for producing



recipients and crucibles for metallurgic processes. Also, biocompatibility and good mechanical properties favored its use for medical and mechanical equipment. The number of application for glass-like carbon kept on increasing along with the technical progresses of its manufacturing technique. In the last twenty years, the strong drive of the MicroElectroMechanical Systems (MEMS) technology brought an incredible interest on the development of glass-like carbon obtained by pyrolysis of photolithographically patterned photoresist. At first and until 2002, only positive photoresists were used. Then, a glass-like carbon material was derived from SU-8, a negative epoxy photoresist, which will be described in the next section of this work. The introduction of SU-8 as carbon precursor opened new perspectives for the glass-like carbon, the carbon MEMS technology, and their possible application to microfluidics, and nanobiosensors manufacturing.

## **2.2 SU-8**

SU-8 is an epoxy-based negative photoresist, which means that exposure to UV light triggers a cross-linking chemical reaction that makes the photoresist unsolvable by the chemicals used during the development. SU-8 is a solution composed by EPON<sup>TM</sup> SU-8 resin, which is a polymeric solid epoxy novolac resin trademark of the Shell Chemical Company ([www.shell.com](http://www.shell.com)), in an organic solvent, such as cyclopentanone, gamma-butyrolactone, or Propylene Glycol Methyl Ether Acetate (PGMEA) [38]. The solution may contain up to 10 wt% of triarylsulfonium/hexafluoroantimonate salt, which generates the acid that initiates the cross-linking reaction.



Specific compositions of SU-8 were patented by IBM in the early 90's, and the first commercial version of the negative photoresist came into the market in 1996, as an exclusive of MicroChem ([www.microchem.com](http://www.microchem.com)). Recently a Swiss company, Gersteltec ([www.gersteltech.ch](http://www.gersteltech.ch)), entered the market so now both companies offer a large spectrum of different SU-8 versions. In particular, varying the percentages of resin and organic solvent, it is possible to obtain photoresists of different viscosities, which affects the thickness of the SU-8 that can be spin coated on the substrate, and consequently the maximum height of the SU-8 features obtainable. At the moment, there are compositions that allow for spin coating in a range between few and 500µm with a single deposition, and up to 3mm with multiple depositions. The possibility of depositing thick layers and the high resolution achieved, allow to obtain features with high aspect ratios (HAR), as reported by Chuang in 2002 (HAR>190) [29].

The possibility of producing features with HAR, high resolution, and smooth lateral surfaces is a peculiarity of the SU-8. The outstanding combination of this peculiarity with the good chemical, mechanical, electrical and thermal properties, erected the SU-8 as one of the most utilized materials for micromanufacturing applications involving photolithography. Low molecular weight gives high solubility, which translates in solution dense in resin, and consequently thicker spin coated layers. The high Young's modulus gives stability to the patterned SU-8, making it usable as structural material. Also, SU-8 has high thermal and chemical resistance. high thermal stability, good adhesion to various substrates and is highly biocompatible.



### 2.3 Photolithography of SU-8

Photolithography is a microfabrication process that reproduce the pattern of an opaque mask onto a photoresist material. A photoresist is a material that reacts to UV light, and it can be defined either positive or negative. Positive photoresists are materials that are naturally resistant to the chemicals used during development, but they become solvable if exposed to an energy source. Conversely, negative photoresists such as the SU-8, are naturally solvable by the development solvents, but they become unsolvable after exposure to UV light. Photolithography processes are defined positive or negative, according to the type of photoresist used. The two processes are conceptually very similar, but differ in two substantial points. In order to fabricate the same geometry with positive and negative photolithography, the masks used in the two processes must be one the negative of the other. This is because in case of positive photoresist, the exposed part is washed away, while in case of negative photoresist, the shaded part is the one that gets removed.

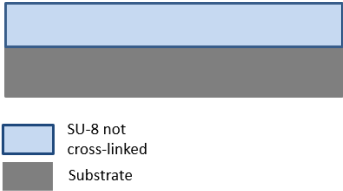
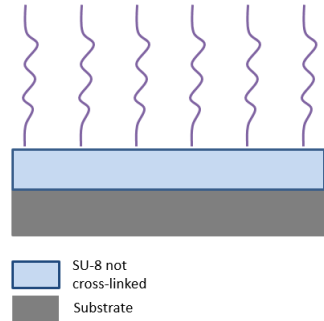
Therefore, to obtain a specific pattern, the SU-8 has to be exposed through an opaque mask with openings in correspondence to the target pattern. Vice-versa, when using a positive photoresist, the UV light has to hit the parts to be removed, therefore the mask has to be the exact negative copy of the one for negative photoresists. The other difference between the two types of photolithography is that the positive does not have a post exposure bake phase, since in this case there is no cross-linking reaction.

A brief step by step overview of the negative photolithography process is given in Table 1. A detailed description of SU-8 photolithography is out of the scope of this thesis and

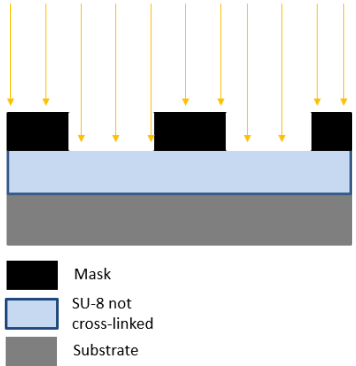
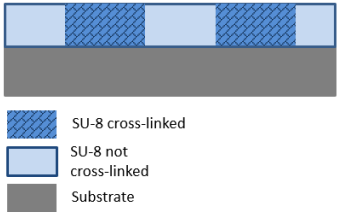


the reader is directed to thorough recent reviews on the topic by Martinez-Duarte and Madou [39] and Abgrall [40]. The exposure step, however, is of particular importance in the fabrication of suspended wires and is described in detail next.

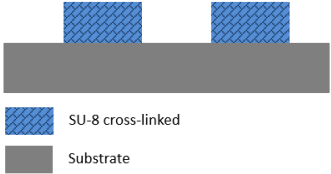
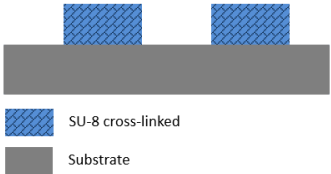
**Table 2.1:** Photolithography process, step by step.

| STEP   | DESCRIPTION   | PARAMETERS OF INTEREST  | REMARKS  |
|--|---|---|--|
| <p><b>Spin Coating</b></p>  | <p>The photoresist is deposited on a clean silicon substrate. There are many options for deposition, but the most common is the spin coating.</p> | <p>Spinning time, speed and acceleration. The Su-8 thickness is inversely proportional to all the three.</p>  | <p>During spinning, the SU-8 tends to accumulate at the edge of the substrate (edge bead). The edge bead has to be removed by either using acetone or including a quick speed peak at the end of the spinning cycle.</p> |
| <p><b>Soft Baking</b></p>   | <p>The photoresist is heated on a hotplate at <math>T &gt; T_{\text{glass}}</math> temperature in order to get rid of the casting solvent.</p>    | <p>Temperature and time. Usually the soft baking is performed at 95°C for a variable time, function of the SU-8 thickness. In certain cases, a prebake at 65 °C is needed to make the process less drastic.</p> | <p>The hotplate is preferable to the oven. When baking in oven, the solvent evaporates first from the top surface, which hardens, trapping the rest of the solvent in (skin effect).</p>                                 |



|   |  |  |   |
|---|--|--|---|
| <p style="text-align: center;"><b>Exposure</b></p>  <p>Mask<br/>SU-8 not cross-linked<br/>Substrate</p>                                | <p>The SU-8 is exposed to UV light through an opaque mask. The exposed SU-8 produces a strong acid that initiate the cross-linking reaction.</p> | <p>Exposure dose<br/>(light intensity <math>\times</math> exposure time)<br/>time of exposure,<br/>type of contact.</p>  | <p>The SU-8 is usually exposed with a UV mercury lamp. Overexposure and light diffraction are responsible for the T-topping, which can be reduced filtering the light of the components with wavelength <math>\lambda &lt; 365</math>. Special exposure techniques are the gray scale mask, and the back-side exposure.</p>                               |
| <p style="text-align: center;"><b>Post Exposure Bake (PEB)</b></p>  <p>SU-8 cross-linked<br/>SU-8 not cross-linked<br/>Substrate</p> | <p>It brings to a completion the cross-linking reactions initiated during exposure</p>   | <p>Temperature and time are the important parameters in PEB. The temperature is usually set at 95°C, but an intermediate step at 65°C could be added, as in the soft bake.</p> | <p>Below 55 °C, there is no polymerization even if the SU-8 is baked for a very long time. Insufficient temperature and/or time might result in a structure not completely cross-linked, and possibly vulnerable to the development. Too high temperature and/or time could cause cracking of the SU-8, and sometimes even peeling from the substrate</p> |



|  |   |   |  |
|--|---|---|--|
| <h3>Development</h3>  <p>SU-8 cross-linked</p> <p>Substrate</p>     | <p>The wafer is immersed in a developer bath. The cross linked parts resist to the chemical but the rest SU-8 gets washed away.</p>                             | <p>Time and agitation speed. Time is important to guarantee a full development. Agitation speed is important to avoid failures.</p> | <p>The development can be due to immersion or spray, and in case of immersion, there is the possibility of having a calm or agitated solvent bath. The immersion is more effective, but at the same time more aggressive than the spray. Agitation enhances the solving capability of the bath, but exposes the SU-8 to mechanical stress.</p> |
| <h3>Rinse and Dry</h3>  <p>SU-8 cross-linked</p> <p>Substrate</p> | <p>The wafer is dried from the developer. There are different drying techniques: nitrogen blowing, spinning, freeze-drying, and supercritical point drying.</p> | <p>Surface tension of the liquid where the wafer is immersed</p>  | <p>High surface tension and HAR posts may cause stiction. Stiction bends and merges the SU-8 posts. To avoid stiction, an intermediate liquid with less surface tension than the solvent can be used for the developing bath.</p>  |



## **2.4 Importance of the Exposure in making suspended structures**

The purpose of the exposure is to provide the necessary energy for the hexafluorantimonate salt to become hexafluorantimonic acid and liberate protons. The protons are received by the SU-8 epoxy rings, which are initially neutral closed chains, but open to receive the protons, becoming positively charged oxoniums. The oxoniums are positively charged ions, but they do not undergo further reactions, until heat is administered to the photoresist. During the post exposure baking, the heat activates the oxoniums, and they start reacting with other ions or with the leftover neutral epoxy rings, generating the cross-links.

The exposure phase is crucial in determining the SU-8 structures that will be microfabricated. In fact, the cross-linking is a reaction localized to the SU-8 parts with ionized epoxy rings, and the amount of the reaction is proportional to the number of oxoniums, and thus, to the exposure dose received. In case of underexposure, the cross-linking reaction may result incomplete, and the SU-8 may not resist to the development. Increasing the exposure dose, will not only fully cross-link the exposed areas, but the reaction will also start penetrating more deeply into the material, and propagating sideways. Therefore, the amount of exposure affects the fidelity of the SU-8 structures to the mask pattern.

In an ideal photolithography process, with infinite resolution and perfect setting of the process parameters, the SU-8 would perfectly match the pattern designed on the mask, and the structures sidewalls would be perfectly smooth and vertical. In practice, patterns are broadened in their dimensions due to overexposure and light diffraction.



Light diffraction is the bending of light rays as they pass in proximity of an opening edge. The amount of bending increases when the opening size is comparable with the light wavelength, and therefore, it is very important in SU-8 photolithography. Because of light diffraction, the exposed area on the SU-8 is actually bigger than the ideal one, and becomes even bigger as the distance in between the mask and the SU-8 increases. This, in combination with the overexposure, will cause undesired phenomena such as T-topping, which is the object of the next section.

## **2.5 T-topping**

T-topping is a loosely defined term in the SU-8 photolithography literature. T-topping defines a broadening of the SU-8 top surface, respect to its designed value and the rest of the features. A vertical section of an SU-8 post would show a peculiar T-profile, from which the phenomenon takes the name of T-topping, as shown in Figure 2.1.



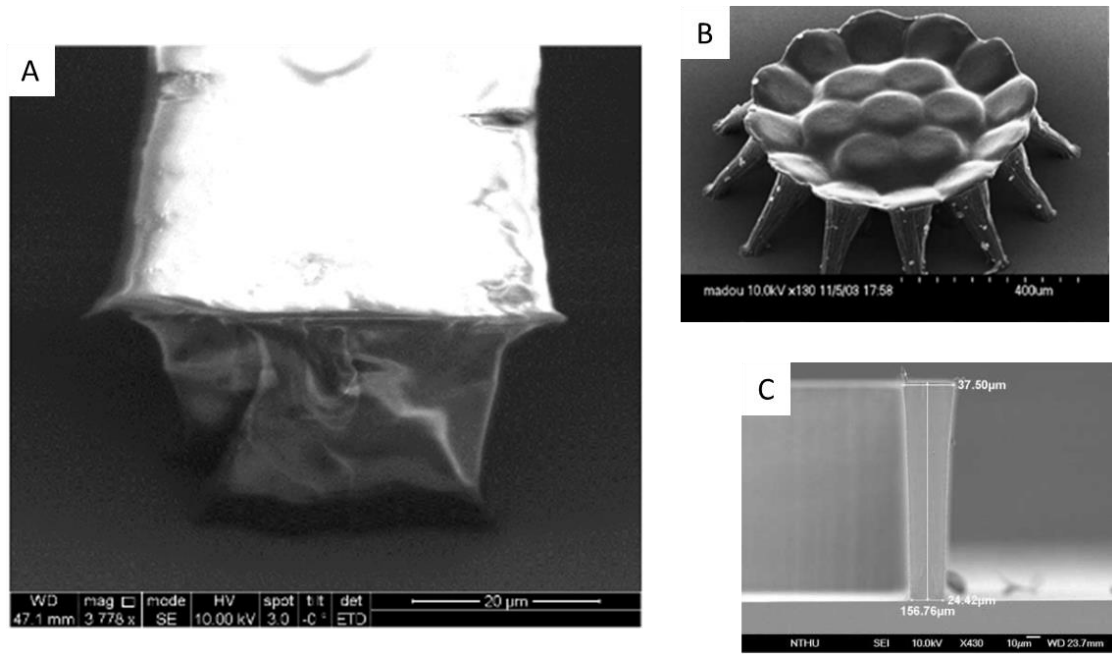


Figure 2.1: A) SEM picture of SU-8 feature overexposed by 100% [41]; B) SEM picture of a carbon plate [32]; C) SEM picture of a T-topped SU-8 ribbon, exposed with 100 μm contact distance [29].

T-topping is essentially a photolithography imperfection, and has been considered by several authors as a problem when fabricating structures that are closely located. Besides the loss of resolution of the process, it precludes the possibility of obtaining perfectly straight walls, and it may also cause a loss of functionality. For example, self-standing vertical SU-8 posts may merge due to T-topping, becoming unusable. For all these reasons, significant efforts have been undertaken to minimize the entity of the T-topping.

A solution to this problem is to reduce the air gap between the mask and SU-8, which can be obtained choosing contact as type of exposure, instead of proximity or



projection. In soft contact photolithography, the mask is directly laying on the SU-8, so the distance is theoretically zero. In reality, however, the mask stops at the first contact of the two surfaces, which happens when the highest peak of one of the two surfaces touches the other. The resulting air gap is variable from point to point based on the topography of the surfaces. In order to minimize the topography variation and reduce the gap, the spin coating parameters have to be optimized, and the edge bead carefully removed. Also, the gap can be reduced by applying a force that pushes the mask against the substrate (hard contact).

Another solution to limit the T-topping, is the introduction of a filter to block the light waves with wavelengths  $<350$  nm. In fact, the SU-8 has the maximal absorption for the light with wavelength 365nm, which can get as deep as 2mm, while its absorption of light wavelengths  $<350$ nm is very shallow. Eliminating such waves means eliminating light that would expose only the surface of the SU-8 layer, and thus reducing the T-topping.

Lastly, the T-topping can be reduced optimizing the exposure time. As mentioned in the previous section, overexposure increases the cross-linked area at the top of the SU-8 layer, thus, limiting the exposure to the minimum required to fully cross-link the nominal, area reduces the T-topping.



## **2.6 Turning T-topping into a microfabrication tool**

The previous section explains in details the phenomenon of T-topping, the problems connected to it, and some possible solutions. Unfortunately, no matter the strategy adopted and the effort spent, it is impossible to completely eliminate it. Nevertheless, on the other hand, it is possible to see the T-topping as a microfabrication resource. The biggest risk with the T-topping is that structures designed to be separated, may come out connected. However, if the ultimate goal is to obtain connected structures, T-topping becomes, all of a sudden, a useful resource. For example, if the objective was obtaining a structural layer of SU-8 minimizing its weight, having SU-8 pillars connected by simple bridges, or entirely covered by a thin SU-8 film, could be preferable respect of a thick layer of SU-8.

Furthermore, thinking of the SU-8 as a precursor of carbon electrodes for C-MEMS applications, a suspended structure connecting two adjacent posts, could be the electrical connection of two carbon electrodes. This is exactly the application envisioned in this thesis, which strives to fabricate SU-8 suspended structures to derive carbon electrodes for C-MEMS and biosensors in the micro and nanoscale. The hypothesis of this work, is that T-topping can be exploited to fabricate suspended bridges and wires. In these terms, the focus of this work is not to eliminate the T-topping, but find a way to control it.

It has been explained that the entity of the T-topping is greatly depending on the exposure dose and the distance between mask and SU-8. These translates immediately into two of the process parameters analyzed in this work: exposure time and type of



contact. Also, it is hypothesized that other parameters will affect the entity of the T-topping, such as the nominal size of the features, their shape and their nominal distance. Therefore, if it possible to define the relationship among the variation of these parameters with the amount of T-topping first, and with the final patterns second, it will be actually possible to consider the T-topping as a powerful microfabrication tool.



## CHAPTER THREE

### PARAMETERS OF INTEREST

#### 3.1 General Assumptions

As previously mentioned, T-Topping indicates the broadening of the top section of the feature respect to its body, in the case of SU-8 posts. An example is given in Figure 3.1.

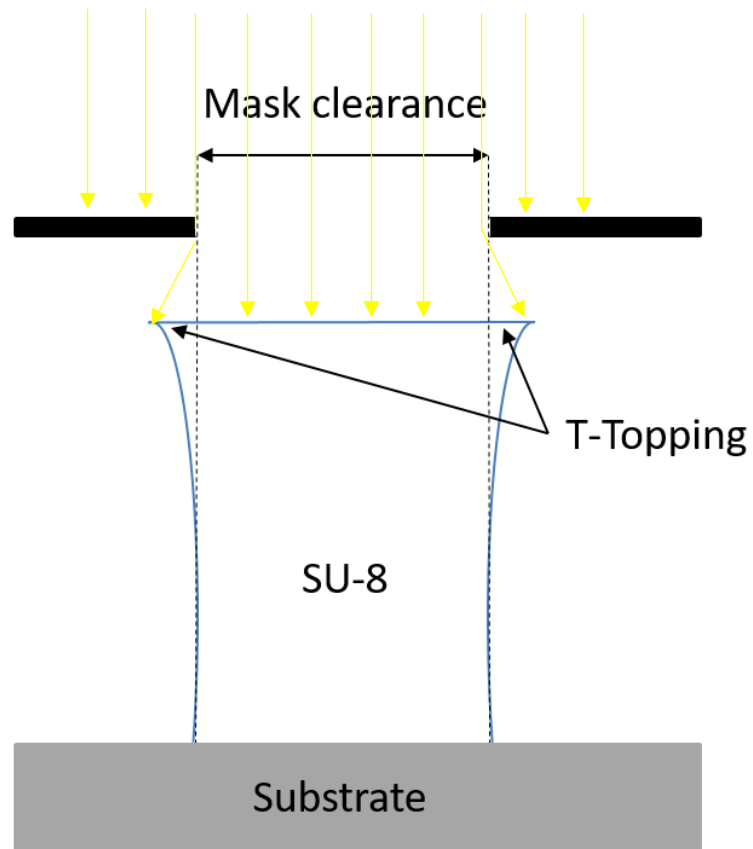


Figure 3.1: Exposure of an SU-8 post in vertical view.



Such broadening is due to the combined effect of multiple process parameters: exposure dose, type of contact, geometry and nominal size of the shape. As the top section broadens, the posts get more packed, eventually leading to the interaction of the adjacent ones, and sometimes, to the formation of suspended structures, as shown in Figure 3.2.

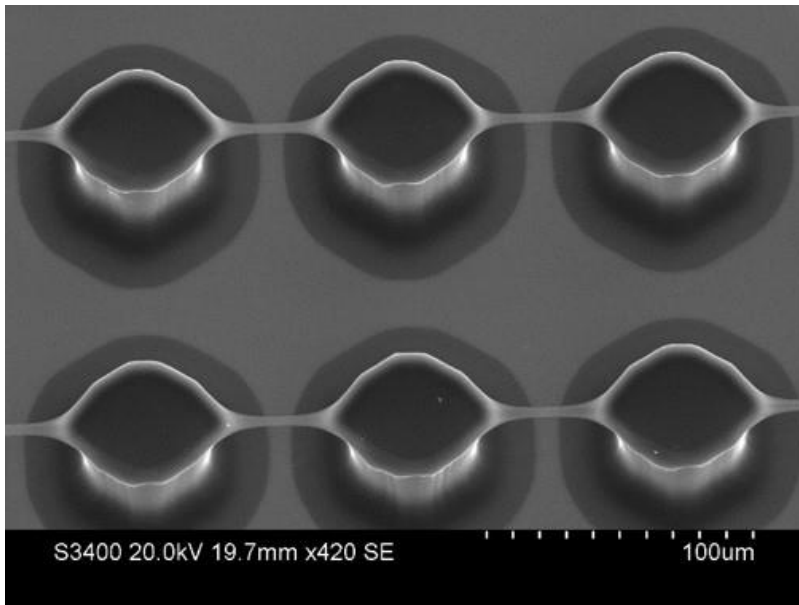


Figure 3.2: SEM picture of an array of hexagonal posts, featuring suspended bridges.

Let us look in greater detail the dynamics behind the formation of the suspended structures. As explained in previous sections, the SU-8 is a negative photoresist, thus the parts of the SU-8 that are desired to stay need to be exposed to light, to initiate the cross-linking reaction. The part exposed to light is the first to cross-link, and successively the cross-linking propagates through the SU-8 layer. The energy given to the cross-linking process is dependent on the intensity of the light source and the time of exposure. The



intensity of the light used for this fabrication process is  $10 \text{ mW/cm}^2$ , and the minimum exposure time is 10 s, which gives an exposure sufficient to crosslink all the way through the bottom of the SU-8 layer. Hence, the regions in correspondence of the mask slots are fully cross-linked and all the post anchors are formed independently from their size or shape.

The areas surrounding the nominal size of the post undergo cross-linking for effect of overexposure and light diffraction from the mask edges. Nevertheless, the diffracted light is not as concentrated as the light that hits the surface straight, so the entity of the cross linking fades as it goes further from the post. Consequently, the broadened area is not necessarily receiving enough energy to fully crosslink the SU-8. Looking at the top view of an SU-8 post, from the center going outward, the following areas can be seen: a fully cross-linked area down to the substrate (A in Figure 3.3), a cross-linked area suspended (B in Figure 3.3), and an area partially cross-linked, but not sufficient to resist the development (C in Figure 3.3).



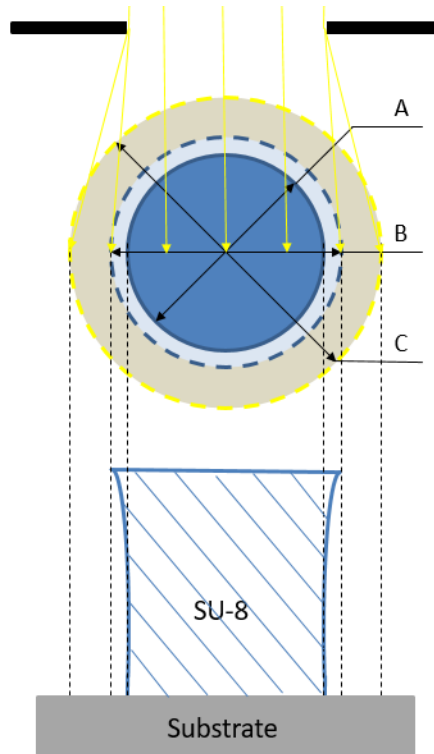


Figure 3.3: Shift from fully cross-linked to partially and not cross-linked areas, in function of the distance from the post center.

Considering an array of posts, so close to each other that the partially cross-linked areas of two adjacent posts intersects, the quantity of energy received by the intersection might be enough to complete the cross-linking process, as shown in Figure 3.4.



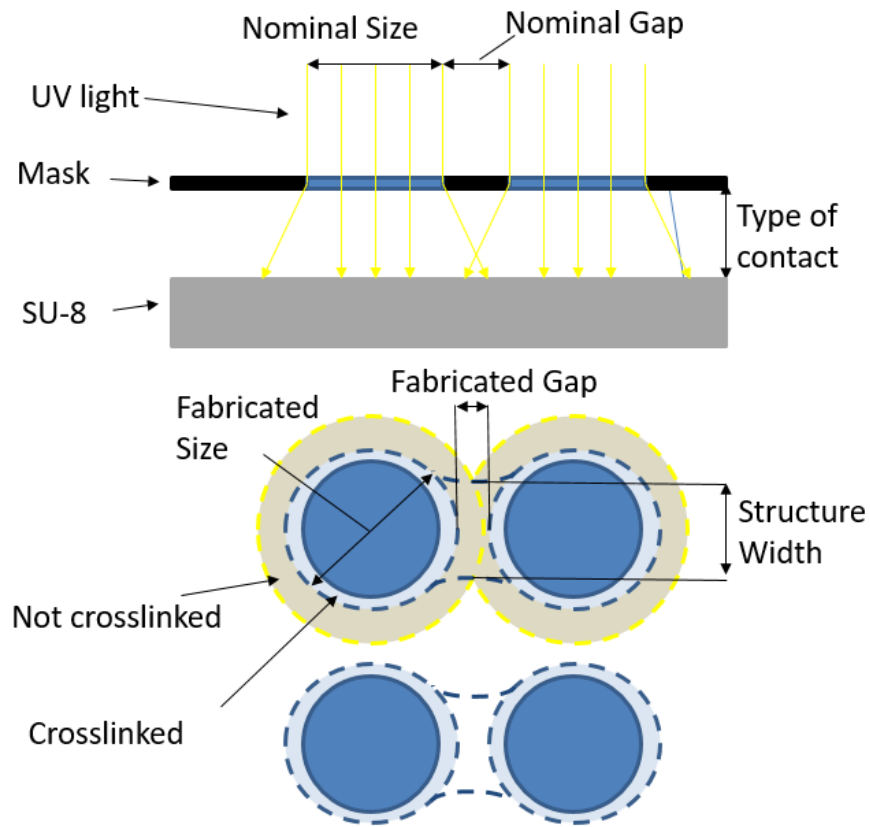


Figure 3.4: Effect of light exposure on the interaction between two adjacent circular posts.

As the time of exposure increases, the SU-8 behaves as follows: the top surfaces stretch towards each other; small spikes start protruding in the same direction, until they connect; the first points to connect are the closest of the two facing profiles, and the connection will most likely be a suspended wire; then, numerous new connections are established along the profiles, forming messy texture of wires and spikes, which eventually become a single, continuous, wide bridge. This explains why the structures form along the vertical and horizontal axis of the array, but not in diagonal (longer distance). If the exposure continues past this point, the structures expand sideways, filling



the gaps within the array, and finally generating a continuous film over the posts. At the same time, the exposure affects the penetration of the cross-linking process, so that the suspended structure in the vertical view is not simply a bar in-between two posts but looks like an arch. As for the width, the thickness will increase with the exposure time, and will eventually generate a wall all the way to the substrate. An example of the effect of overexposure on a suspended bridge is shown in Figure 3.5, where the bridge in between two triangular posts is already half way to the bottom, and tiny connections are progressively filling the gap.

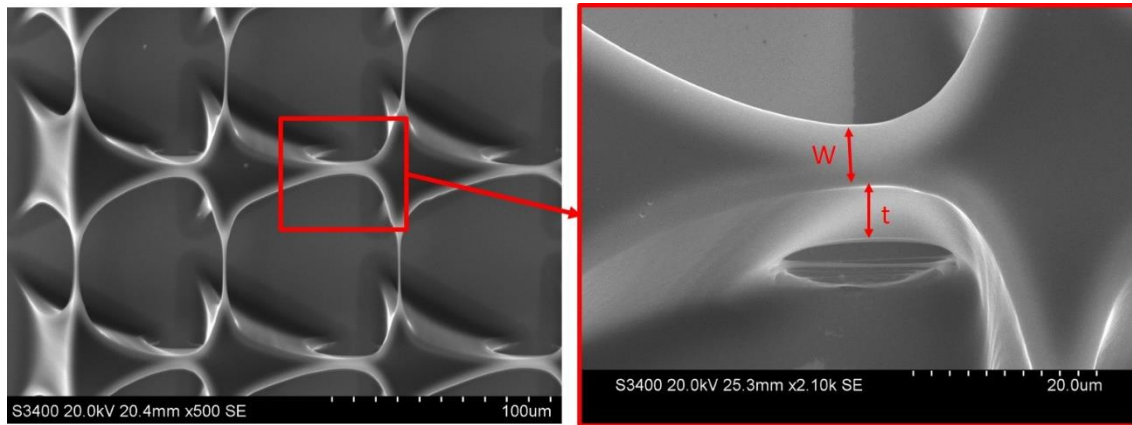


Figure 3.5: SEM picture of the effect of overexposure on the width ( $w$ ) and thickness ( $t$ ) of a suspended bridge in between triangular posts BTB.

Since the final product of the photolithography process is the result of the combined influence of the type of contact, exposure dose, type of gap, nominal gap, nominal size, and SU-8 thickness, it is not possible to identify the exact influence of a single parameter on the process (all parameters are explained in detail in the following



subsections). Therefore, in order to formulate a hypothesis and later on to analyze the results, it is necessary to fix all the parameters but the one of interest at a time. The result of such analysis is still dependent on the values chosen for the fixed parameters but the single “degree of freedom” of the system allows to determine common trends that repeat throughout the different setups.

### **3.2 Type of Contact**

There are three possible types of contacts: hard contact, soft contact, and proximity.

Proximity indicates that the mask is fixed to a distance of  $20\text{ }\mu\text{m}$  from the SU-8 layer. In soft contact, the mask is laying directly on the SU-8 layer, touching, but with no additional pressure applied. Hard contact indicates that the mask is laying on the SU-8, and a sort of clamping force is applied to keep them pressed against each other. The type of contact determines the clearance between the bottom of the mask and the top of the SU-8. The maximum clearance is obtained in proximity because there is no actual contact. In the case of soft contact, the distance between the two surfaces is, in theory, zero, but, in practice, the surface roughness of the two surfaces sets a stop whenever a point of the mask enters in contact with a point of the SU-8 layer. Therefore, the distance in between the two bodies varies from point to point, according to the topography of their surfaces. In hard contact, the mask is stopped at the same distance of the soft contact but the extra force applied on the mask presses it against the SU-8, flattening the roughness peaks that set the stop point and, consequently, reducing the clearance.



To understand the influence of the distance between the mask and SU-8, let us consider parallel light rays hitting the mask surface perpendicularly and from above, which is the outcome of a light source fixed far enough above the mask. The mask, as described in the photolithography section, is made of an opaque material where slots have been patterned in correspondence of the features desired on the photoresist layer. The rays hitting the opaque mask are totally absorbed and reflected. In correspondence of the slots, the rays pass unobstructed and unaltered and hit the surface of the SU-8 perpendicularly and with full intensity. Instead, around the slots edges, a part of the rays is deflected at a certain angle, which causes a larger area of SU-8 to be exposed to light comparably to the nominal profile. The projection of the initial straight light rays is actually a cone, after passing through the mask slots. Hence, the further the SU-8 layer is from the mask, the larger the area exposed to light will be.

Based on the previous considerations, the first hypothesis is that as the distance in-between the mask and the SU-8 increases so does the entity of the T-Topping, facilitating the formation of suspended and merged structures. Thus, the wafer obtained by proximity should be clearly the one featuring the most number of bridges, and the longest nominal gaps between adjacent posts. Following these two criteria for the ranking of the types of contact, the second type should be soft contact, and the third one, hard contact. In particular, in hard contact, the distance between the mask and the SU-8 is theoretically zero and practically very small, so suspended bridges are expected only at the shortest nominal gaps.



### 3.3 Exposure Dose

The exposure dose is probably the parameter that influences the most the process outcome. Exposure dose is the product of the light intensity and the time of exposure. The light intensity is a constant determined by the type of lamp used for the photolithography, in this case,  $10\text{ mW/cm}^2$ . The time of exposure can be varied freely and such variation does not require any additional change of mask or setup. The influence of the exposure dose is quite straightforward. As previously seen, the cross-linking process of the SU-8 is the direct consequence of the exposure dose. The amount of cross-links increases with the exposure dose, and when a part is fully cross-linked, that part will become resistant to the development process, and will, consequently, be included in the final product. Also, as the time of exposure increases, the cross-linking process penetrates into the SU-8 layer until the substrate and propagates sideways on the lighted surface. This leads to the following hypothesis for the exposure dose. A longer exposure time: (1) increases the area of the SU-8 that will cross-link till the bottom, resulting in larger posts; (2) increases the area that will fully crosslink on the top surface of the material (bigger T-topping); (3) facilitates the formation of suspended structures, walls, and merged shapes.

In this experiment, each wafer was divided in quarters, and each quarter of a wafer was exposed for: 10s, 20s, 30s, and 40s, respectively. The minimal exposure, 10 seconds, is enough to fully crosslink the SU-8 till substrate in the area hit by the unobstructed light rays, but not enough to fully crosslink the entire lighted area. Thus, observing in sequence arrays of posts that get exposed to 10s, 20s, 30s, and 40s, while keeping all other parameters fixed, it is expected to find larger shapes, new bridges where



there were not before, or wider bridges than the previous ones, and eventually walls and merged shapes where there were previously suspended bridges.

### **3.4 Nominal Gap**

The nominal gap indicates the minimal distance in vertical and horizontal directions, in-between two consecutive slots of the mask and it depends on the shape of the slots. If the slots have a square shape, the nominal gap is the distance between the sides of two squares. If the slots are triangles, it is the distance between two points, or two sides, or a point and a side, depending on the orientation of the shapes. A significant difference of the nominal gap comparably to the other parameters, is that the nominal gap is decided before even starting the photolithography process, when the mask is produced, and changing it, would mean having to produce a new mask. It is worth to note that the actual distance between two shapes is not the actual nominal gap, but the fabricated gap.

To obtain the fabricated gap, the increase of the actual SU-8 shapes respect to their nominal size on the mask has to be subtracted from the nominal gap. Due to the T-topping effect, the actual shapes are either larger or equal to their nominal size (they are equal in the ideal case where there is no T-topping at all), thus the fabricated gap can only be smaller or equal to the nominal gap.

As previously explained, shapes closer to each other are more likely to interact and form a connection. Therefore, the hypothesis is that decreasing the nominal gap, the formation of suspended structures, and eventually merged shapes will be facilitated. Two posts far apart would show no bridges. Repeating the experiment for shorter gaps, the



outcomes would be spikes, broken bridges, stable bridges, walls, and finally merged structures, in this exact order. If the nominal gap was the only parameter under examination, it would be relatively easy to find out a reasonable range of distances to obtain each of the outcomes. Nonetheless, since there are other parameters that come into play, such correlation is not possible because two pairs of posts at the same distance, might have or not bridges, depending on the combination of the other parameters.

In this experiment, there are 7 different nominal gaps: 45 $\mu\text{m}$ , 30 $\mu\text{m}$ , 25 $\mu\text{m}$ , 20 $\mu\text{m}$ , 15 $\mu\text{m}$ , 10 $\mu\text{m}$ , and 5 $\mu\text{m}$ , for each exposure type and shape of the posts. The features obtained when all the other parameters are fixed, are expected to obey to the trend previously mentioned, in the same order, but repeating some of the outcomes, and skipping others.

The nominal gap and the exposure dose are the two parameters that influence the most the formation of suspended structures, and they are dependent on each other. Fixing the exposure time at any value, suspended structures could be obtained in the majority of cases if the nominal gap was decreased just enough. Vice-versa, for a fixed nominal gap, suspended structures could be obtained in the majority of cases, increasing the time of exposure just enough.

### **3.5 Type of Gap**

The type of gap is a parameter created in this study to refer to two actual parameters of the process, the shape and orientation of the posts in the arrays. The shapes used for this experiment are all regular geometrical figures, and precisely: hexagons,



squares, diamonds, triangles, circles. These shapes are aligned along an axis of symmetry, so that adjacent posts in vertical and horizontal direction may be facing each other differently, with a point or a side. There are cases where the elements facing each other are: two points (point-to-point or “PTP”), two sides (side-to-side or “STS”), one point and a side (point-to-side or “PTS”), and two circular elements.

The hypothesis, for the type of gap, is that when the closest elements of the two adjacent posts are sides, the interaction of the two shapes is easier than when the two elements are points. The explanation of such hypothesis is that in the case of sides, the conditions for the initial connection between the shapes are met simultaneously all along the sides. Hence, it is possible that the initial connection happens in more than one point at the same time, facilitating the outcome of a suspended structures. An additional consideration is that, even though generic structures are more likely in the STS case, if the outcome desired is a suspended wire (thinner than  $1\mu\text{m}$ ), the odds are in favor of the PTP case.

Circular elements and PTS are two exceptions, the former happens only in the case of circles and the latter only in the case of triangles with the vertex facing the base. However, their behavior is similar to shapes STS and PTP respectively, and thus they are considered part of those two groups



### 3.6 Nominal Size

The nominal size refers to the characteristic dimension of the particular shape considered. For example, in the case of the circles, it indicates the diameter. For all the other shapes, it indicates the length of a side. This parameter is defined nominal because it refers to the ideal dimensions carved on the mask. The SU-8 posts' size is actual bigger than the nominal, due to the T-topping effect induced by diffraction of light and overexposure of the photoresist. At a first thought, a change of the shape size should not significantly influence the interaction of adjacent posts, as long as the gap in between them is the same. Nevertheless, it is foreseeable that the broadening due to T-topping is more conspicuous when the nominal size is bigger. Conversely, the nominal gaps remain the same, resulting in a reduction of the fabricated gap, and consequently, influencing indirectly the formation of suspended structures.

The nominal size is once again a parameter set during the mask fabrication and cannot be varied without reworking the mask, or creating a new one. In this experiment, 6 nominal sizes have been taken into consideration: 160 $\mu\text{m}$ , 80 $\mu\text{m}$ , 40 $\mu\text{m}$ , 30 $\mu\text{m}$ , 20 $\mu\text{m}$ , and 10 $\mu\text{m}$ .

The hypothesis is that among arrays with different nominal size, there is not a significant difference in the formation of suspended structures, although bigger sizes may slightly favor it. Also, a larger nominal size is hypothesized to help the posts remain straight upright during the development phase, when they are in danger of bending and sticking together due to stiction (the arrays failing in such way are considered irregular



and have no use for the purpose of this study). In other words, irregular features are expected to be found for the 10 $\mu$ m and 20 $\mu$ m arrays, but not for the 160 $\mu$ m.

### **3.7 SU-8 Thickness**

The SU-8 thickness is the height of the SU-8 layer, which has been spin coated on the wafer substrate. It is the same height of the SU-8 posts after exposure and development. This thesis does not provide a comprehensive study of this parameter. However, it is possible to assume that the SU-8 thickness does not directly affect the formation of suspended structures, but it is important for the stability of the posts themselves. In fact, as previously mentioned, slender posts are more subjected to stiction. Therefore, the wafers with a SU-8 thickness of 300 $\mu$ m, are expected to have many more irregular arrays than the wafers with SU-8 thicknesses 50 $\mu$ m and 100 $\mu$ m. This parameter will be the subject of future studies.



## **CHAPTER FOUR**

### **MATERIALS AND METHODS**

This section starts with a detailed description of the microfabrication process that produced the specimens analyzed in this study. A depiction of a sample specimen will follow, explicating the geometrical shapes and dimensions, as they would have been if the SU-8 was a perfect copy of the photolithography mask. Finally, the last part of this section will focus on the methodology which was followed to collect and analyze the data.

#### **4.1 Microfabrication**

All the specimens produced were fabricated through photolithography of SU-8 (GM1075 Gersteltec, Switzerland). An exhaustive introduction on both, SU-8 and photolithography, has been already given in chapter two. Therefore, this section will not reiterate the theory behind the microfabrication process, but will present, step-by-step, the choice of the photolithography parameters.

The process starts with a clean silicon substrate. The wafer has a cylindrical shape with diameter 10.16cm, and thickness roughly 550 $\mu$ m. The circular profile of the wafer has two perpendicular cuts close to the borders, which allow to align the substrate to the mask. Figure 4.1 shows a sample wafer.



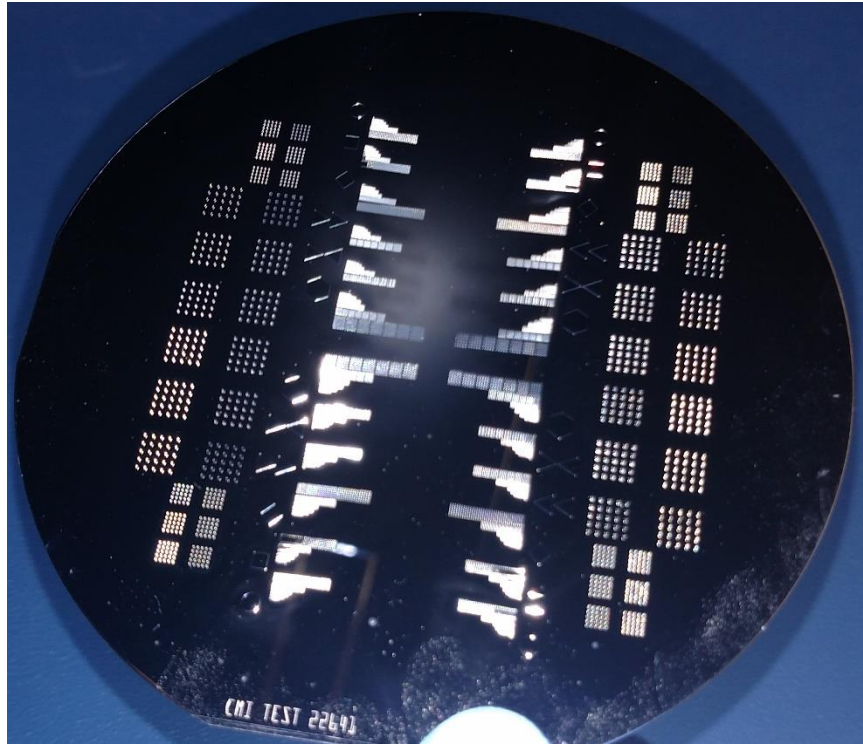


Figure 4.1: Wafer #22641 (100 $\mu$ m-hard contact).

Starting from analogous substrates, 14 different wafers have been obtained, varying the SU-8 thickness and the type of contact of the photolithography mask. Possible values for the thickness are 50 $\mu$ m, 100 $\mu$ m and 300 $\mu$ m, while possible types of contact are soft, hard and or proximity. Since this study does not include an analysis of the influence of the SU-8 thickness, only wafers with SU-8 thickness of 50 $\mu$ m have been analyzed.

For these wafers, a layer 50 $\mu$ m-thick SU-8 was spin coated and soft baked following the recommended guidelines. Figure 4.2 shows the spin coating operation in a graph, with rotational speed in rpm in the y-axis, and time in seconds in the x-axis.



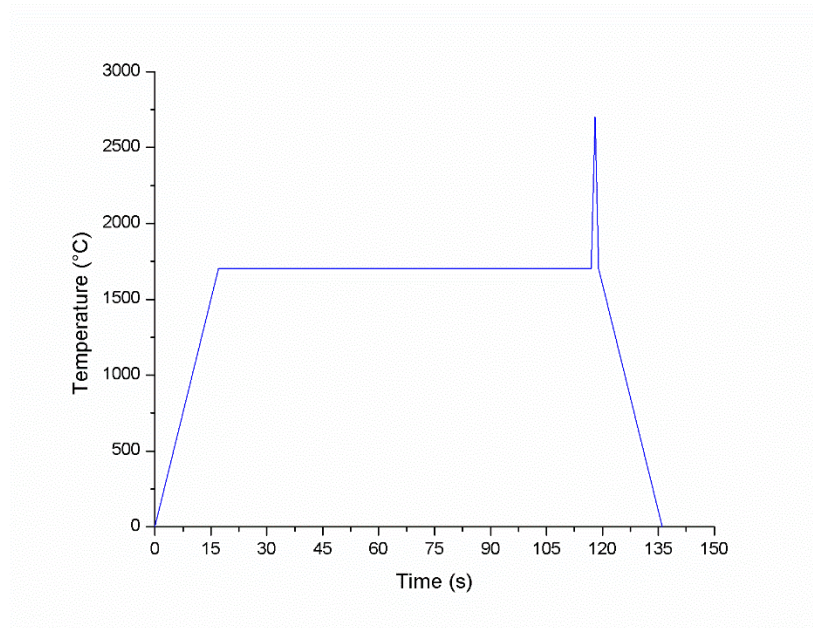


Figure 4.2: Spin coating cycle.

The rotational speed goes from 0 to 1700rpm in 17 seconds, with a constant acceleration of 100rpm/s. The speed is kept constant for 100s, to ensure a good diffusion of the SU-8 throughout the whole substrate. The operation is concluded with a sudden speed peak, to remove the edge bead, which is the SU-8 accumulated at the substrate edge. The speed goes to 2700 rpm and back to 1700rpm in just 2s, and finally decreases till stopping with a constant deceleration of 100rpm/s (same as the acceleration).

After spin coating, the wafer was soft baked on a hotplate, following the cycle shown on Figure 4.3.



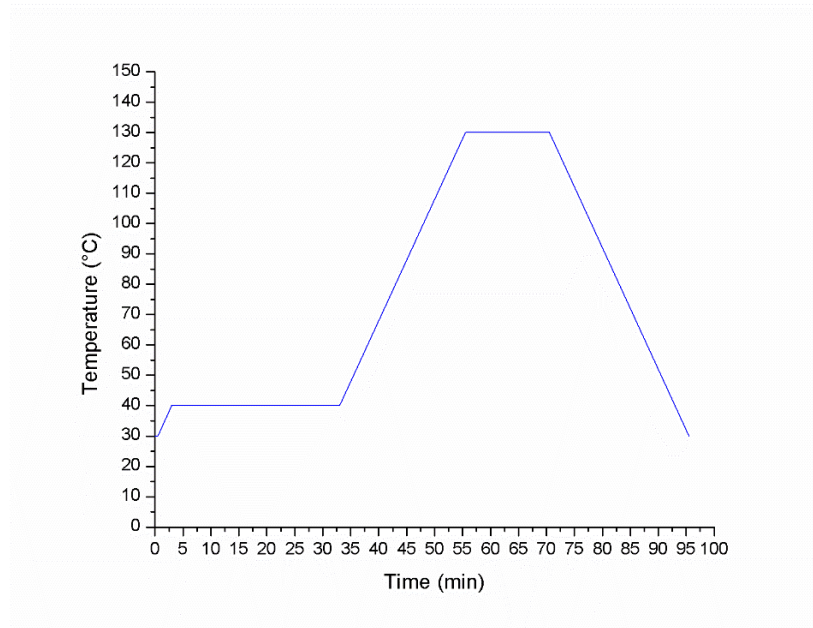


Figure 4.3: Soft baking cycle.

The heat treatment consists of two baking steps, the prebaking at 40°C for 30 min, and the soft baking at 130°C for 15 min. The preheat is useful to make the treatment smoother, limiting the formation of cracks in the SU-8. All the temperature gradients, both heating and cooling, have the same slope of 4°C/min. The baking takes complessly 95.5 min.

The exposure of the photoresist was done in a Suss MA6 Mask Aligner. A parameter of study here was the time of exposure, which translates directly into the exposure dose received by the SU-8. The light source was a mercury lamp with intensity of 10 mW/cm<sup>2</sup>, and light emissions of wavelength 365nm. The times of exposure studied were 10, 20, 30 and 40s. In order to obtain 4 different exposure doses on the same wafer, the exposure was performed in 4 phases of 10s each. For the first 10s, all the wafer was



exposed through the patterned photomask. For the next phase, one quarter of the wafer was shielded with a second mask, while the others were exposed for other 10s, so on and so forth, covering an additional quarter each phase.

The post exposure bake was a single step heat treatment at 95°C for 25 min. Regarding the soft baking, both heating and cooling were performed with a gradient of 4°C/min. The post exposure bake cycle is shown in Figure 4.4.

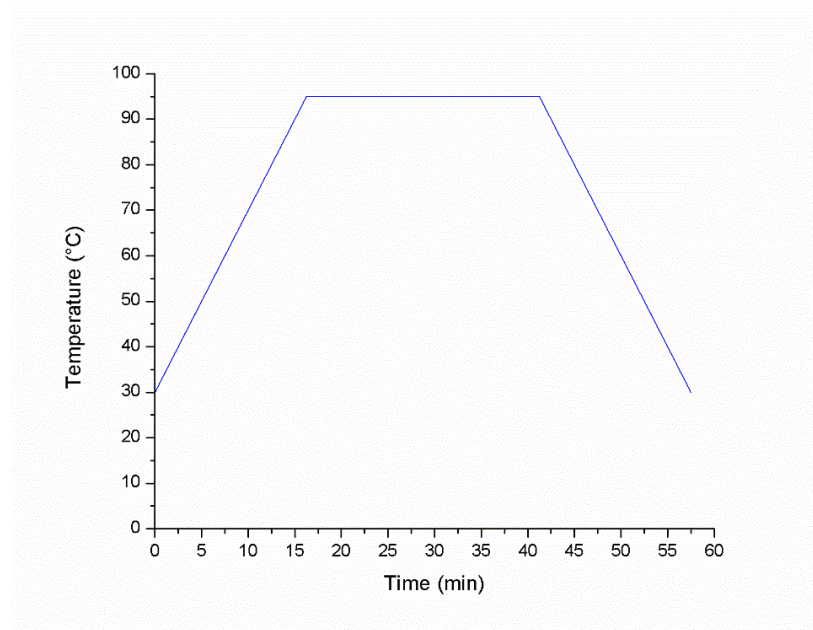


Figure 4.4: Post Exposure Baking cycle.

The final steps of the photolithography process are the development, which was performed by 3-5min immersion in PGMEA bath, with manual agitation, and hard bake at 190°C for 15 min.



## 4.2 Geometry and Dimensions

A wafer is divided into 4 quadrants, depending on the exposure time. Aligning the wafer with the long straight side on the bottom, the exposure time of the top left quadrant is 10s, and increases by 10s clockwise for each quadrant. Within one quadrant, posts are grouped primarily by their shape, and secondarily by their size and distance. In this section, all geometrical and dimensional values are nominal values, as they were theoretically designed on the photolithography mask. In reality, the SU-8 is not a faithful reproduction of the pattern carved in the mask, due to the effect of T-topping and other imprecisions. Although not corresponding to the real measurements on the wafers, the nominal values are fixed and comparable, making them suitable parameters for studying the photolithography process.

The possible geometrical sets are 6: hexagons, diamonds, squares, circles and two groups of triangles. One of the two sets of triangles has all the shapes oriented in the same way, so that the point of one triangle faces the side of the next one. In the other group, every row is rotated by  $180^\circ$ , so that, alternatively, consecutive rows are facing by two points or two sides.

Every set contains 42 subsets, which differ in terms of size and distance of the posts. The sizes studied are: 160, 80, 40, 30, 20 and  $10\mu\text{m}$ , while the distances studied are: 45, 30, 25, 20, 15, 10 and  $5\mu\text{m}$ . Each subset is a  $5\times 5$  array of SU-8 posts, where both distance and size are fixed. Therefore, for each of the 42 possible combinations of size and distance (252 combinations considering all the three: shapes, sizes and distance),



there are at least 20 possible structures in the x-axis and other 20 in the y-axis, which are enough to collect a significant amount of measurements.

The whole pattern of shapes, sizes and distances repeats for every exposure time. The 20, 30 and 40s patterns can be obtained from the 10s one, by symmetrically projecting them through the y-axis, origin and x-axis respectively. Finally, 3 different wafers were analyzed, one for each type of contact. The last parameter to take into account would be the SU-8 thickness, which was neglected in this study.

### **4.3 Methodology**

The SU-8 structures were first analyzed using optical microscopy (Nikon Eclipse LV100) and the native Nikon NIS Elements BR software. The optical microscope in our laboratory is mounted on a 3 degrees of freedom support, which allows the objectives to translate in x, y and z direction. The microscope has 4 Nikon TU PLAN ELWD objectives, with magnifying power 5x, 10x, 20x and 50x. The objective in use is the one aligned with the z-axis of the microscope. The output is recorded by a Zyla SCMOS (Andor Technology) camera, which is installed on the vertical eyepiece on top of the objectives. The camera records the images and sends them in real time to a desktop computer. Measurements can be taken directly on the screen, through the measurement toolbox of the NIS software. The SU-8 features were observed from top view, with the wafer fixed onto the microscope Tabletop, perpendicular to the z-axis of the machine, and with the straight sides aligned to the x and y-axis.



Considering all the different parameters, more than 3000 sets (arrays 5×5) were obtained, unique for their combination of type of contact, exposure, shape, size and distance. Despite the large number of different sets, not all of them are of interest in this specific study. Since the focus of this study is the characterization of suspended wires and bridges, only arrays featuring suspended wires and bridges are considered interesting, while arrays where the majority of the posts are merged, irregular, presenting broken bridges or no bridges at all, were neglected. However, the fact that the process parameters vary discretely, and not continuously, has to be considered. While extensive measurements were only taken for the arrays featuring suspended structures, the information of which parameters combination generates no bridges or merged structures is important as well. Therefore, a double step approach is adopted as methodology, first a qualitative analysis of the whole wafer is conducted, followed by quantitative analysis of the sets of interest.

In the qualitative analysis, a color and a code are assigned to each possible SU-8 features, as shown in Table 4.1.



Table 4.1: Colors and codes used for the qualitative analysis.

|    |                |
|----|----------------|
| NB | No Bridge      |
| S  | Spikes         |
| BB | Broken Bridges |
| SB | Stable Bridges |
| M  | Merged         |
| IR | Irregular      |

Then, for every type of contact, exposure dose and type of gap, colored Tables 7×6 were generated. Each Table contains 42 cells, one for each of the 42 subsets sharing the same values of three parameters. Every subset is associated to the proper color and code, according to the feature that repeats more frequently within the 5×5 array. Also, every set is numbered with numbers ranging from 1 to 42, to identify the particular combination of size and nominal gap. In the Tables, as in the wafer, the sets are ordered by size in columns and by nominal gaps in rows. The numeration starts from the top left, with set number 1 being the array with size 160μm and nominal gap 45μm. The count increases going down the first column, and then proceeds to the 45μm gap of the next column. When a particular shape has associated two or more types of gap, two different Tables were generated, for example, hexagons STS and hexagons PTP. Table 4.2 is the sample Table for hexagons side to side, 50μm thickness, exposed in soft contact for 30s.



Table 4.2: Sample qualitative analysis for hexagons STS, obtained with 30s exposure in soft contact.

| Size Gap ( $\mu\text{m}$ ) \ Size ( $\mu\text{m}$ ) | 160 | 80 | 40 | 30 | 20 | 10 |
|---|-----|----|----|----|----|----|
| 45  | SB  | NB | NB | NB | NB | NB |
| 30  | SB  | BB | SB | S  | NB | NB |
| 25  | SB  | SB | SB | SB | SB | NB |
| 20  | SB  | SB | SB | SB | SB | SB |
| 15  | M   | M  | M  | M  | M  | M  |
| 10  | M   | M  | M  | M  | M  | M  |
| 5   | M   | M  | M  | M  | M  | M  |

The most direct information illustrated by the colored Table 4.2 is the position of the sets with stable bridges, making the second step of the methodology, the quantitative analysis, much faster. Also, the point where the subsets switch from NB to SB, indicates that somewhere in the range between the nominal gaps of the two subsets, there is the maximum distance allowed to have suspended structures. Analogously, the range of the minimum distance can be found where the SB switch to M. Finally, comparing multiple Tables is a quick way to identify possible trends regarding the formation of bridges.

Once the qualitative analysis is completed, all the SB sets have been identified, and the quantitative analysis can start. In this part, actual measurements were taken and recorded, to obtain a database containing the real dimensions of the fabricated shapes, the



length of the bridges (or the gap in between two posts if the set has no bridges), and the width of the bridges. To give statistical significance to the analysis, a minimum of 4 measurements of each type was taken. With the x-y view, it was not possible to measure anything in the z-axis, but it was still possible to get an idea of the depth from the different gray scale of the features, depending on their position on the z-axis.

Further analysis was conducted via Scanning Electron Microscopy (SEM S3400N, Hitachi, Japan). Images obtained through SEM have much more resolution, making it possible to see wires as thin as 200nm. Also, the scanning electron microscope allows to incline the wafer, and consequently obtain 3D views of the posts. Three dimensional images make more easy the identification of suspended structures, respect the ones that are connected to the bottom, which was particularly helpful in the start, while trying to interpret the meaning of the gray shades in the pictures taken with the optical microscope.

After completing the analysis on the SU-8, the wafers were pyrolyzed to obtain the desired carbon structures. The pyrolysis was performed in a furnace (TF1700, Across International), in nitrogen atmosphere. The carbonization heat cycle is shown in Figure 4.5.



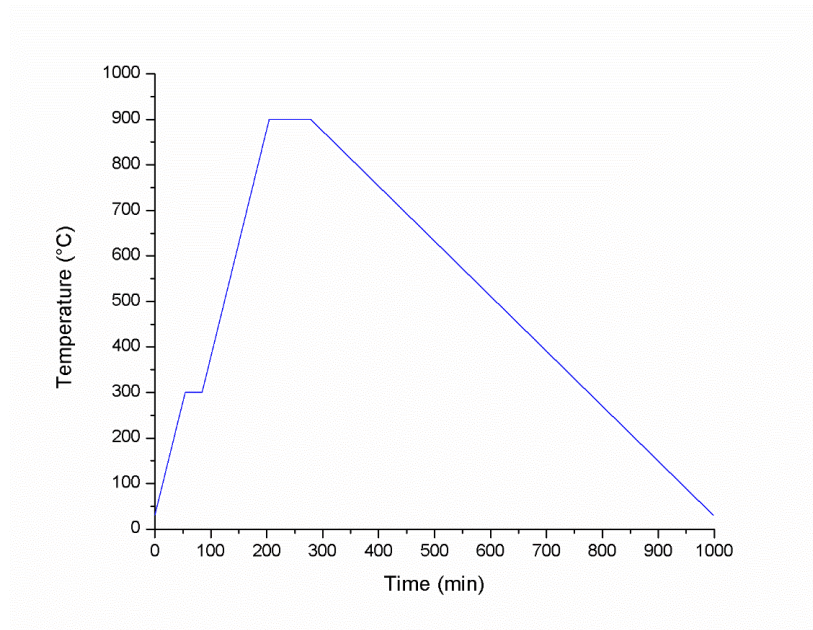


Figure 4.5: Carbonization cycle.

The heat treatment has two steps. The temperature is initially brought to 300°C where it remains for 30 min. During this phase, also called pre-carbonization, the solvent is eliminated from the SU-8. Then, the SU-8 is carbonized at 900°C for 75min. The heating rate is, in both cases, a constant 5°C/min, while for the cooling, the wafer is left inside the turned off furnace for 12h. Carbonization induces stresses and shrinkage, which definitely change the geometry of the suspended structures previously measured. Therefore, after carbonization, the wafers have to be analyzed again, with the same two steps methodology used for the SU-8. The results of both, SU-8 and carbon analysis, are the focus of Chapter 5 “Results”.



## CHAPTER FIVE

### RESULTS

In this chapter the results of the qualitative and quantitative analysis are presented. Every process parameter is analyzed in a dedicated section for the SU-8 fabrication, while the same analysis is repeated for structures obtained post carbonization. The chapter ends with a discussion section, which summarizes the results obtained and develops a mathematical model for the prediction of the formation of suspended structures.

#### 5.1 General considerations

Upon characterization of the different structures, the following cases were identified: No Bridges (NB), Broken Bridges (BB), Stable Bridges (BB), Walls/Merged (M) and Irregular/Missing (IR). The possible features obtainable from the photolithography process are shown in figure 5.1.A-E.

- A. No Bridges (NB): the posts are vertical and self-standing, there is no visible interaction in-between the posts.
- B. Broken Bridges (BB): there is an obvious attempt of the two posts to connect but the structure is either visibly cracked, interrupted, or incomplete.
- C. Stable Bridges (SB): regular, homogeneous and continuous suspended structures.

A structure is classified as “bridge” if it is more than 1 $\mu$ m wide, like the horizontal ones in the picture. Otherwise, the structure is classified as “wire”, like the vertical ones.



- D. Merged/Walls (M): the first case indicates that the posts are actually intersecting, so that is not possible to identify single posts anymore; the second case indicates that the structure is not suspended, but extends all the way to the bottom. These two are grouped, since they are equally undesirable.
- E. Irregular (IR): whenever the posts are not straight upwards, but bent, strongly deformed, or completely missing, they are considered irregular.

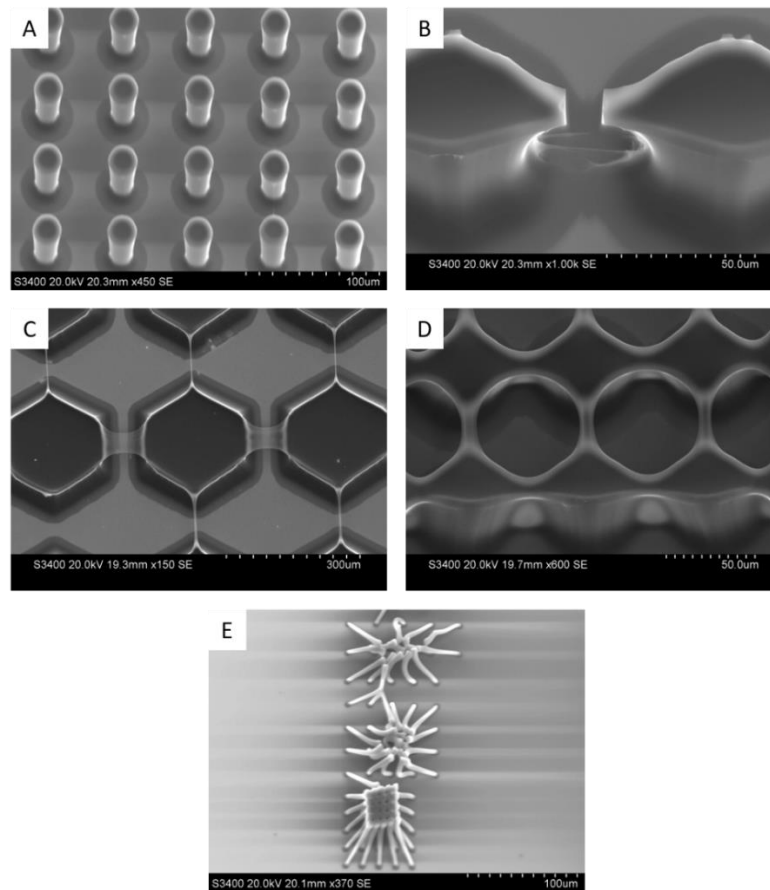


Figure 5.1: SEM images of: A) No Bridges; B) Broken Bridge; C) Suspended Bridges (Horizontal) and Wires (Vertical); D) Merged, note that the wall extends throughout the height of the posts; E) Irregular.



The possible outcomes illustrated above are the result of the combined influence of all the photolithography parameters. The ones analyzed in this work, as mentioned previously, are: type of contact, exposure time, nominal size, nominal gap, and type of gap. In order to obtain information on the influence of a single parameter on the formation of suspended structures, each parameter was studied fixing all the other parameters at the same time. This allowed to generate graphs where the characteristic dimensions of the bridges, length and width, were a function of the single parameter of interest.

The graphs obtained this way are not very informative by themselves, but become very meaningful when compared to each other. The graphs can be grouped and compared to identify possible trends. For example, examining the exposure time, the information sought is the behavior of the bridges formation as the exposure goes from 10s to 40s. There are no data that can tell a priori whether a specific time of exposure will result in self-standing, connected or merged structures. The reason is that, within the same quadrant with fixed exposure, there are bridges, merged structures, and self-standing posts depending on the shape, size, and distance of the posts. A possibility is plotting a curve for every exposure time, in a graph where the y-axis is either the fabricated length or the width of the suspended structure (which are the two characteristic dimensions of a bridge), and the x-axis is the nominal gap. Such graph allows to determine whether the bridges are longer or shorter, wider or thinner, as the exposure increases from 10s to 40s, for a specific nominal gap.



The results shown in the exposure/gap plot do not take into consideration the type of contact, type of gap, and size of the shape. For a complete analysis, a different graph for each of the possible combinations of these parameters has to be obtained, and then, the results have to be compared altogether to determine if there is a trend associated with the exposure time. Finally, all the parameters have to be analyzed in the same way as the exposure time. Moreover, not all the combinations produced enough suspended structures. Therefore, for the sake of brevity and clarity, in order to demonstrate the hypotheses formulated in Chapter 3 only a set of representative graphs will be presented in the results section.

## **5.2 Type of contact**

As seen in Chapter 3, type of contact refers to the distance in between photomask and SU-8 layer, during the exposure step of the photolithography process. According to the hypothesis formulated, the formation of suspended structures should be “facilitated” as the distance increases. “Facilitated” is a controversial term, and requires a further explanation because it does not necessarily mean that the number of suspended structures will be increased. The formation of bridges is facilitated in the sense that increasing the distance, the probability of creating structures at higher nominal gaps increases. At the same time, the probability of obtaining merged structures at higher nominal gaps also increases. Therefore, the number of subsets featuring stable bridges does not always increase, but these subsets are usually shifted to larger nominal gaps (the top of the colored tables in the qualitative analysis).



Figure 5.2A-F illustrates plots of fabricated gaps against the nominal ones for 6 different types of gap. Each graph has 3 curves: soft contact, hard contact, and proximity. Before talking about the actual results, a few remarks to better understand the graphs will be made. The fabricated gaps in Figure 5.2.A-F are plotted in function of only two parameters, type of contact and nominal gap. The exposure time was fixed to 40s, and the size of the shapes to 160 $\mu$ m. Among all the possible combinations of parameters, this particular one was chosen as representative, because it has the highest number of subsets with stable bridges. A selection was also made on the types of gap. Figure 5.2 contains: A) hexagons PTP; B) hexagons STS; C) triangles BTB facing by the points adjacent to the bases; D) diamonds; E) squares; and F) circles. Triangles PTB and triangles BTB facing by the bases or by the points opposite to the bases were neglected in most of the analysis, because they did not generate many reliable structures respect to other types of gap. Furthermore, in the graphs, every point indicates a specific subset, which is identified by the nominal gap on the x-axis. With all the other parameters fixed and the nominal gap free to vary, a curve can have a maximum of seven points, one for each nominal gap: 5, 10, 15, 20, 25, 30, and 45 $\mu$ m. Since the y-axis represents the length of the structures, there are only points for the subsets corresponding to stable bridges. Also, these subsets can only be consecutive, since it is not possible, for example, to have bridges at 20 and 30 $\mu$ m, but not at 25 $\mu$ m, unless the structures of the middle subset broke for reasons independent from the process parameters. Therefore, in all the figures, all the subsets with nominal gap values at the right of the curves, have associated either broken bridges or no bridges, while all the subsets at the left of the curves have associated walls



and merged structures. For example, the blue curve of figure 5.2A shows that, for hexagonal posts of dimension  $160\mu\text{m}$ , facing point to point and exposed for 40 seconds in proximity contact: at nominal gaps 5 and  $10\mu\text{m}$ , there are merged structures; at 15, 20 and  $25\mu\text{m}$  there are stable structures; and at 30 and  $45\mu\text{m}$  there are no bridges or broken ones.



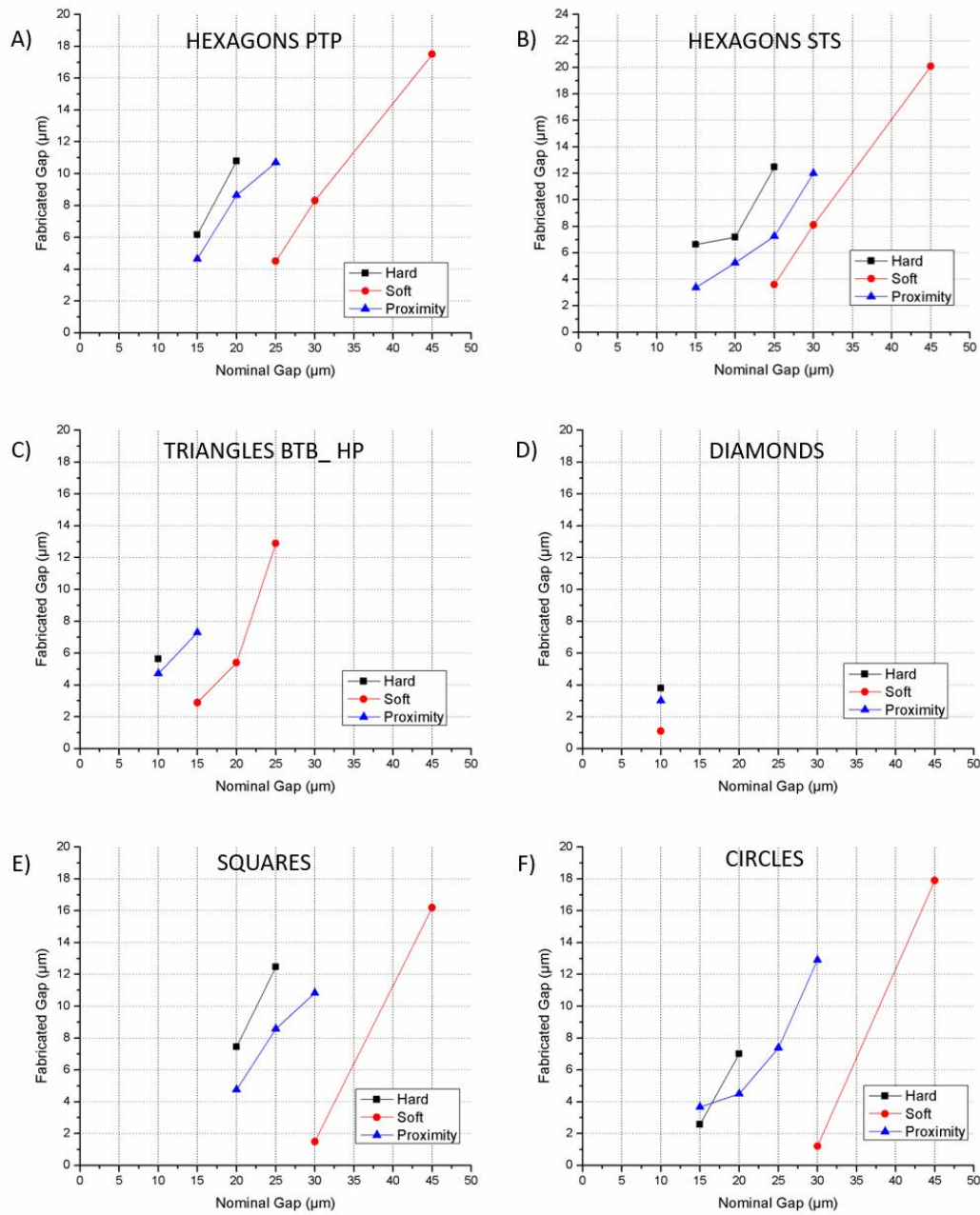


Figure 5.2A-F: Fabricated gap against nominal gap for different types of contact. The results are shown for the case of exposure fixed to 40s, and nominal size of 160 $\mu\text{m}$ .



In Figure 5.2, it can be observed that every type of gap and type of contact produces 1 to 4 subsets with stable bridges when 160 $\mu$ m shapes are exposed for 40s. The curves, analyzed singularly, show that the fabricated gap increases as the nominal gap increases. Diamonds and triangles have less stable bridges, mostly concentrated at smaller nominal gaps. The other gap types are characterized by more stable bridges, mostly concentrated in the nominal gaps middle values. An interesting trend emerging from Figure 5.2A-F is the shift of the curves towards right (larger nominal gaps), when passing from hard contact, to proximity and then to soft contact. Exposing the SU-8 in soft contact produces bridges at larger nominal gaps than proximity, and hard contact. At the same time, the fabricated gap for a fixed nominal gap decreases in the same order, causing the posts in soft contact to merge at longer nominal gaps.

The other characteristic dimension of the suspended structures is the width, which is analyzed in Figure 5.3.A-F, analogously to the fabricated gap. The remarks mentioned above also apply to this case, and to every further graph shown in this chapter, independently from the parameters in study.



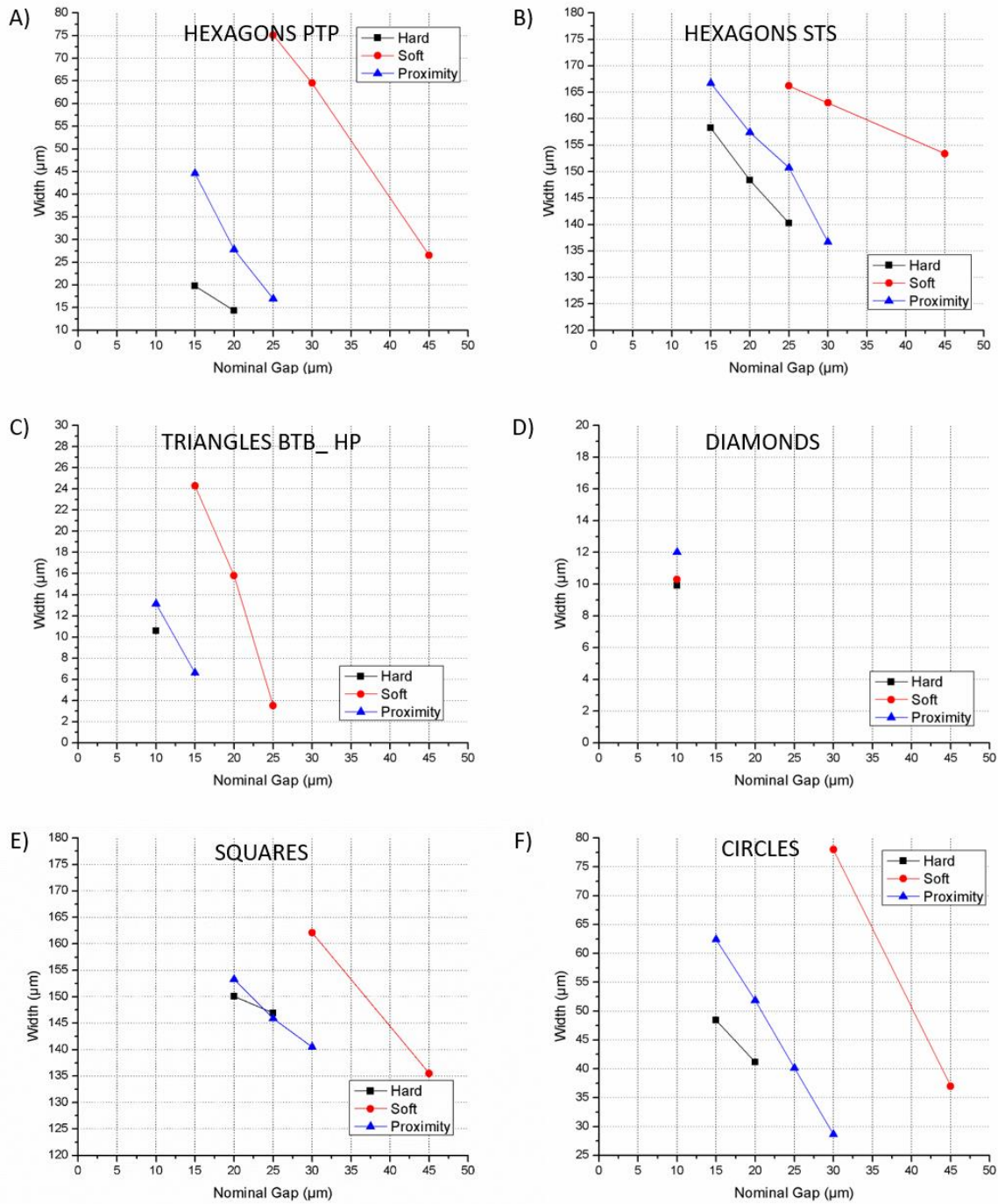


Figure 5.3.A-F: Width against nominal gap for different types of contact. The results are shown for the case of exposure fixed to 40s, and nominal size of 160μm.



The curves plotted in Figure 5.3 show that the width of the bridges decreases with the nominal gap, and increases passing from hard to proximity and, eventually, to soft contact, confirming the trend observed in Figure 5.2.

To summarize the results for the type of gap, passing from hard contact to proximity and, eventually, to soft contact, the T-topping increases, allowing suspended structures to form between posts nominally further, and generating broader posts, which reduce the fabricated gap and consequently increase the bridge width. Although the trends observed were partially expected, the fact that soft contact is generating more T-topping than the proximity contact is, surprisingly, in contrast with the hypothesis formulated. Since the distance between the mask and the SU-8 increases passing from hard contact to soft contact, and finally to proximity, the shift was expected to follow this order as well. While the hard contact clearly shows a disadvantage for the formation of suspended structures, proximity was supposed to work better than soft contact.

A possible reason for such incongruence is the topography of the SU-8 layer after spin-coating. Theoretically, the distance between the mask and the SU-8 is supposed to be  $20\mu\text{m}$  in proximity, and 0 in soft and hard contact. Nevertheless, analyzing the topography of the wafer, the average height of the SU-8 layer resulted  $612.8 \pm 8.6\mu\text{m}$ , varying within the wafer surface in a range of about  $30\mu\text{m}$ , which is larger than the proximity distance itself. In hard contact, the mask is pressed against the SU-8, and the pressure could be sufficient to flatten the SU-8 topography. Instead, in soft contact, the mask stops as soon as it touches the highest peak, which could explain why the hard contact behaved as expected and the soft contact did not.



In Figure 5.4, a new parameter, the gap reduction ( $\Delta g$ ) is introduced. The gap reduction is obtained subtracting the fabricated gap from the nominal gap. From a geometrical point of view, the gap reduction is equivalent to the increase of the shape size in direction of the gap, and can be obtained from the fabricated gap ( $g_f$ ) and the nominal gap ( $g_n$ ) using the equation:

$$\Delta g = g_n - g_f$$

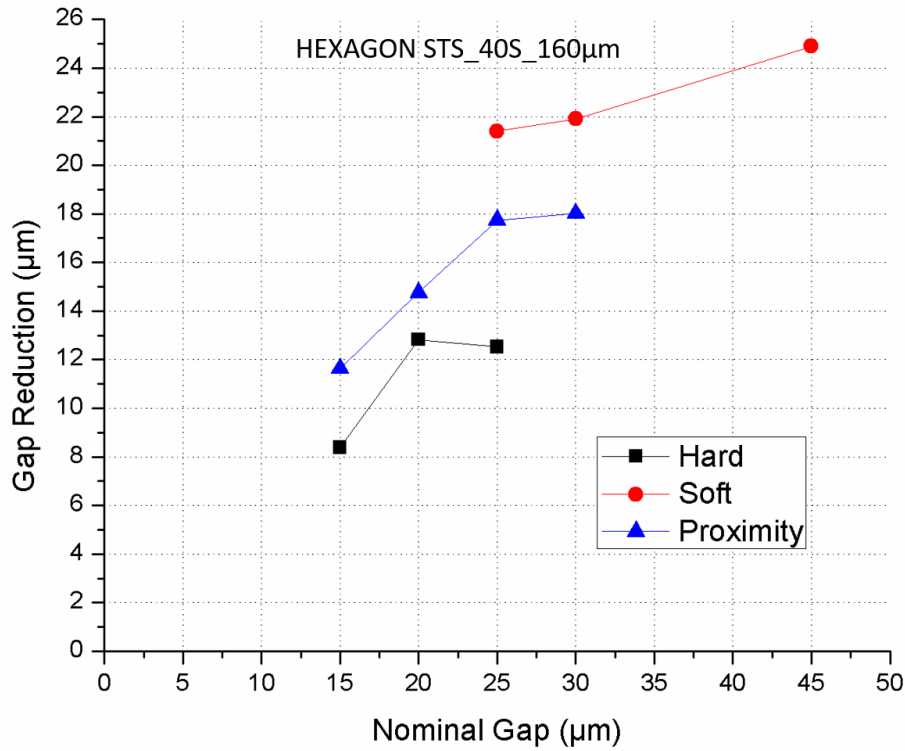


Figure 5.4: Gap reduction against nominal gap for different types of contact. The results are shown for the case of exposure fixed to 40s, and nominal size of 160μm.

The graph of the gap reduction is a further confirmation of the trend observed in the previous two Figures. The highest gap reduction is witnessed for soft contact,

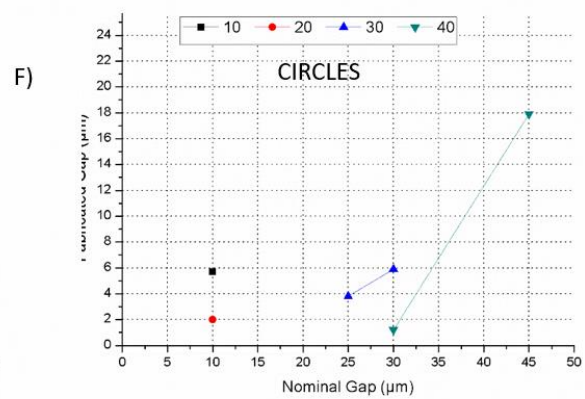
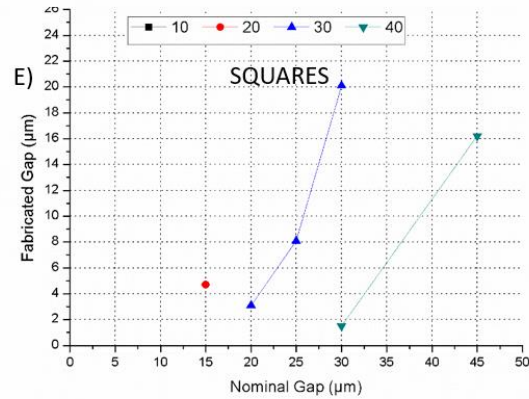
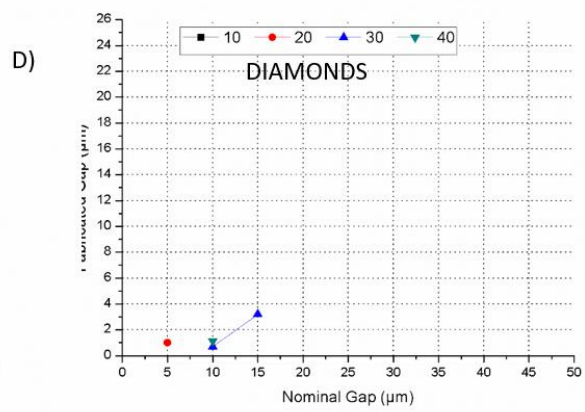
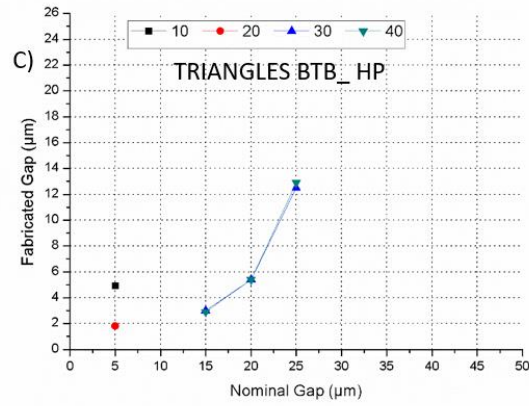
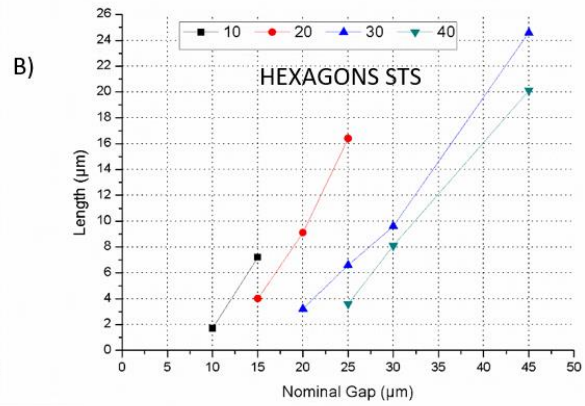
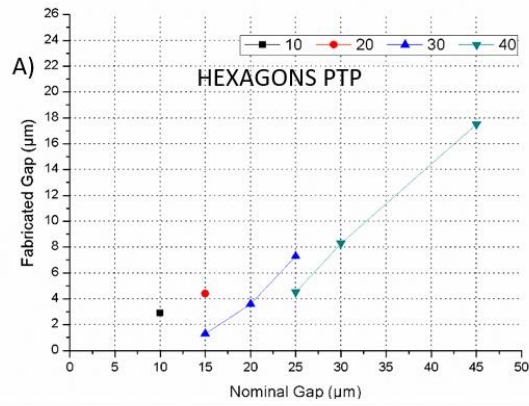


followed by proximity, due to the increase of the shapes respect to the nominal. Also, the gap reduction decreases with the nominal gap.

### **5.3 Exposure dose**

As seen in chapter 3, the exposure dose is defined as the product of the power of the light source multiplied by the time of exposure. Keeping the light source power constant, the parameter of interest is the time of exposure. It was hypothesized that a close correlation between exposure time and the amount of T-topping exists. Thus, it is expected that an increase of the exposure time will generate larger shapes, reducing fabricating gaps, and facilitating the formation of suspended structures. Figure 5.5 contains graphs of the same 6 types of gap considered in the analysis of the type of contact. Each graph displays the fabrication gap in function of the nominal gap, for the 4 different time of exposures. All the graphs of Figure 5.5 refer to shapes of size  $160\mu\text{m}$ , exposed in soft contact.





5.5A-F: Fabricated against nominal gap for different exposure times. The results are shown for the case of soft contact exposure, and nominal size of 160μm.



After having analyzed the results for the type of contact, a similar trend for the exposure can be immediately recognized. The longer exposure time, the further the curves shift to the right of the graphs, generating suspended structures at larger nominal gaps, and featuring more merged subsets as well, as shown in Table 5.1.

Table 5.1: Maximum and minimum gaps with stable bridges for different types of gap and exposure times. The results are shown for the case of soft contact exposure, and nominal size of 160 $\mu$ m. All dimensions are in  $\mu$ m.

| Type of Gap         | Feature         | Exposure |     |     |     |
|---------------------|-----------------|----------|-----|-----|-----|
|                     |                 | 10s      | 20s | 30s | 40s |
| Hexagons<br>PTP     | Min gap with SB | 10       | 15  | 20  | 25  |
|                     | Max gap with SB | 15       | 25  | 45  | 45  |
| Hexagons<br>STS     | Min gap with SB | 10       | 15  | 15  | 25  |
|                     | Max gap with SB | 10       | 15  | 25  | 45  |
| Triangles<br>BTB_HP | Min gap with SB | 5        | 5   | 15  | 15  |
|                     | Max gap with SB | 5        | 5   | 25  | 25  |
| Diamonds            | Min gap with SB | -        | 5   | 10  | 10  |
|                     | Max gap with SB | -        | 5   | 15  | 10  |
| Squares             | Min gap with SB | -        | 15  | 20  | 30  |
|                     | Max gap with SB | -        | 15  | 30  | 45  |
| Circles             | Min gap with SB | 10       | 10  | 25  | 30  |
|                     | Max gap with SB | 10       | 10  | 30  | 45  |



Table 5.1 refers only to the nominal gaps. From a quantitative point of view, for a fixed nominal gap, the fabrication gap reduces as the exposure time increases. The reduction of the fabrication gap is shown in Table 5.2, for the sample hexagons STS and PTP, at fixed nominal gap 25 $\mu$ m. These particular gap and shapes were chosen because they are from the most representative, since they feature stable bridges at 3 different times of exposures.

Table 5.2: Fabrication gaps for Hexagons STS and PTP in function of the exposure time. The results are shown for the case of soft contact exposure, nominal size of 160 $\mu$ m, and nominal gap of 25  $\mu$ m. All dimensions are in  $\mu$ m.

| Type of Gap | Exposure 10s |        | Exposure 20s |        | Exposure 30s |        | Exposure 40s |        |
|-------------|--------------|--------|--------------|--------|--------------|--------|--------------|--------|
|             | Average      | St.Dev | Average      | St.Dev | Average      | St.Dev | Average      | St.Dev |
| Hexagons    | -            | -      | -            | -      | 7.3          | 0.34   | 4.5          | 0.99   |
| PTP         | -            | -      | -            | -      | -            | -      | -            | -      |
| Hexagons    | -            | -      | 16           | 0.63   | 7.25         | 0.56   | 3.6          | 0.4    |
| STS         | -            | -      | -            | -      | -            | -      | -            | -      |

In Figure 5.6A-F, the curves of the bridges width in function of the nominal gap for different time exposures and types of gap, fixed sizes to 160 $\mu$ m, exposed in soft contact, are shown.



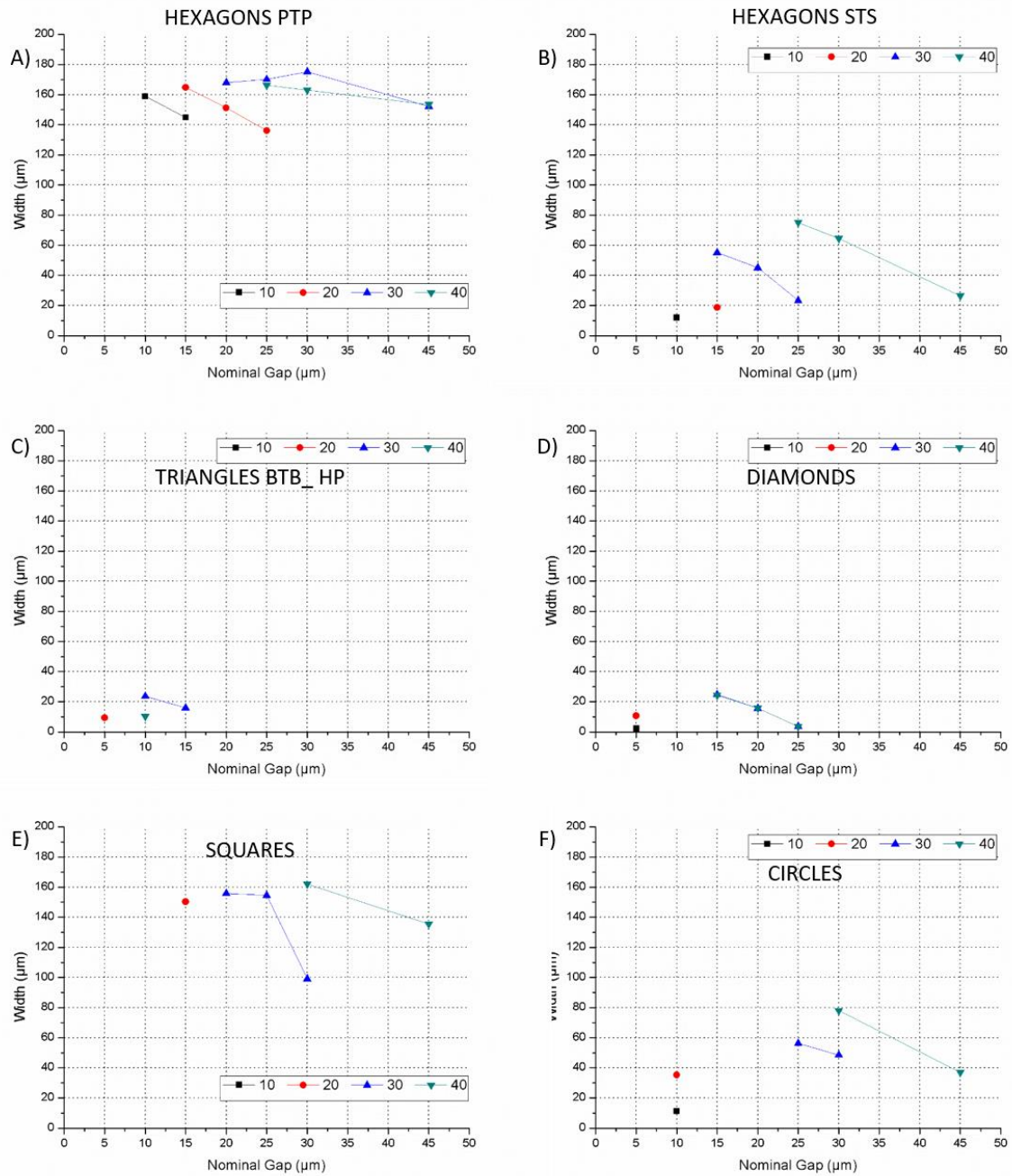


Figure 5.6A-F: Width against nominal gap for different exposure times and types of gap.

The results are shown for the case of soft contact, and nominal size of  $160\mu\text{m}$ .



Regarding the type of contact, the bridge width decreases with the nominal gap and increases with the fabricated gap. Therefore, for fixed nominal gaps, a longer exposure time produces wider suspended structures. The same trend is confirmed by the behavior of the gap reduction. Since, in this section dedicated to the exposure, the type of contact was not taken in consideration, but simply fixed to soft contact, Figure 5.7A-C displays the graphs of the gap reduction in function of the nominal gap for different exposure times and types of contact.

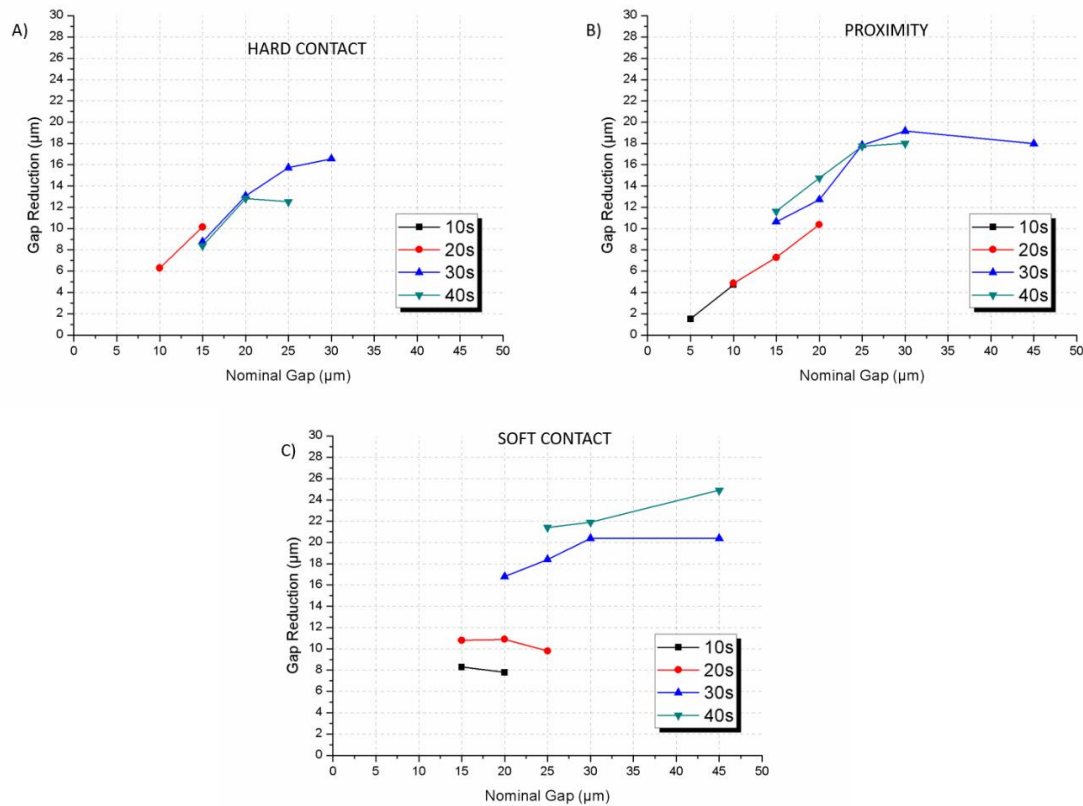


Figure 5.7A-C: Gap reduction against nominal gap for different types of contact and exposure times. The results are shown for the case of hexagons STS of nominal size 160μm.



The data analyzed shows an increase of the gap reduction in function of the exposure time. The trend is very clear in Figure 5.7C while the curves for 30s and 40s (Figure 5.7A-B), are too close to each other to observe any tendency. As previously mentioned, the gap reduction is equivalent to the increase of the post shapes respect to the nominal. Therefore, to close the circle and furtherly validate the trend identified, Table 5.3 shows the area broadening in function of the exposure time, for all the different shapes, with fixed size 160 $\mu$ m and soft contact exposure.

Table 5.3: Cross section in function of the time of exposure, for different shapes with characteristic dimension 160 $\mu$ m. All dimensions in  $\mu$ m.

| Shape                  | Nominal size | Size for 10s | Size for 20s | Size for 30s | Size for 40s |
|------------------------|--------------|--------------|--------------|--------------|--------------|
| Hexagons <sup>1</sup>  | 277.18       | 288          | 291          | 298          | 303          |
| Triangles <sup>2</sup> | 138.5        | 151          | 155          | 162          | 165          |
| Diamond <sup>3</sup>   | 226.3        | 227          | 232          | 238          | 242.5        |
| Squares                | 160          | 168          | 170          | 182          | 190          |
| Circles                | 160          | 165          | 168          | 184          | 190          |

<sup>1</sup> For hexagons the measurement taken was the distance between two parallel sides.

<sup>2</sup> For triangles the measurement taken was the height.

<sup>3</sup> For diamonds the measurement taken was the diagonal.

The data in Table 5.3 shows that the broadening of the cross section is directly proportional to the time of exposure. In particular, the increment of the cross sections in the case of 10 and 20s is quite limited compared to the higher exposure times. This is the explanation of the fact that the 30 and 40s quadrants present many more merged subsets, and usually more suspended structures, respect to the 10 and 20s. The fact that for 10 and 20s exposure time the broadening is limited, generates thinner suspended structures, and sometimes allow their formation at the lowest nominal gaps (5-10 $\mu$ m), which is the key to obtain the very thin wires, which are the final objective of this work.



In the case of the exposure time, all the hypotheses formulated in chapter three have been confirmed.

#### **5.4 Nominal size**

Each set (defined in chapter 4 as the group containing all the posts with the same geometrical shape) has subsets of posts of 6 different sizes: 160, 80, 40, 30, 20 and 10 $\mu$ m. Such values refer to the characteristic dimension of the shape, which is the side for the polygonal shapes, and the diameter for the circles. Figure 5.8A-F represents the fabricated gaps in function of nominal gap and shape size, for exposure time of 40s in soft contact.



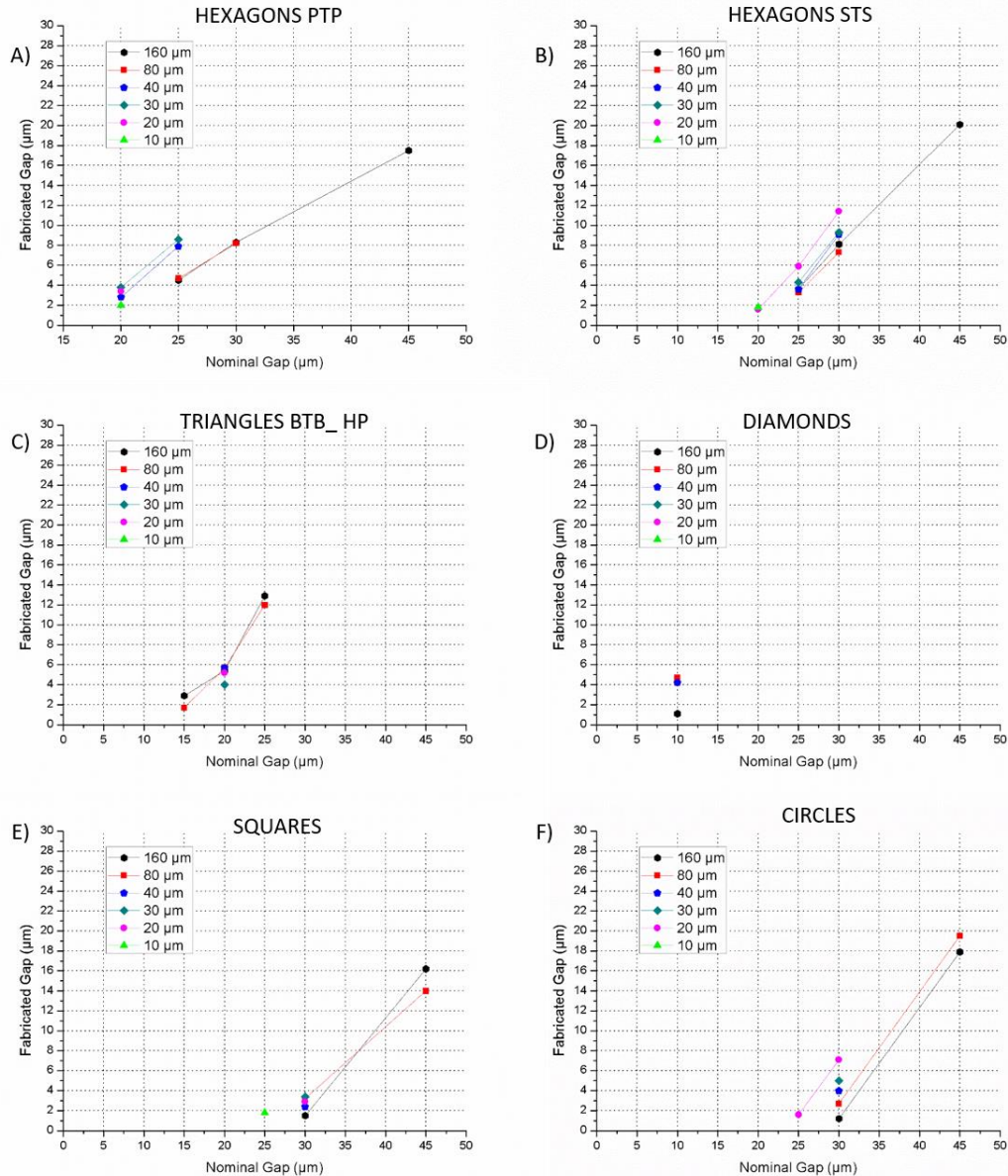


Figure 5.8A-F: Fabricated gap against nominal gap for different nominal sizes and types of gap. The results are shown for the case of exposure 40s in soft contact.

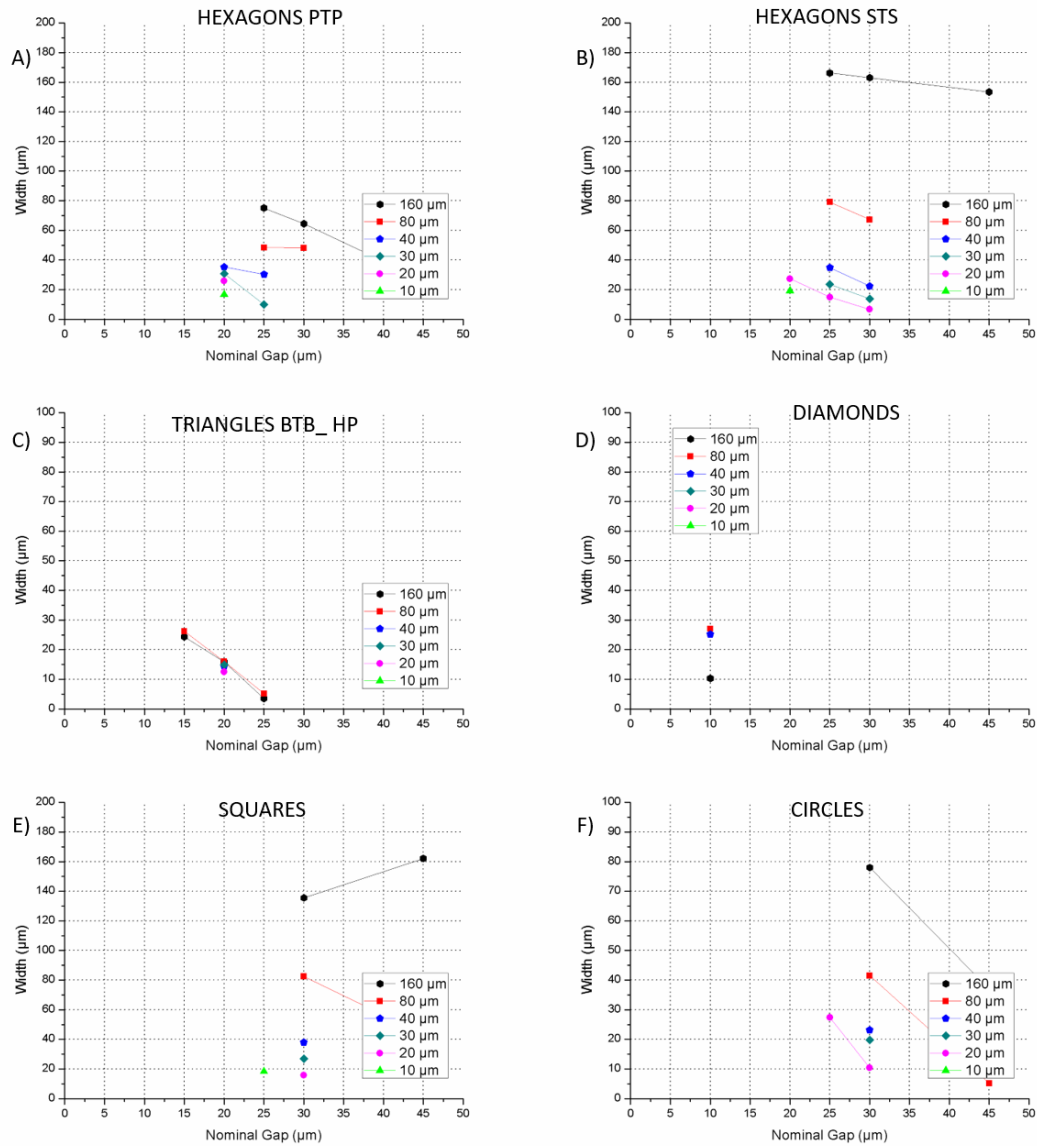
The data analyzed shows that varying the nominal shape does not significantly influence the formation of suspended structure so there is not a clear influence between



the size of the posts and the formation of suspended structures. Even considering great changes in the nominal size, passing from 10 to 160 $\mu\text{m}$ , most of the points are still aligned in columns. This means that for a specific set, if the subset of size 160 $\mu\text{m}$  and nominal gap 30 $\mu\text{m}$  features stable bridges, there are high chances that all the other subsets with different nominal sizes but same nominal gap 30 $\mu\text{m}$  will have stable bridges as well. A clear example is given by the hexagon STS in Figure 5.8B, where all the nominal sizes but the 10 $\mu\text{m}$  have bridges at 25 and 30 $\mu\text{m}$ .

Although the formation of bridges is not affected by variation of the nominal size, the width of the suspended bridges is directly proportional to the shape size. In fact, two adjacent posts, facing each other by sides instead of points, tend to develop bridges all along the sides. This explains why subsets with type of gap STS features wider bridges than the subsets PTP. For the same reason, the bigger the side, the wider the bridge. This hypothesis can be verified analyzing the graphs in Figure 5.9A-F.







graphs, which represent gaps PTP, the influence of the nominal size is strongly reduced.

This is perfectly in accordance with the hypothesis, since, in these sets, the posts are facing by points, which do not increase particularly with the nominal size. The hypothesis is furtherly quantitatively verified by the data in Table 5.4, which proves the small influence of the nominal shape on the fabrication gap, and the big influence on the suspended structures width, for hexagons STS exposed for 40s in soft contact.

TABLE 5.4: Bridges length and width in function of the nominal size. The results are shown for hexagons STS, exposed in soft contact for 40s. All dimensions are in  $\mu\text{m}$ .

|                                | Nominal Size      |                  |                  |                  |                  |                  |
|--------------------------------|-------------------|------------------|------------------|------------------|------------------|------------------|
|                                | 160 $\mu\text{m}$ | 80 $\mu\text{m}$ | 40 $\mu\text{m}$ | 30 $\mu\text{m}$ | 20 $\mu\text{m}$ | 10 $\mu\text{m}$ |
| <b>Nominal gap</b>             | 30                | 30               | 30               | 30               | 30               | 30               |
| <b>Average measured length</b> | 7.64 $\pm$ 1.37   | 7.47 $\pm$ 1.33  | 9.19 $\pm$ 0.6   | 9.3 $\pm$ 0.71   | 11.47 $\pm$ 0.56 | 13.81 $\pm$ 0.63 |
| <b>Average measured width</b>  | 163.42 $\pm$ 3.36 | 67.29 $\pm$ 0.51 | 22.26 $\pm$ 0.13 | 13.77 $\pm$ 1.7  | 6.86 $\pm$ 0.3   | No Bridge        |

Figure 5.10A-D display the gap reduction in function of the nominal gap, for different nominal sizes and exposure times, in the case of hexagons STS in soft contact.



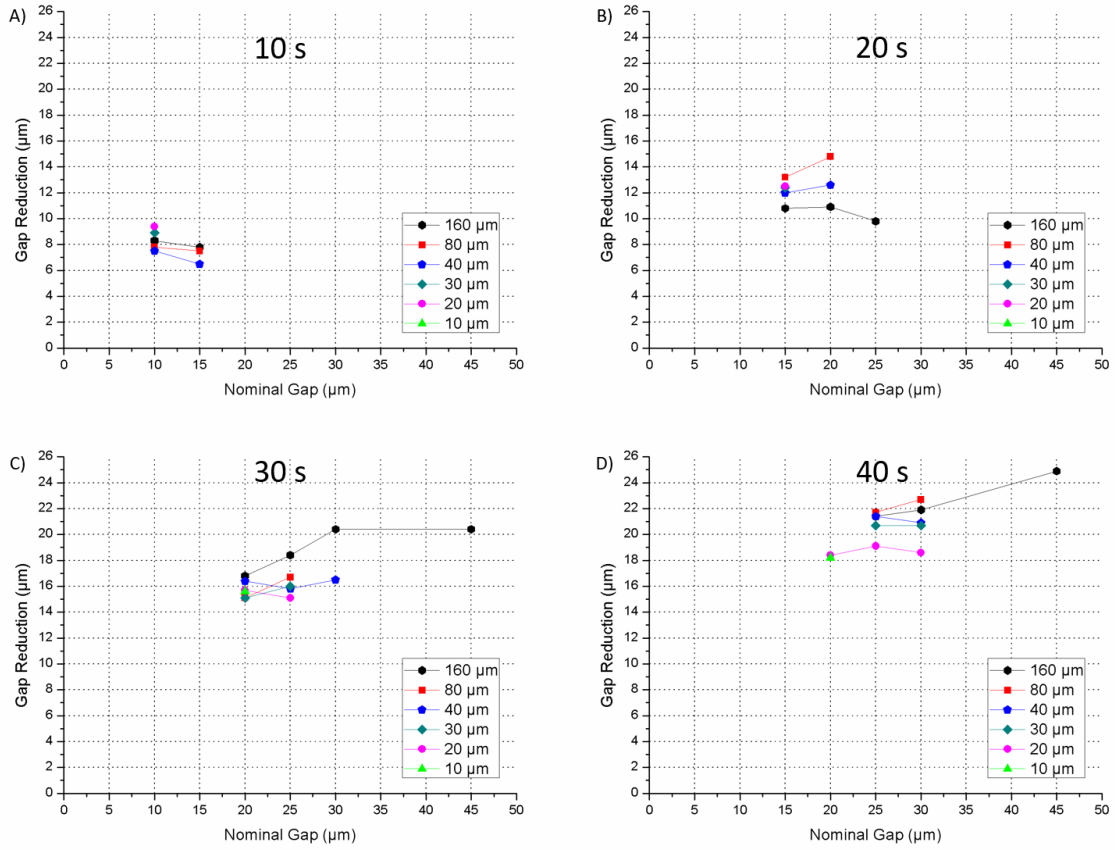


Figure 5.10A-F: Gap reduction against nominal gap for different nominal sizes and exposure times. The results are shown for hexagons STS exposed in soft contact.

As expected, the data analyzed do not suggest any trend of the gap reduction in response to nominal size variations.

The last consideration about the nominal size, is that it directly affects the resistance of the SU-8 posts to stiction. Stiction is a phenomenon due to the surface tension of the liquid meniscus that is formed in-between two adjacent posts during the photolithography development. The risk of stiction increases for high aspect ratio posts



closely packed. The resistance of a post to this phenomenon depends on its height and moment of inertia, which is determined by the geometry and dimensions of the cross section [38]. High aspect ratio posts with smaller cross sections are slenderer, and thus more inclined to bend and stick in an irreversible fashion.

## **5.5 Type of Gap**

The type of gap depends on both the geometry and orientation of the shape. From a geometrical point of view, the subsets are regrouped in 5 different shapes: hexagons, squares, diamonds, triangles and circles. A further differentiation is done taking also in consideration the orientation of these shapes. In this sense, the types of gap are grouped and defined as side-to-side (STS), point-to-point (PTP), point-to-side (PTS), and circle-to-circle (CTC), depending on which extremities of the shapes are facing two consecutive posts. Squares are defined as STS, diamonds as PTP, shapes such as hexagons can be both. For example, aligning two parallel sides of hexagons to the x-direction, the type of gap, in the x-direction, is hexagons PTP, while, in the y-direction, is hexagons STS. The only PTS case is the triangles where the vertex of a triangle faces the base of the following one. The triangles PTS are not included in most of the graphs shown in the results section, because they often connect diagonally, in an unpredictable manner, and hence, they are not considered interesting for the goal of this study. The circles have a behavior in-between PTP and STS, but since they are closer to the latter, they are considered to belong to the STS group for simplicity. The fabrication gap in function of



the nominal gap, for different types of gap and time of exposures, is shown in Figure 5.11A-D.

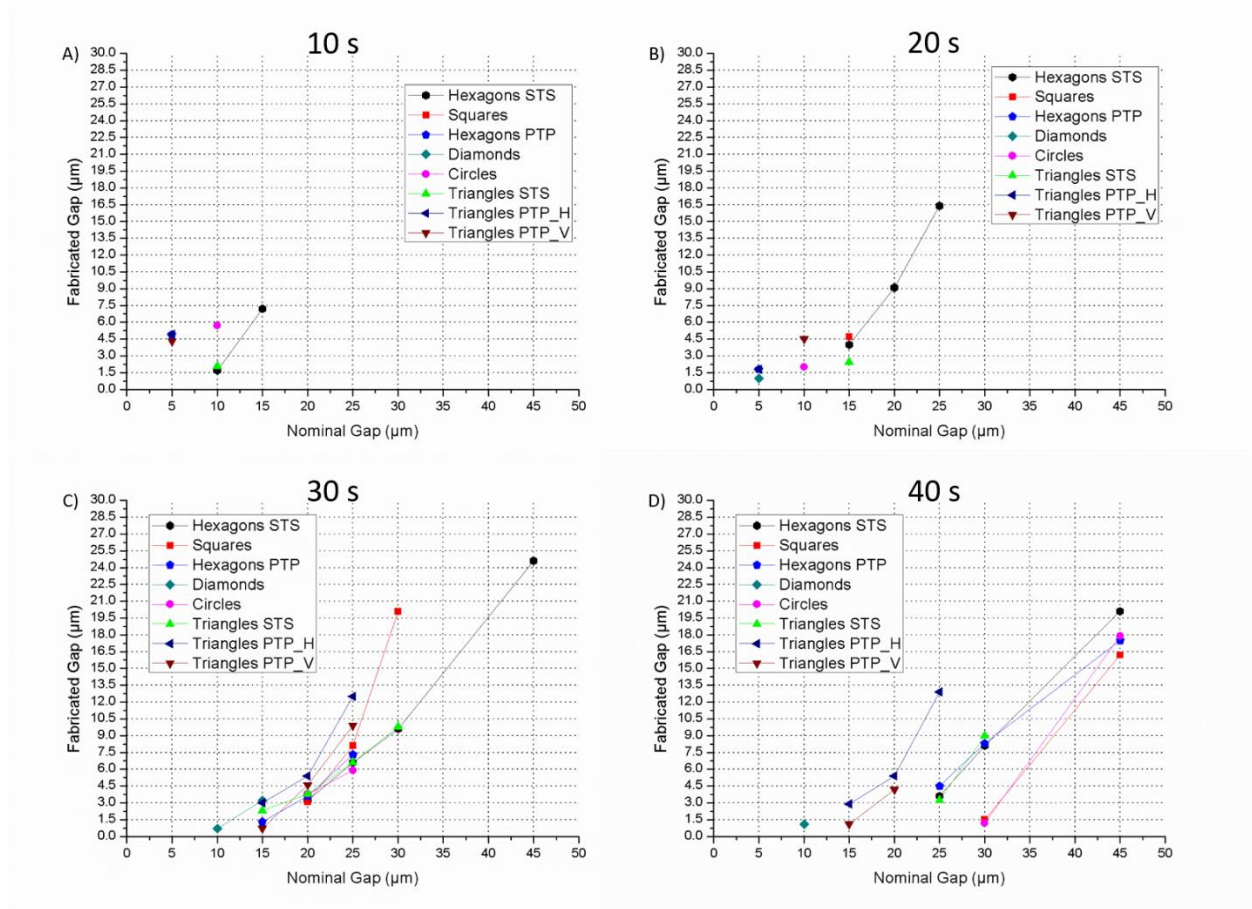


Figure 5.11A-D: Fabrication gap against nominal gap for different types of gap and exposure times. The results are shown for nominal size 160μm exposed in soft contact.

It can be observed that the shapes STS usually present suspended structures at longer nominal gaps than the PTP. In particular, hexagons STS appear to be the most effective type of gap when the goal is to achieve suspended long and wide bridges in a large range of nominal gaps. The other shapes that facilitate the formation of bridges are



squares, circles and triangles, followed by the PTP shapes. The PTP shapes tend to form less suspended bridges, at lower nominal gaps and, as shown in Figure 5.10.A-D, PTP shapes produce much thinner structures than the STS ones. Thus, the PTP shapes are the only ones capable of generating suspended wires with width lower than  $1\mu\text{m}$ . Among the PTP shapes, the number of subsets with suspended structures and the dimensions of the structures decrease in descending order from hexagons to diamonds and finally to triangles. This trend confirms the hypothesis that shapes with more material facing each other are facilitated in creating connections. The theory is also supported by the graphs in Figure 5.12A-D, where it is shown that shapes with more material at the interface with the adjacent posts result in wider bridges. Once again, the hexagons STS appear at the top right of the plots, followed by the other STS shapes, while the PTP are confined at the bottom left.



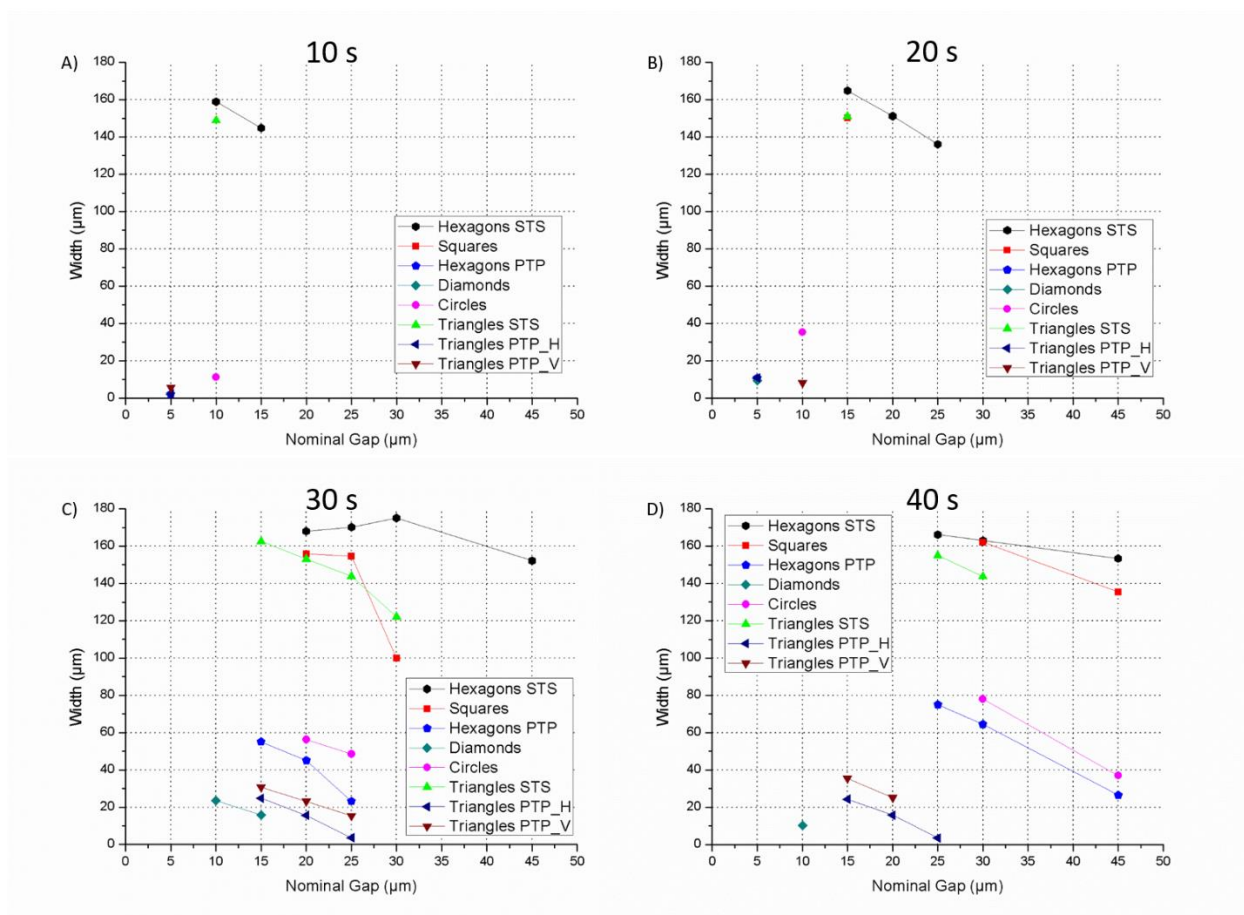


Figure 5.12A-D: Width against nominal gap for different types of gap and exposure times. The results are shown for nominal size 160 $\mu\text{m}$  exposed in soft contact.

Plots of the gap reduction are given in Figure 5.13A-D. The data does not suggest any particular trend associated to the type of gap.



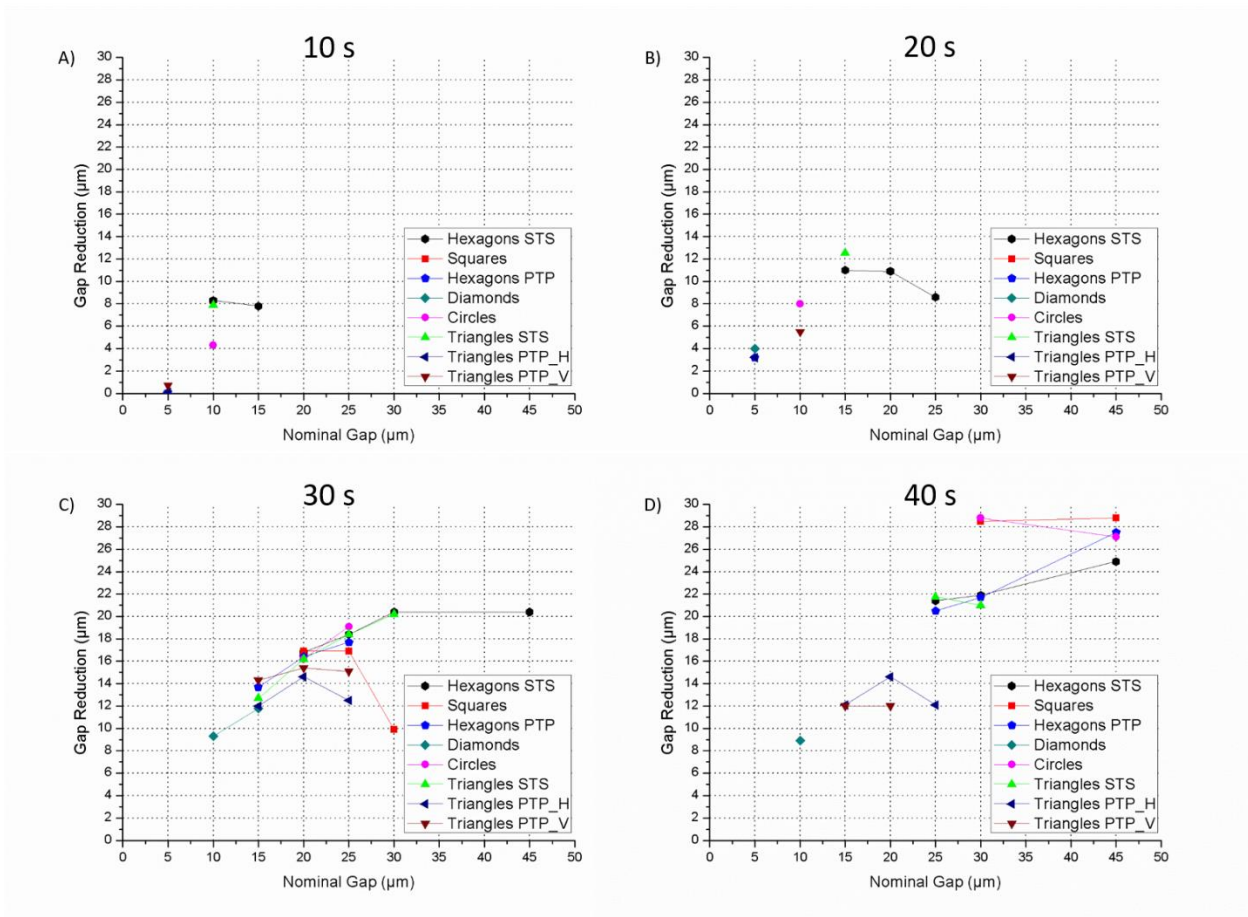


Figure 5.13.A-D: Gap reduction against nominal gap for different types of gap and exposure times. The results are shown for nominal size 160μm exposed in soft contact.

## 5.6 Nominal Gap

Nominal gaps of 45, 30, 25, 20, 15, 10 and 5μm were explored. There are no graphs dedicated to this parameter, because it was included in the graphs of all the previously mentioned parameters. In fact, for every parameter under analysis, the variables were plotted in function of that parameter and the nominal gap. The nominal gap is the most influent parameter on the formation of bridges, along with the exposure



time. When all the other parameters are fixed, all the types of feature can be obtained varying the nominal gap appropriately. In particular, going from high gaps to smaller ones, the features follow always a specific order: no bridges, spikes, stable bridges, walls and merged structures. The fact that not all of them appear in every set is not in contrast with the previous statement. As a matter of fact, all the mentioned features would appear if the nominal gap was a continuous variable and not limited to 7 discrete values, which may cause some of the features to be skipped. .

## **5.7 SU-8 thickness**

The influence of the SU-8 thickness has not sufficiently been analyzed yet to be included in the results of this work. Preliminary results were obtained from the comparison of two wafers with SU-8 posts, 50 $\mu\text{m}$  and 300 $\mu\text{m}$  high, exposed in soft contact. The qualitative analysis for these two wafers does not show a significant influence of the SU-8 thickness in the formation of suspended bridges, although the 300 $\mu\text{m}$  tall posts have a much higher aspect ratio than the 50 $\mu\text{m}$  ones, making them more sensitive to stiction. This trend can be verified observing Table 5.5, where all the parameters were fixed, except the SU-8 thickness. It is noticeable that the 300 $\mu\text{m}$  thick wafer features a much higher number of irregular subsets, even at higher nominal gaps, than the 50 $\mu\text{m}$  thick.



Table 5.5: Qualitative analysis for triangles PTB, exposed in soft contact for 20s in the case of 50 $\mu$ m (top chart), and 300 $\mu$ m (bottom chart) SU-8 thickness.

|    |    |    |    |    |    |
|----|----|----|----|----|----|
| NB | NB | NB | NB | NB | IM |
| NB | NB | NB | NB | NB | IM |
| NB | NB | NB | NB | NB | IM |
| NB | NB | NB | NB | NB | IM |
| NB | NB | NB | NB | NB | IM |
| SB | SB | SB | SB | NB | IM |
| M  | M  | M  | M  | M  | M  |

|    |    |    |    |    |    |
|----|----|----|----|----|----|
| NB | NB | IM | IM | IM | IM |
| NB | NB | IM | IM | IM | IM |
| NB | NB | IM | IM | IM | IM |
| NB | NB | IM | IM | IM | IM |
| NB | S  | IM | IM | IM | IM |
| SB | SB | M  | M  | IM | IM |
| M  | M  | M  | M  | M  | IM |

## 5.8 Carbonization

The SU-8 structures shrink significantly during the carbonization process. The characteristic dimensions for the different geometries were reported to shrink up to the 50% of their original value, as shown in Figure 5.14A-B.



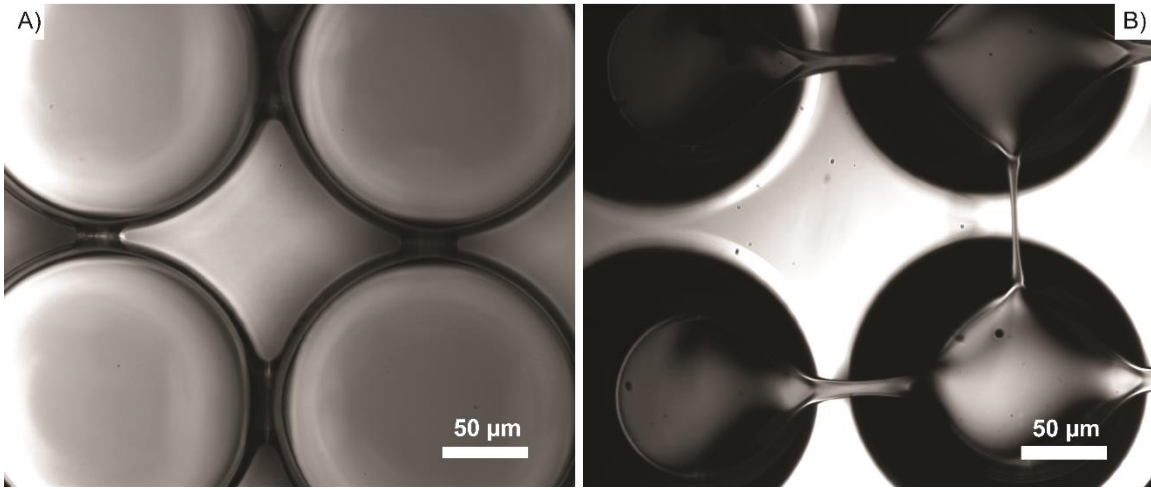


Figure 5.14A-B: Circular shapes obtained for nominal size  $160\mu\text{m}$ , nominal gap  $30\mu\text{m}$  and exposure time 30s in soft contact. A) SU-8; B) carbonized.

Figure 5.14A-B displays the same 4 posts before and after carbonization. During the treatment, the posts underwent a contraction of about 49.5% of their average diameter, ranging from  $186\mu\text{m}$  for the SU-8 to  $94\mu\text{m}$  for the carbon. The posts retreated due to the shrinkage, making the fabricated gap increase at equally to the diameter reduction, forcing the suspended structure to stretch. The average values of the bridges length increased from  $6.1\mu\text{m}$  to  $93.1\mu\text{m}$ , while the width got reduced from  $39.4$  to  $8.5\mu\text{m}$ . It is important to notice that suspended structures may break due to the tensional stress caused by the stretching, as happened to the vertical bridge on the left in Figure 5.14B.

As a direct consequence of the shrinkage, long and thin structures in the SU-8 have high chances to break under the effect of the stretching-induced stress, causing a reduction in the maximum nominal gap that allows subsets with suspended structures. Under the same principle, some subsets that were characterized as walled or merged, may



become actual suspended structures as the SU-8 posts retreat. The two effects of the shrinkage can be summarized with a shift of the subsets with suspended structures towards lower gaps. This trend is shown qualitatively in Table 5.6, as the maximum and minimum nominal gaps feature stable bridges, in the case of SU-8 and carbon, for different nominal sizes. The type of gap is fixed to hexagons STS, and the exposure time to 30s in soft contact.

TABLE 5.6: Value of maximum and minimum gaps with stable bridges in function of the nominal size, for hexagons STS, exposed for 30s in soft contact.

| Feature                           | Material | Nominal Size     |                  |                  |                  |                  |                   |
|-----------------------------------|----------|------------------|------------------|------------------|------------------|------------------|-------------------|
|                                   |          | 10 $\mu\text{m}$ | 20 $\mu\text{m}$ | 30 $\mu\text{m}$ | 40 $\mu\text{m}$ | 80 $\mu\text{m}$ | 160 $\mu\text{m}$ |
| Max gap with SB ( $\mu\text{m}$ ) | SU-8     | 20               | 25               | 25               | 30               | 25               | 45                |
|                                   | Carbon   | 20               | 25               | 25               | 25               | 15               | 45                |
| Min gap with SB ( $\mu\text{m}$ ) | SU-8     | 20               | 20               | 20               | 20               | 20               | 20                |
|                                   | Carbon   | 20               | 15               | 15               | 25               | 15               | 25                |

The quantitative entity of the shift can be observed in Figure 5.15A-D for the fabricated gap, and in Figure 5.16A-D for the width.



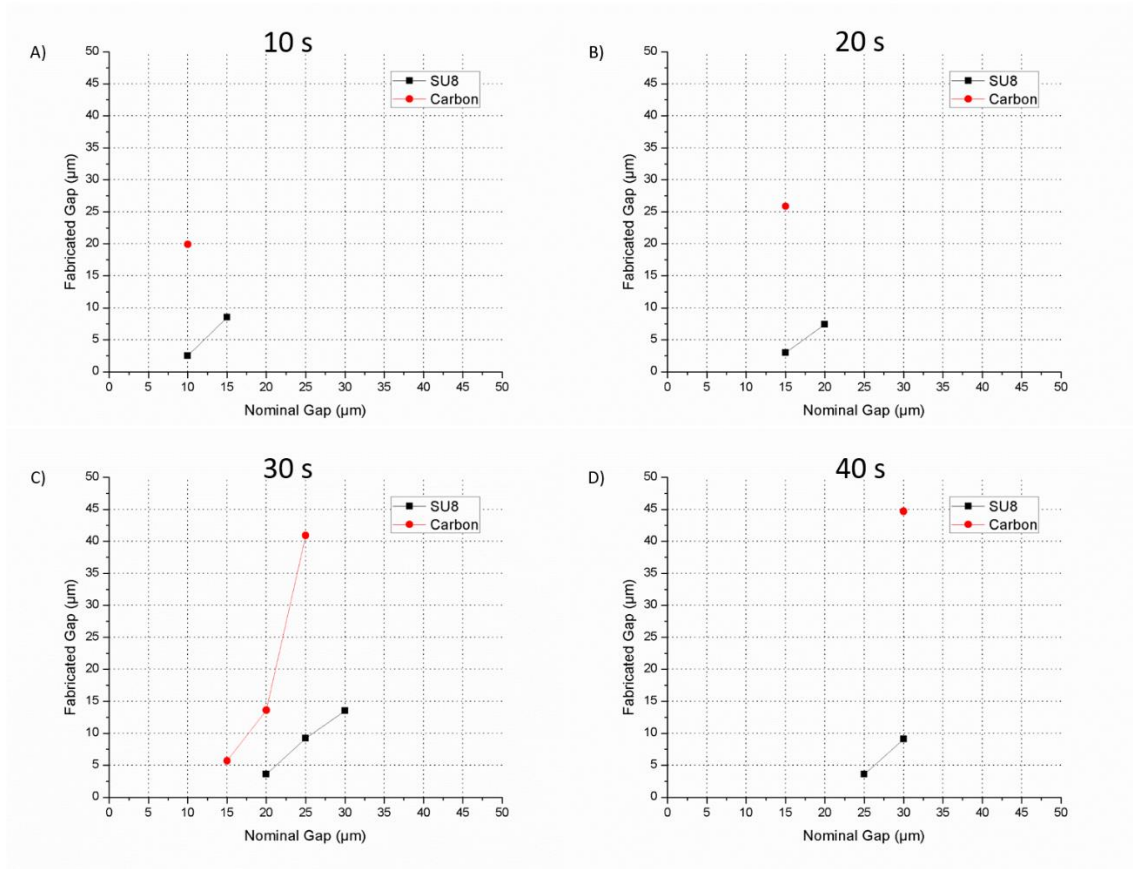


Figure 5.15A-D: Fabrication gap in function of the nominal gap in the case of SU-8 and carbon structures, for different times of exposures. The results shown are for hexagons STS with nominal size 40μm

Although there are not enough subsets with carbon suspended structures to define all the curves, the shift of the carbon curves towards top-left in the fabrication gap graphs is shown in Figure 5.13C, and also confirmed in 5.13A, B and D



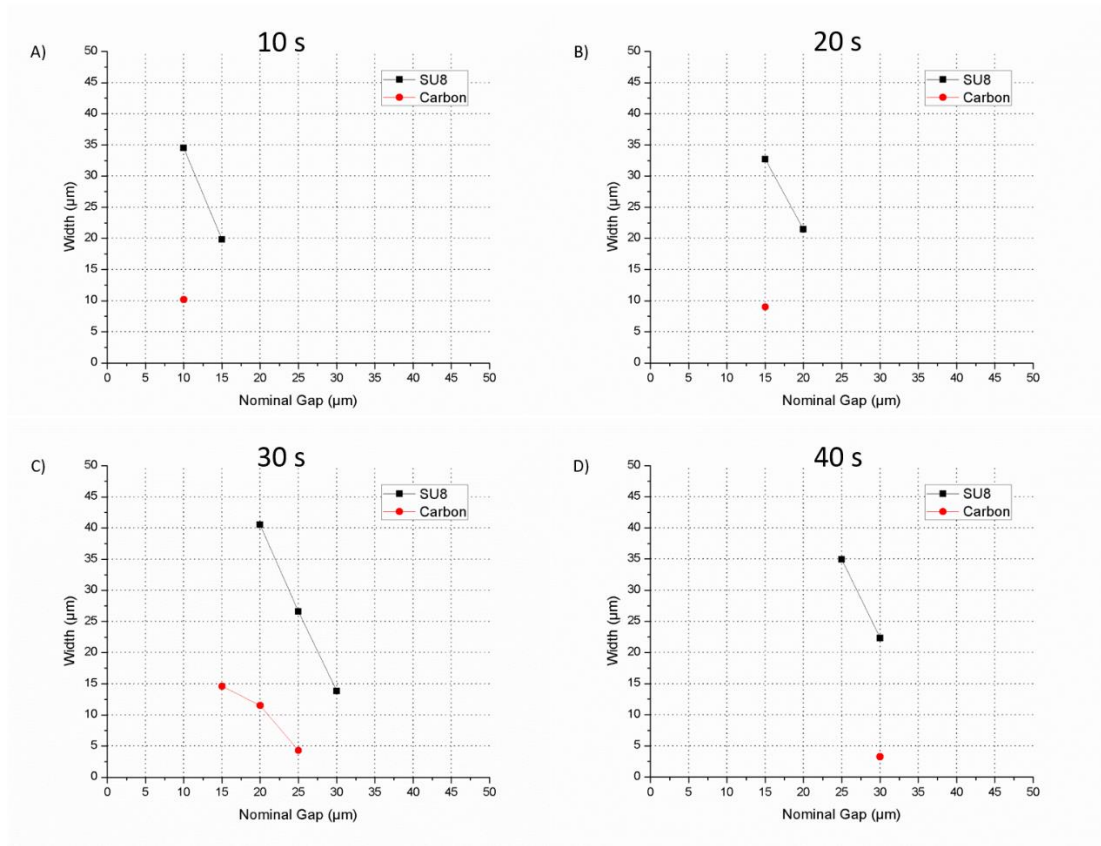


Figure 5.16A-D: Width in function of the nominal gap in the case of SU-8 and carbon structures, for different times of exposures. The results shown are for hexagons STS with nominal size  $40\mu\text{m}$

Similarly, the shift of the curves towards bottom-left in the width graphs is shown in Figure 5.16C, and confirmed by the other graphs.

All the trends associated to the photolithography parameters are still valid for the carbon. In fact, the carbonization process cannot generate connections in between posts that were not previously connected in the SU-8. As a consequence, the parameters that facilitate the formation of SU-8 suspended structures, will also facilitate the formation of



carbon suspended structures. To verify this assertion, a brief analysis of the data collected on the carbon suspended structures will follow. For this analysis, the different combinations of parameters respect to the SU-8 case will be showed. After carbonization, there are less subsets featuring stable bridges, thus, it is tougher to find combination of parameters that produce enough subsets of interest. The type of contact is examined in Figure 5.17A-D.

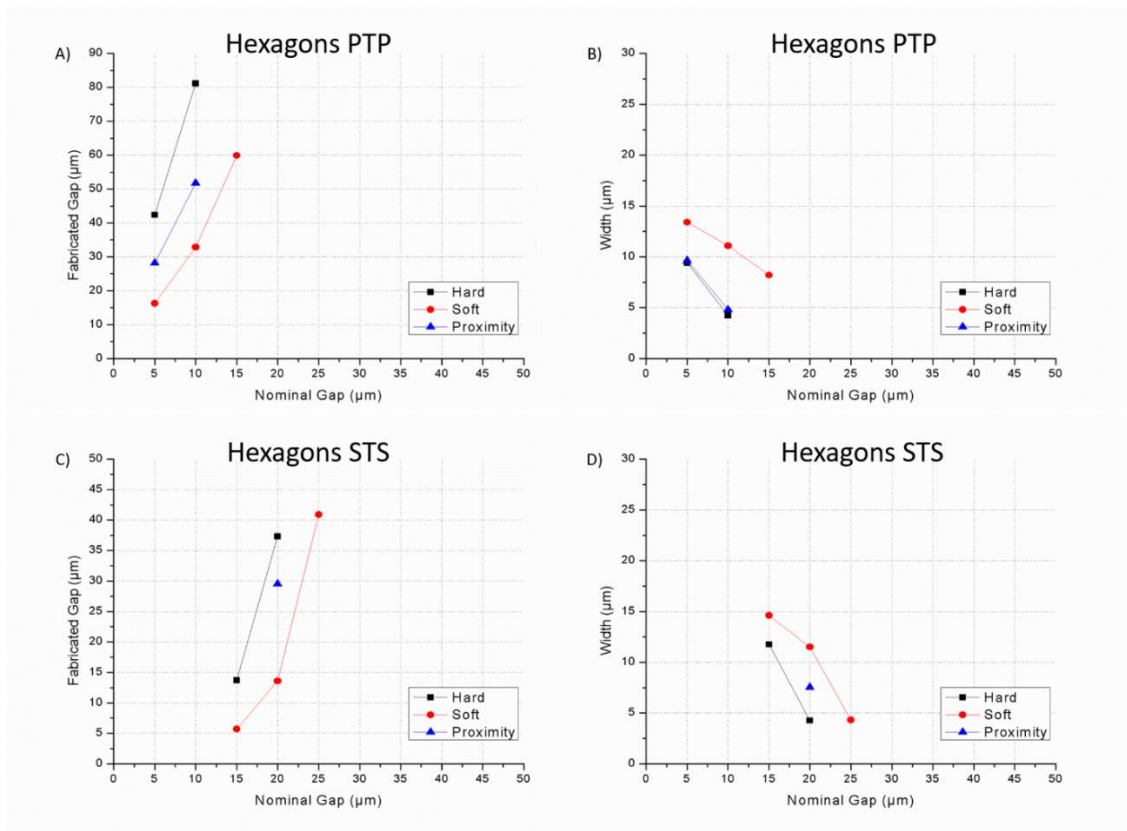


Figure 5.17: A, C) Fabrication gap and B, D) width, in function of the nominal gap, for nominal size  $80\mu\text{m}$ , and exposure time 30s, with different types of contact. Post carbonization.



The curves in Figure 5.17A-D confirm the trend observed for the type of contact, in the case of SU-8 structures. Passing from hard contact to proximity and to soft contact, suspended structures appear at bigger nominal gaps. Also, for fixed nominal gap, the fabricated gap decrease and the width increase. The influence of the exposure is investigated in the graphs of Figure 5.18A-D.

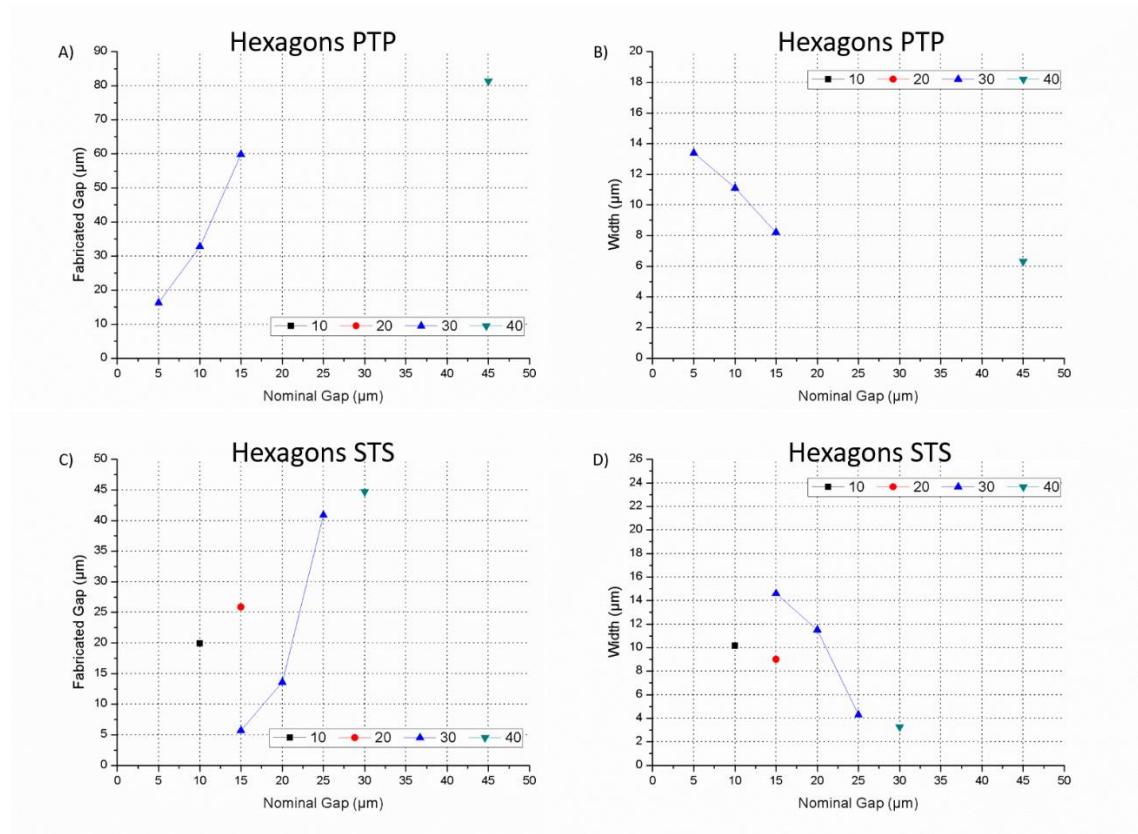


Figure 5.18: A, C) Fabrication gap and B, D) width, in function of the nominal gap, and time of exposure, for nominal size 80μm, exposed in soft contact. Post carbonization.

Even if only the 30s exposure time generates an actual curve, the points obtained with the other exposures follow the trend described for the exposure time in the SU-8



section. In fact, proceeding from small nominal gaps to bigger ones (from left to right in the graphs), the first point found corresponds to the 10s exposure time, and the 20, 30, and 40s exposure points follow. Also, looking at the subsets with nominal gap 15 $\mu$ m, the 30s exposure produces shorter fabricated gap and wider suspended structures.

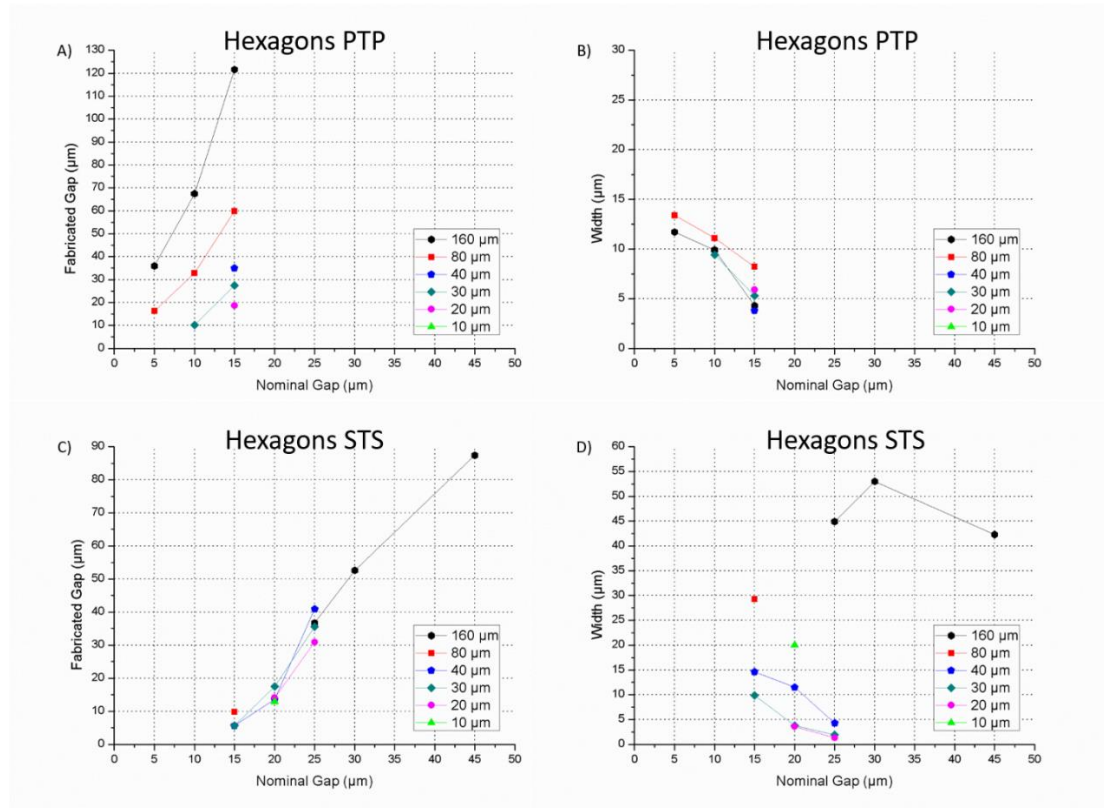


Figure 5.19: A, C) Fabrication gap and B, D) width, in function of the nominal gap and nominal size, for exposure time 30s in soft contact. Post carbonization.

In Figure 5.19A-D, the different nominal sizes, with exposure time 30s in soft contact, for hexagons STS and PTP are compared. As observed for the SU-8, Figure 5.17A shows that every nominal size generates suspended structures only for 5, 10 and



15 $\mu$ m, confirming that varying the nominal size does not affect significantly the presence of subsets with suspended structures. In Figure 5.17A, it is also shown that the fabrication gap increases with the nominal size, which is particularly interesting, since, in the SU-8, it was slightly decreasing with an increment of the nominal size. This is due to the fact that the shrinkage during carbonization prevails the increase of cross section due to the T-topping during the exposure time. This fact can be best explained by the scheme in Figure 5.20 (the numbers in this example are rounded for simplicity, but they are still very close to the real ones).

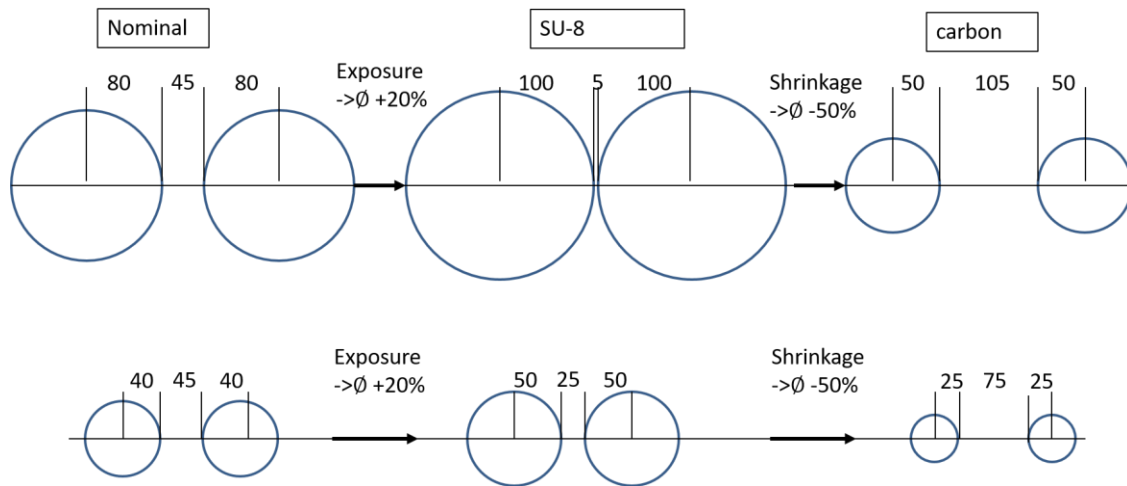


Figure 5.20: Different increase of fabrication gap in function of nominal size.

Lastly, the types of gap are compared in Figure 5.21A-B.



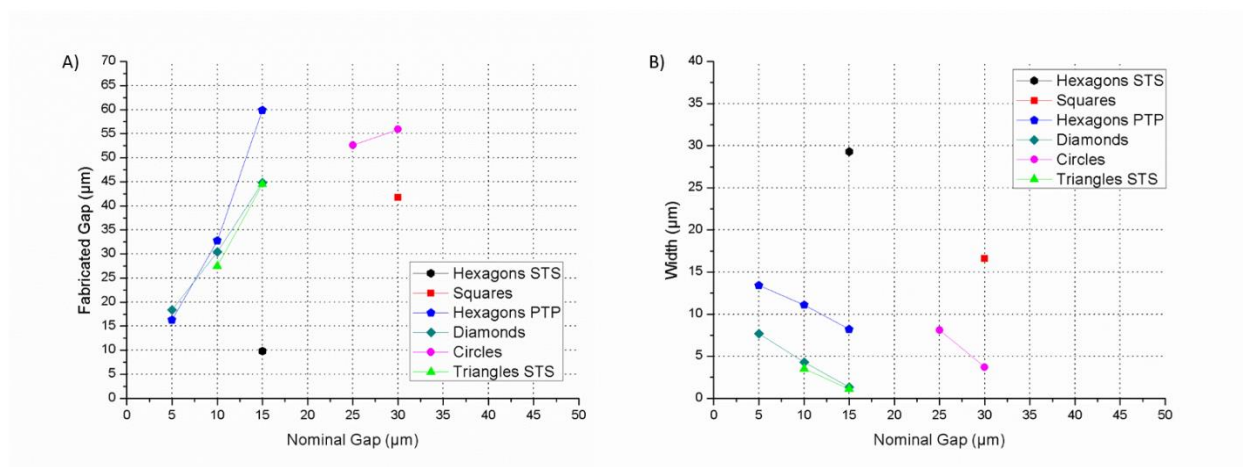


Figure 5.21: A) Fabrication gap and B) width, in function of the nominal gap, for different types of gap. The results are shown for nominal size of 80μm, exposed for 30s in soft contact.

There is not an appreciable trend for the fabrication gap curves in Figure 5.21A. In Figure 5.21B, it is shown that as in the case of the SU-8, the width of the suspended structures increases with the amount of material facing the adjacent post. The STS shapes have the widest structures, followed by circles, and then PTP shapes, starting with hexagons PTP and getting to the triangular shapes. Based on the analysis, the PTP shapes appear to be the only types of gap that allow to obtain suspended carbon wires. In order to obtain structures thinner than 1μm, the posts have to face each other with the least material possible, and the exposure time can only be 10 or 20s. In particular, the thinnest wires were obtained by triangular shapes facing by the points adjacent to their base, and for a time of exposure of 10s.



Another interesting fact is that the shapes STS suffer a drastic reduction of the number of subsets with suspended structures. That is mostly due to the fact that the carbonization process induces thermal stress in the SU-8, which can create cracks in the material. An example of two consecutive arrays of squared posts cracked during carbonization is given in Figure 5.22.

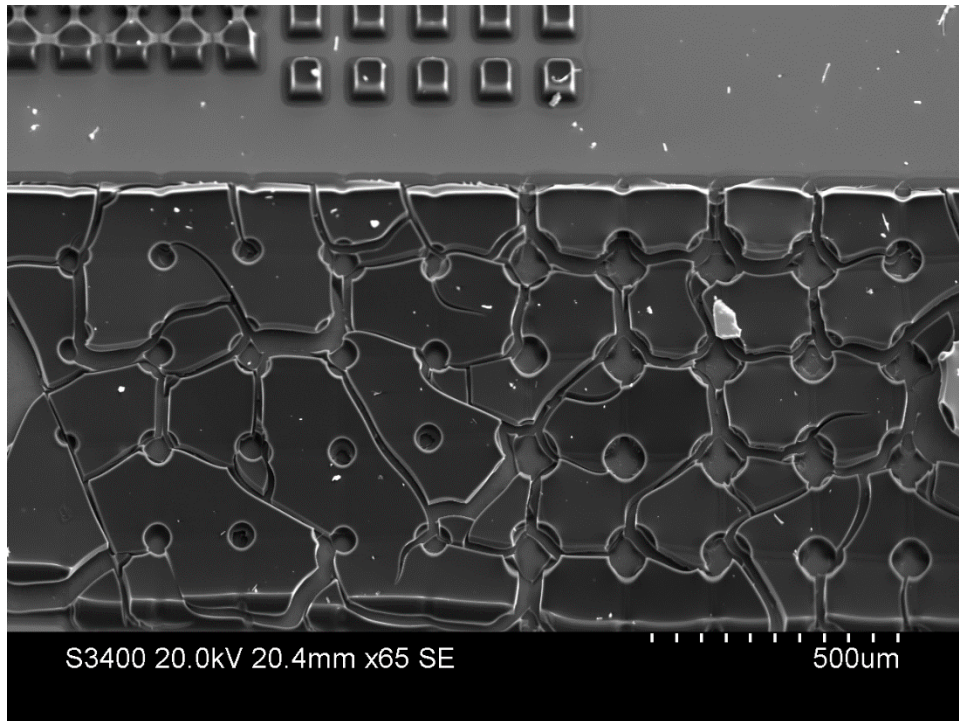


Figure 5.22 – Effect of the thermal stress induced by carbonization on 2 arrays of squared posts.

The cracks are not necessarily preventing the formation of suspended structure, but they make the subset unusable. Therefore, the cracked subsets were excluded from the graphs. Since the entity of the induced stress is proportional to the shapes quantity of material, the STS shapes suffer from the carbonization process more than from the PTP.



Also, as shown for the nominal size, bigger shapes retreat more while shrinking, inducing a higher tensional stress on the SU-8 structures, and consequently increasing the probability of breaking them.

## 5.9 Discussion

It has been shown that choosing wisely the photolithography parameters, a variety of SU-8 structures such as: self-standing posts (Figure 5.23A), suspended bridges (Figure 5.23B), and wires (Figure 5.23C) can be obtained.

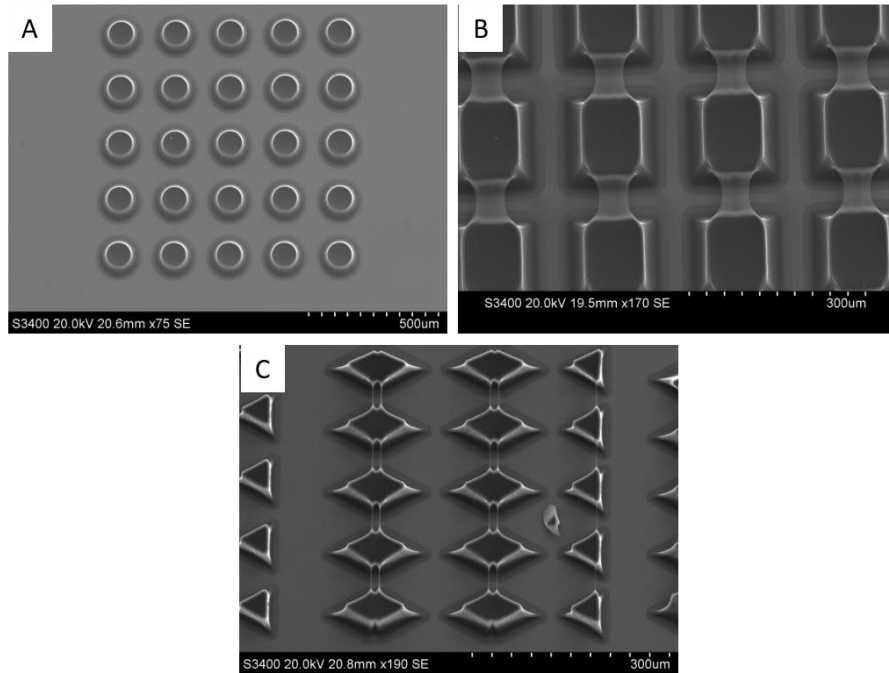


Figure 5.23: Examples of SU-8 structures obtained. A) Circular self-standing posts; B) Squared posts featuring suspended bridges; C) Triangular posts featuring suspended wires.



Suspended bridges and wires were fabricated using a large amount of different combinations of parameters. Judging from the structures repeatability, continuity and width, the optimum parameters to fabricated bridges and wires were found, and are given in Table 5.7

Table 5.7: Optimum fabrication parameters for obtaining repeatable, reliable and continuous bridges and wires.

| <b>Suspended Structure</b> | <b>Type of Contact</b> | <b>Exposure time (s)</b> | <b>Type of gap</b> | <b>Size (μm)</b> | <b>Gap (μm)</b> | <b>Average width of structure (μm)</b> | <b>Average length of structure (μm)</b> |
|----------------------------|------------------------|--------------------------|--------------------|------------------|-----------------|--|---|
| Wires                      | Soft                   | 10                       | Triangles<br>60°H  | 80               | 5               | 0.81±0.18                              | 39.71±4.39.                             |
| Bridges                    | Soft                   | 30                       | Hexagon<br>STS     | 160              | 45              | 53.55±6.73                             | 74.42±1.77                              |

Figure 5.24A-B displays images from the optical microscope, for the subsets featuring bridges and wires fabricated with the optimum parameters.



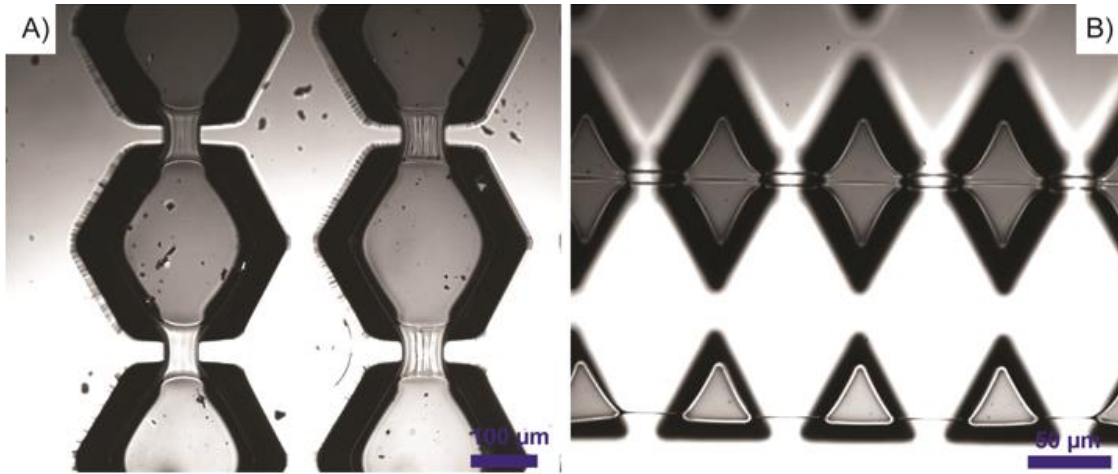


Figure 5.24: A) Hexagonal subset featuring optimal bridges and B) Triangular subset featuring optimal wires.

Wires as thin as  $0.47\mu\text{m}$  were obtained but they were not repeatable within the subset. Also, analyzing triangular arrays with the SEM, even thinner wires of width  $< 0.1\mu\text{m}$  were found coming out from the sidewalls of the structures. These features were too small to be observed at the optical microscope and were found not repeatable. However, their extremely low width makes them interesting for further research.

Characterizing the fabricated structures was not the only goal of this work. The second objective is the determination of a mathematical model able to predict the process results, given a particular combination of parameters. It has been observed that structures with same length or width can be obtained with different combination of the parameters. For example, bridges of a specific length could be fabricated at a determined nominal gap, with a certain combination of the other parameters, but also, at a higher nominal gap, increasing the exposure time accordingly. However, none case where both the same



length and width were obtained from two different subsets was recorded. At the same time, all the posts within the same subset behave similarly. These are very good premises because they suggest that it is possible to associate the choice of the parameters with a unique and repeatable outcome.

Predicting the characteristics of the structures is not a straightforward operation, since all the photolithography parameters are correlated, and their dependency on each other is not clear. Previously in this chapter, each parameter was examined individually, analyzing the data related to that parameter, while all the other parameters were fixed. Even in such a system, with a singular degree of freedom, the influence of a parameter on the formation of bridges cannot be defined accurately, because it still depends on the particular choice of all the other parameters.

Strictly focusing on the formation or not of suspended structures, without addressing their width, it was found that the two most important parameters are the distance in-between the posts and the time of exposure. Decreasing the distance in-between the posts increases the probability of forming suspended structures, and the same effect is caused by increasing the time of exposure. Therefore, with an extremely simplified model, the system could be described as follows: choosing a gap as large as desired, there would always be a large enough value of the exposure time to generate a bridge; vice-versa, choosing an exposure as small as desired, there would always be a small enough value of gap to generate a bridge. Obviously, upper and lower boundaries limit the choice of the two parameters, to guarantee the feasibility of the process.

This model could be mathematically described with a simple linear relationship.



$$K_b \stackrel{\text{def}}{=} \frac{e}{g_f} \quad (1)$$

$$\text{if } K_b \geq \overline{K_b} \xrightarrow{\text{yields}} \text{bridge} \quad (2)$$

Where  $e$  is the exposure time,  $g_f$  is the fabricated gap (distance in-between the posts), and  $\overline{K_b}$  is a constant that has to be determined experimentally. In order for this model to work, the presence of a bridge or not has to be predicted based only on the time of exposure and the fabricated gap measured, for every combination of the other parameters. For every type of contact, exposure time, and nominal size, the constant  $K_b$  of the subsets featuring no bridges with the lowest nominal gap ( $K_{b,NB}$ ), and the ones featuring bridges with the highest nominal gap ( $K_{b,SB}$ ), have been calculated. The average values of  $K_{b,NB}$  and  $K_{b,SB}$  are shown in Table 5.8, where the results have been grouped by type of gap, since usually the type of gap influences the formation of bridges.



Table 5.8: Average values of  $K_{b,NB}$  and  $K_{b,SB}$ , and acceptable interval for  $\overline{K_b}$ . All values are grouped by type of gap.

| Type of Gap       | $K_{b,NB} [s/\mu m]$ | $K_{b,SB} [s/\mu m]$ | $\overline{K_b} [s/\mu m]$                                    |
|-------------------|----------------------|----------------------|---|
| Hexagons STS      | 1.37±0.31            | 4.48±1.41            | $1.65 \leq \overline{K_b} \leq 3.07$                          |
| Hexagons PTP      | 1.92±0.57            | 5.71±1.39            | $2.49 \leq \overline{K_b} \leq 4.32$                          |
| Squares           | 1.45±0.41            | 6.76±3.47            | $1.86 \leq \overline{K_b} \leq 3.29$                          |
| Circles           | 1.7±0.34             | 6.53±1.88            | $2.04 \leq \overline{K_b} \leq 4.64$                          |
| Diamonds          | 3.11±1.08            | 13.58±5.3            | $4.19 \leq \overline{K_b} \leq 8.28$                          |
| Triangles PTB_PTS | 1.94±0.53            | 5.56±2.03            | $2.47 \leq \overline{K_b} \leq 3.53$                          |
| Triangles PTB_PTP | 2.17±0.79            | 7.39±5.14            | $\overline{K_b} \geq 2.96$ , and $\overline{K_b} \leq 2.26^*$ |
| Triangles BTB_STS | 1.54±0.38            | 11.01±5.82           | $1.92 \leq \overline{K_b} \leq 5.2$                           |
| Triangles BTB_PTP | 2.95±0               | 7±0.93               | $2.95 \leq \overline{K_b} \leq 6.1$                           |

\*Note: the fact that there are not possible values for  $\overline{K_b}$ , means that the model fails to describe this shape.

For most gap types, the lowest value of the confidence interval of  $K_{b,SB}$  is still higher than the highest value of the confidence interval of  $K_{b,NB}$ . These two values are used to define a safety interval, within which the constant  $\overline{K_b}$  can be chosen to ensure that most subsets with stable bridges will have a  $K_b \geq \overline{K_b}$ , and most subsets with no bridges will have  $K_b < \overline{K_b}$ . The  $\overline{K_b}$  safety intervals, calculated for every shape, are shown in Table 5.8 outermost right column. Analyzing these intervals, the constant  $\overline{K_b}$  was set to  $2.5s/\mu m$ , which respects the constraints for all the types of gap but diamonds and triangles PTP.



In this model,  $g_f$  refers to the actual fabricated gap, which is equal with the length of the bridge  $L$  (when there is one) and is depending from the process parameters.

$$L = f(g_n, \Delta D_n) \quad (3)$$

Where  $g_n$  is the nominal gap, and  $\Delta D_n$  is the variation of the characteristic dimension, respect to its nominal value  $D_n$ . The characteristic dimension is the side in the case of polygonal shapes, and the diameter in case of the circle. The length formula can be expressed in function of a shape factor  $c_S$ , depending on the geometry of the shape.

$$L = g_n - c_S \Delta D_n \quad (4)$$

In the sample case of the squares,  $L = g_n - \Delta D_n$  and  $c_S = 1$ . The illustration of the square shapes geometry, explaining the result for  $c_S$ , is given in Figure 5.25.



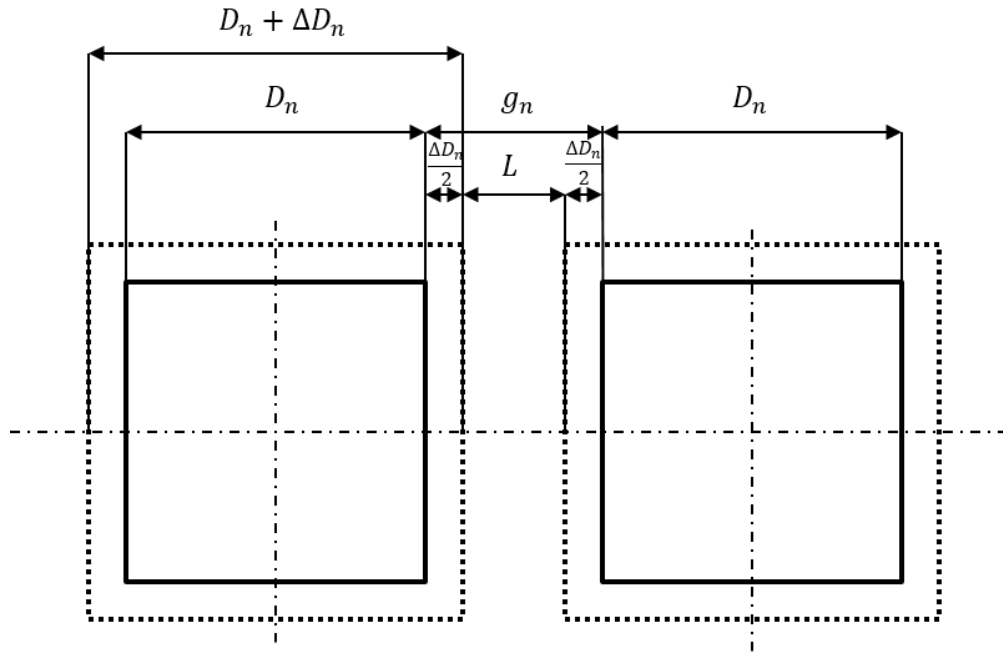


Figure 5.25: Shape factor  $c_s$  for squares.

The illustrations of the geometry of all the other types of gap can be found in Appendix A. The summary of the values found for each shape factors  $c_s$  are given in Table 5.9.



Table 5.9: Shape factor  $c_s$  grouped by type of gap.

| Type of Gap       | $c_s$        | $L = g_n - c_s \Delta D_n$                |
|-------------------|--------------|---|
| Hexagons STS      | $\sqrt{3}$   | $L = g_n - \sqrt{3} \Delta D_n$           |
| Hexagons PTP      | 2            | $L = g_n - 2 \Delta D_n$                  |
| Squares           | 1            | $L = g_n - \Delta D_n$                    |
| Circles           | 1            | $L = g_n - \Delta D_n$                    |
| Diamonds          | $\sqrt{2}$   | $L = g_n - \sqrt{2} \Delta D_n$           |
| Triangles PTB_PTS | $\sqrt{3}/2$ | $L = g_n - \frac{\sqrt{3}}{2} \Delta D_n$ |
| Triangles PTB_PTP | 1            | $L = g_n - \Delta D_n$                    |
| Triangles BTB_STS | $1/\sqrt{3}$ | $L = g_n - \frac{1}{\sqrt{3}} \Delta D_n$ |
| Triangles BTB_PTP | $2/\sqrt{3}$ | $L = g_n - \frac{2}{\sqrt{3}} \Delta D_n$ |

The increase of the characteristic dimension is the consequence of the T-topping, and thus is a function of all the process parameters

$$\Delta D_n = f(e, S, D_n, d) \quad (5)$$

Where  $e$  = exposure time,  $S$  = shape,  $D_n$  = nominal size,  $d$  = contact distance

Hypothesizing that the partial increment of the characteristic dimension due to a single parameter is a function of only that parameter, and that the total  $\Delta D_n$  is given by the product of all the partial increments,  $\Delta D_n$  can be modeled as follows:



$$\Delta D_n = K(\Delta D_{n,e} \cdot \Delta D_{n,S} \cdot \Delta D_{n,Dn} \cdot \Delta D_{n,d}) \quad (6)$$

Where  $K$  is an experimental constant and

$$\Delta D_{n,e} = f(e), \quad \Delta D_{n,S} = f(S) \quad (7)$$

$$\Delta D_{n,Dn} = f(D_n), \quad \Delta D_{n,d} = f(d) \quad (8)$$

In order to determine the relationship between the exposure  $e$  and the corresponding  $\Delta D_{n,e}$ , a group of subsets differing only by the exposure time was analyzed. Since the other parameters were fixed, their contribution to the size increment was considered constant, and included in the  $K$  of equation (6). Thus,  $\Delta D_n$  can be expressed as:

$$\Delta D_n = J\Delta D_{n,e} = Jf(e) \quad (9)$$

Where  $J$  is a convenience constant that contains the previous  $K$  and the constant factors due to  $D_n$ ,  $d$  and  $S$ . Plotting the values of  $\Delta D_n$  taken from the actual measurements against the values of  $e$ , it was possible to approximate the real curves with linear relationships of the type:

$$\Delta D_{n,e} = m_e e + q_e \quad (10)$$



Where  $m_e$  and  $q_e$  are coefficient to be determined case by case. It was found that the same equation can describe subsets with different nominal sizes and types of contact, but not different shapes. Therefore, a different equation was derived to approximate every shape, as shown in Figure 5.26

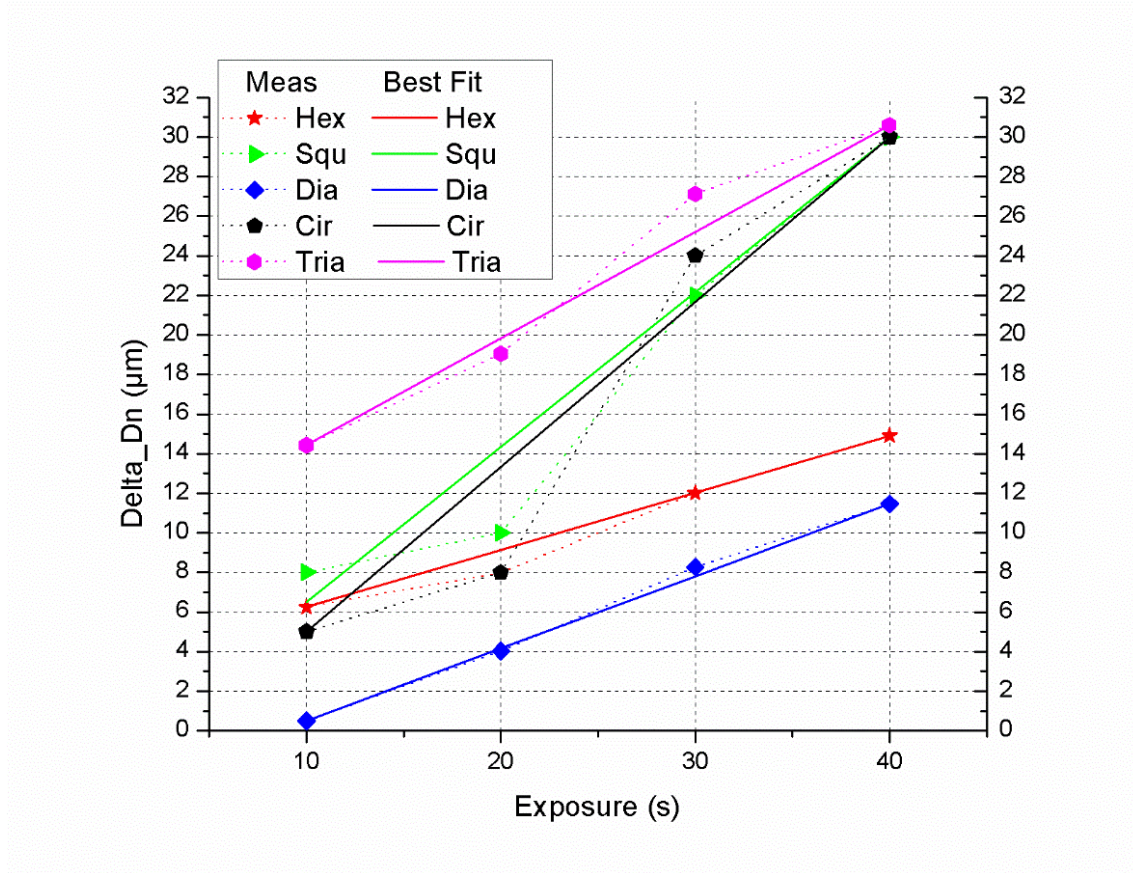


Figure 5.26: Linear approximation of the influence of the time exposure on the cross-section increment, for every shape.

The values of the coefficients  $m_e$  and  $q_e$  for each shape, and the corresponding equations for  $\Delta D_{n,e}$ , are listed in Table 5.10.



Table 5.10: Equations to calculate  $\Delta D_{n,e}$ , shape by shape.

| Shape     | $m_e$ | $q_e$ | $\Delta D_{n,e}$            |
|-----------|-------|-------|-----------------------------|
| Hexagons  | 0.29  | 3.36  | $\Delta D_n = 0.29e + 3.36$ |
| Squares   | 0.78  | -1.33 | $\Delta D_n = 0.78e - 1.33$ |
| Circles   | 0.83  | -3.33 | $\Delta D_n = 0.83e - 3.33$ |
| Diamonds  | 0.36  | -3.16 | $\Delta D_n = 0.36e - 3.16$ |
| Triangles | 0.54  | 9.04  | $\Delta D_n = 0.54e + 9.04$ |

Using a different equation for every shape, makes the presence of the factor  $\Delta D_{n,s}$  unnecessary. Thus, the increment due to the shape  $\Delta D_{n,dS}$  can be simplified, and equation (6) can be rewritten, for the sample case of hexagons, as:

$$\Delta D_{n,Hex} = K \cdot (0.3e + 3) \cdot \Delta D_{n,Dn} \cdot \Delta D_{n,d} \quad (11)$$

Where  $\Delta D_{n,Hex}$  is the total size increment in the case of hexagonal shapes. The procedure used to calculate the partial increment due to the exposure time, was repeated to determine equations for the nominal size, analyzing subsets with constant exposure of 30s in soft contact, but variable nominal size. As for the exposure case, the increment due to the nominal size was found directly proportional to the size.

$$\Delta D_{n,Dn} = m_{Dn} D_n + q_{Dn} \quad (12)$$



Where  $D_n$  is the nominal value of the characteristic dimension, and can be 10, 20, 30, 40, 80 or 160 $\mu\text{m}$ .  $m_{Dn}$  and  $q_{Dn}$  are coefficients depending on the shape in exam. The linear approximations are shown in Figure 5.27.

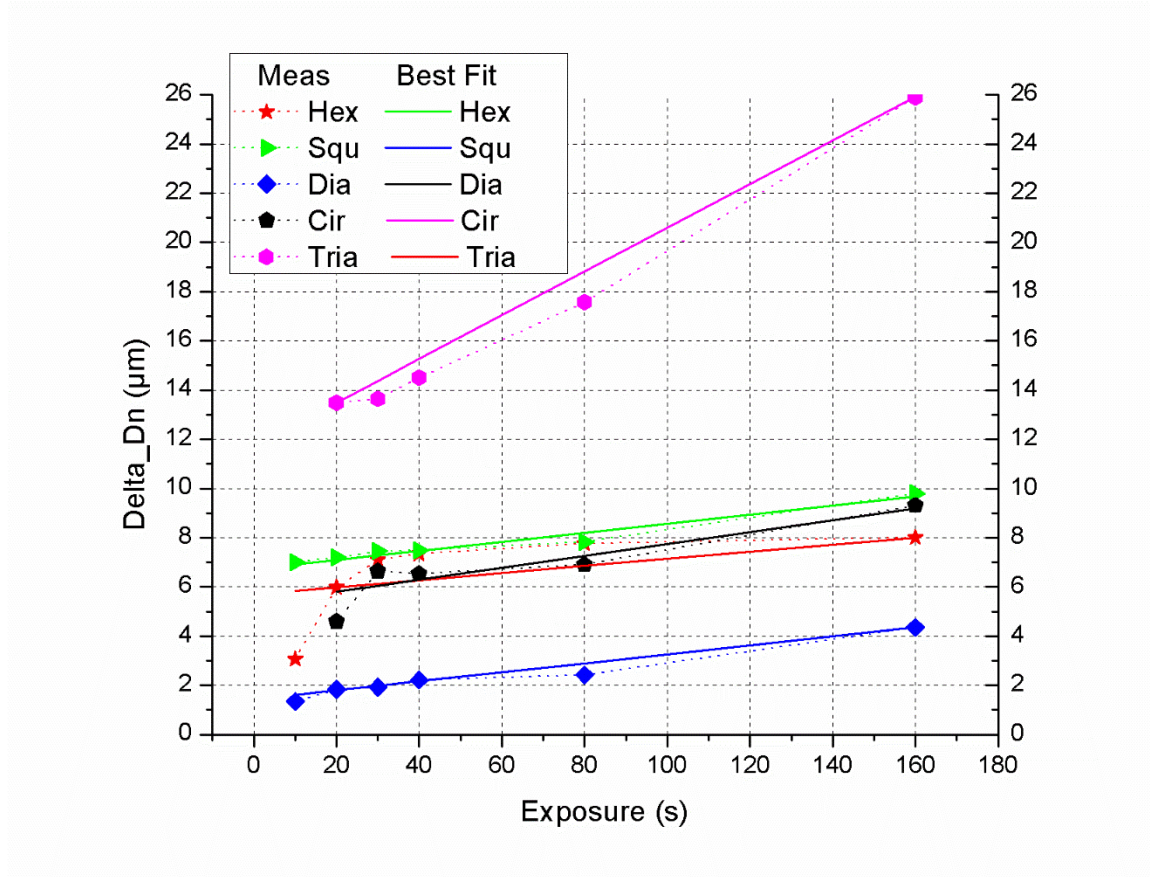


Figure 5.27: Linear approximation of the influence of the nominal size on the cross-section increment, for every shape.

The values of the coefficients  $m_{Dn}$  and  $q_{Dn}$  for each shape, and the corresponding equations for  $\Delta D_{n,Dn}$ , are listed in Table 5.11.



Table 5.11: Equations to calculate  $\Delta D_{n,Dn}$ , shape by shape.

| Shape     | $m_{Dn}$ | $q_{Dn}$ | $\Delta D_{n,Dn}$                |
|-----------|----------|----------|----------------------------------|
| Hexagons  | 0.014    | 5.691    | $\Delta D_n = 0.014D_n + 5.691$  |
| Squares   | 0.018    | 6.733    | $\Delta D_n = 0.018D_n + 6.733$  |
| Circles   | 0.024    | 5.314    | $\Delta D_n = 0.024D_n + 5.314$  |
| Diamonds  | 0.018    | 1.436    | $\Delta D_n = 0.018D_n + 1.436$  |
| Triangles | 0.089    | 11.712   | $\Delta D_n = 0.089D_n + 11.712$ |

A problem arose when trying to consider the type of contact, since it is not a numerical value. Considering that changing the type of contact changes the distance between the mask and SU-8, it was thought to use that distance as parameter. Unfortunately, its values are also unknown. In fact, the theory suggests  $20\mu\text{m}$  for proximity, and  $0\mu\text{m}$  for hard and soft contact. The “0” is clearly an unfeasible value, which cannot be reached in practice. Also, soft contact was proved to behave as if it had been actually further than the proximity, for the specific wafers examined. Therefore, arbitrary values of  $d = 10, 20$  and  $30\mu\text{m}$  were assigned to hard contact, proximity and soft contact, respectively. Once again, linear best fit curves were adopted:

$$\Delta D_{n,d} = m_d D_n + q_d \quad (13)$$

Differently from the previous coefficients,  $m_d$  and  $q_d$  had to be calculated for every type of gap, and are given in Table 5.12.



Table 5.12: Equations to calculate  $\Delta D_{n,d}$ , for each type of gap.

| Type of gap       | $m_d$     | $q_d$   | $\Delta D_{nd}$                       |
|-------------------|-----------|---------|---------------------------------------|
| Hexagons STS      | 0.0028    | 0.115   | $\Delta D_{nd} = 0.0028d + 0.115$     |
| Hexagons PTP      | 0.0025    | 0.093   | $\Delta D_{nd} = 0.0025d + 0.093$     |
| Squares           | 0.0004    | 0.033   | $\Delta D_{nd} = 0.0004d + 0.033$     |
| Circles           | 0.0042    | 0.079   | $\Delta D_{nd} = 0.0042d + 0.079$     |
| Diamonds          | 0.0049    | 0.173   | $\Delta D_{nd} = 0.0049d + 0.173$     |
| Triangles BTB_STS | 0.000545  | 0.0094  | $\Delta D_{nd} = 0.000545d + 0.0094$  |
| Triangles BTB_PTP | 0.0000233 | 0.0013  | $\Delta D_{nd} = 0.0000233d + 0.0013$ |
| Triangles PTB_PTS | 0.000576  | 0.00553 | $\Delta D_{nd} = 0.000576d + 0.00553$ |
| Triangles PTB_PTP | 0.000544  | 0.0036  | $\Delta D_{nd} = 0.000544d + 0.0036$  |

Plugging the equations (11), (12), and (13) into equation (6), and the latter into (4), the most general expression for the length of the bridges  $L$  is obtained:

$$L = g_n - c_s K (m_e e + q_e) (m_{Dn} D_n + q_{Dn}) (m_d d + q_d) \quad (14)$$

The value of  $K$  was extrapolated from the parameters and the measured fabricated gap. Also, in this case, a different value for each type of gap was found. The results are shown in Table 5.13.



Table 5.13: Values of  $K$ , for each type of gap.

| Type of gap       | $K$          |
|-------------------|--------------|
| Hexagons STS      | 0.938±0.35   |
| Hexagons PTP      | 0.846±0.259  |
| Squares           | 2.059±0.684  |
| Circles           | 1.373±0.367  |
| Diamonds          | 1.114±0.524  |
| Triangles BTB_STS | 3.109±1.153  |
| Triangles BTB_PTP | 13.213±6.584 |
| Triangles PTB_PTS | 2.997±1.676  |
| Triangles PTB_PTP | 3.049±1.829  |

The values given in Table 5.13 are already considering the shape factor  $c_s$ , which can be eliminated. The values from Tables 5.9-13 can be used to determine the specific equation (14) for each type of gap. For example, in the case of hexagons STS, (14) becomes

$$L = g_n - 0.938(0.28e + 3.36)(0.014D_n + 5.691)(0.0028d + 0.115) \quad (15)$$

Finally, this equation can be used to determine the value of the bridge length, since all the other variables are known process parameters. The model was tested on the



total amount of fabricated bridges, grouped by type of gap. The values of the absolute ( $E_a$ ) and relative ( $E_r$ ) errors of the bridges length respect to the data measured for the fabricated gap are given in Table 5.14

Table 5.14: Absolute and relative error of the length calculated respect to the measured value. The results have been grouped by type of gap.

| <b>Type of gap</b> | $E_a$ [ $\mu m$ ] | $E_r$ [#]        |
|--------------------|-------------------|------------------|
| Hexagons STS       | 2.9 $\pm$ 2.2     | 0.05 $\pm$ 0.87  |
| Hexagons PTP       | 2.29 $\pm$ 2.05   | -0.02 $\pm$ 0.77 |
| Squares            | 3.83 $\pm$ 2.49   | -0.04 $\pm$ 1.08 |
| Circles            | 2.9 $\pm$ 2.28    | 0.14 $\pm$ 1.46  |
| Diamonds           | 6.33 $\pm$ 4.86   | 2.71 $\pm$ 3.41  |
| Triangles BTB_STS  | 5.31 $\pm$ 3.37   | -0.07 $\pm$ 2.79 |
| Triangles BTB_PTP  | 3.57 $\pm$ 2.08   | -1.19 $\pm$ 0.67 |
| Triangles PTB_PTS  | 6.21 $\pm$ 3.81   | 0.41 $\pm$ 3.78  |
| Triangles PTB_PTP  | 4.25 $\pm$ 3.28   | 0.59 $\pm$ 1.86  |

It can be observed that, once again, the model gives good results for hexagons, squares and circles, but not for diamonds and triangles. The fact that the relative error is very small, but its standard deviation is high, suggests that this model is accurate but not precise, as confirmed by the absolute error. Nevertheless, it has to be taken into account



that the model was derived from experimental data, which are not absolutely precise as well. Analyzing the measurements themselves, was registered an average absolute error of  $1.38 \pm 1.37$ , which is quite normal for manual data collection on features that are so close to the microscope maximum resolution. Therefore, with such an error in the measurements, the fact that an error of the same scale was found in the predictions is very satisfactory, and the model can be considered successful for hexagons, squares and circles.

For diamonds and triangles, the variability of measurements and results is due to the fact that these types of gap produced many less subsets featuring suspended structures, respect to the others. In most cases, the number of subsets are not statistically significant to correctly determine the coefficients of equation (14). The reason of this difference in the outcome is that these shapes are mostly PTP types, which tend to form thin bridges and wires. These connections are more fragile and can snap more easily than the wider structures. Thus, the suspended wires are mostly present at the smallest nominal gaps and in very small number. To give an example as support to the previous statements, consider that the total number of subsets with different parameters combinations for triangles BTB\_PTP are 504. Among these, only 11 subsets produced suspended bridges/wires.

Although not very reliable, diamonds and triangles are the shapes that produced the best wires, and thus, more dedicated research is needed in the future, focusing on the combinations of parameters that successfully generated wires.



Once the length has been calculated, the model has to be extended to calculate the width  $W$  of the bridges. In the previous sections of this chapter, it was shown that the width is a function of all the photolithography parameters.

$$W = f(g_n, e, D_n, S, d) \quad (15)$$

The width  $W$  increases with the time of exposure  $e$ , and the type of gap  $d$ , since their increment is a cause of more cross-linking. Also, the profile of the shapes matters because more material at the interface between two posts facilitates the formation of bridges, and increases their width. The width is directly proportional to the nominal size as well, since eventually the posts tend to develop bridges as wide as the entire length of the side (which is the nominal size). It is intuitive that as the distance in-between the posts is reduced, the width increases, and vice-versa. However, it was observed that the nominal gap does not represent the real distance of the posts, and thus, it makes sense to substitute the nominal gap with the fabricated one, which is inversely proportional to the width.

$$W = K_W \frac{f_1(e, d, D_n, S)}{L} = K_W \frac{f_1(e, d, D_n, S)}{g_n - f_2(e, d, D_n, S)} \quad (16)$$

Where  $K_W$  is once again, an experimental constant, and  $f_1$  and  $f_2$  are two unknown functions.



In the case of the hexagons, for which we already determined the expression of  $L$ , equation (15) can be rewritten as

$$W = K_W \frac{f_1(e, d, D_n, S)}{g_n - 0.938(0.28e + 3.36)(0.014D_n + 5.691)(0.0028d + 0.115)} \quad (17)$$

The problem of determining  $K_W$  and the function  $f_1$  was approached in the same way as in the length that was determined previously.

Unfortunately, the data analysis did not lead to any representative result in determining any of the two. Plotting the measured width against the length did not show any repeating pattern. An example of a such width-length plot is given in Figure 5.28, which illustrates 20 different bridges in the hexagons, circles, squares, diamonds and triangles sets, for different exposure times and types of contact.



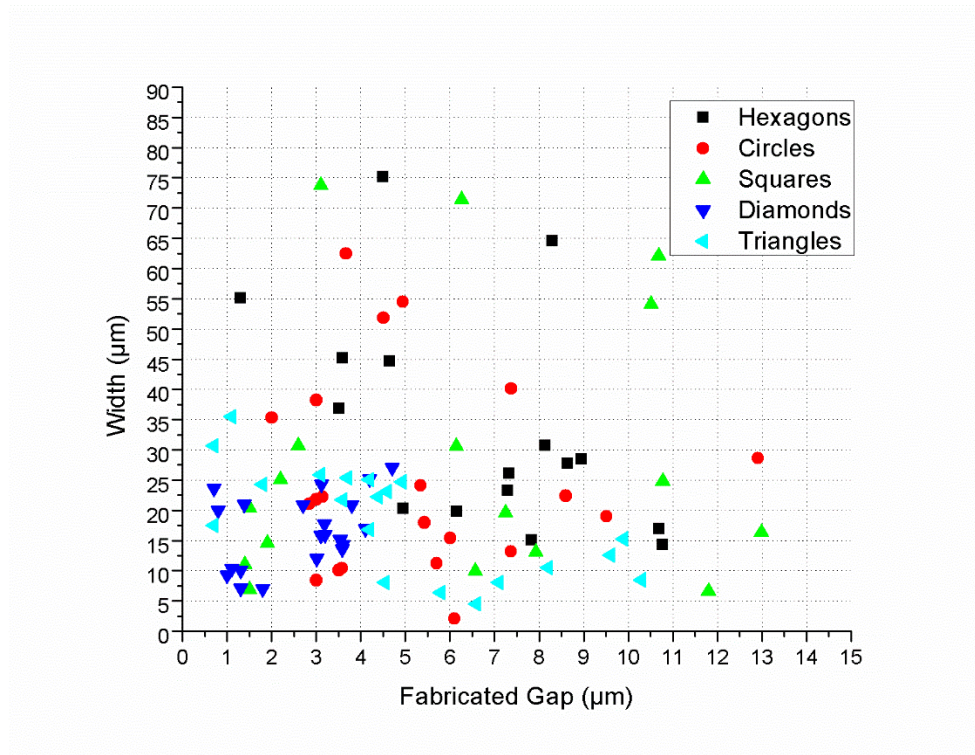


Figure 5.28: Width against length for 20 subsets of hexagons, circles, squares, diamonds and triangles.

Trying to isolate a single parameter did not work either, since, this time, considering the width and the length, there are, always, at least 2 parameters varying. In order to use the same methodology used for the length, it would have been necessary to have a series of bridges differing only by the variation of one of the parameters and the resulting width. In that case, the different results for the width, could have been linked directly to the variation of the parameters under analysis. Instead, when any of the parameters changes, the length changes as well, making the isolation of one parameter impossible.



## **CHAPTER SIX**

### **CONCLUSIONS AND FUTURE WORK**

In this work, the possibility of using pyrolysis of photolithographically patterned SU-8 photolithography to obtain carbon suspended structures in the micro and nano-scale, was investigated. The suspended structures obtained are intended to be used in the future as carbon electrodes contributing to the advance of the C-MEMS technology and of the micro and nano-biosensor industry.

More than 60000 different pairs of SU-8 posts were analyzed, in order to find common trends that could define the influence of the variation of photolithography parameters on the process outcome. It was found that the formation of suspended structures strongly depends on the type of contact, exposure time, type of gap and nominal gap. The formation of SU-8 connections in-between two posts, whether the structure is suspended or merged, is facilitated by an increase of the distance in-between photomask and SU-8, the exposure time, and the quantity of material facing from the side of two adjacent posts. The gap in-between the two posts is the only parameter contributing against the formation of bridges, thus, more bridges and merged structures form at short distances. Variations of the nominal size of the post anchors do not have a significant influence on the formation of suspended structures, but greatly affect the width of the structure, when there is one.

In order to obtain wide bridges, high exposures in soft contact or proximity are required. Theoretically, proximity contact is supposed to be the most effective for the



formation of bridges, but soft contact was proved to work better. This is the only hypothesis that was not confirmed by the data analysis, and is explained considering that the distance in soft contact could have been comparable, if not higher, to the proximity one, because of the topography of the SU-8 layer. Suspended bridges are obtained from a variety of circular and squared post anchors, but the type of gap that gives the best results in terms of suspended, reliable, continuous and uniform bridges, is the case of hexagons facing by their sides.

Suspended wires, as thin as  $0.81\mu\text{m}$ , can be reproducibly obtained with low exposures and point to point gaps. In particular, the thinnest bridges were obtained from triangular post anchors.

A model was developed in order to predict the formation of SU-8 bridges and their characteristic dimensions (length and width), according to the particular choice of photolithography parameters. The ultimate goal for the model is to be able to determine the values of the photolithography parameters needed to fabricate suspended structures of desired length and width.

It was proved that the model successfully predicts the presence of a bridge, given the fabrication gap and the time of exposure, for any combination of the other parameters. In the subsets featuring suspended structures, the fabricated gap coincides with the length of the bridges, and has to be determined. Using as input the nominal gap, exposure gap, contact distance and nominal size of the posts, the length is predicted accurately, but not precisely, for hexagons point to point, hexagons side to side, squares and circles. In those cases, the absolute error of the prediction was found comparable to the absolute error of



the measurements, and thus, the model is validated. The absolute and relative errors in the cases of triangles and diamonds are too high to consider the model valid. The main reason for this imprecision is the lack of data to analyze, since diamonds and triangles are the least prolific in terms of suspended structures. Therefore, the author is confident about the possibility of calibrating the model for these shapes as well, provided that further research is conducted on these shapes, targeting the combinations of parameters that produced suspended structures.

An attempt was made to implement the model to predict the width of the bridges, but it was not possible to find a relationship between the width and the other parameters.

In conclusion, good advancements, towards the understanding and use of carbonization and SU-8 photolithography as microfabrication techniques for obtaining micro-patterned carbon electrodes, were made for the electrochemical society. This work places itself in a niche of the electrochemistry literature, not very popular yet, but rapidly developing, and it is intended to be a pioneer work of future implementation.

The model proposed in this thesis needs to be optimized and calibrated through the analysis of additional experimental data with higher quality. Also, the possibility of predicting the width of the structures needs to be further investigated. Moreover, the effect of the SU-8 thickness variation needs to be integrated, and finally, the model has to be extended to the structures obtained post carbonization.

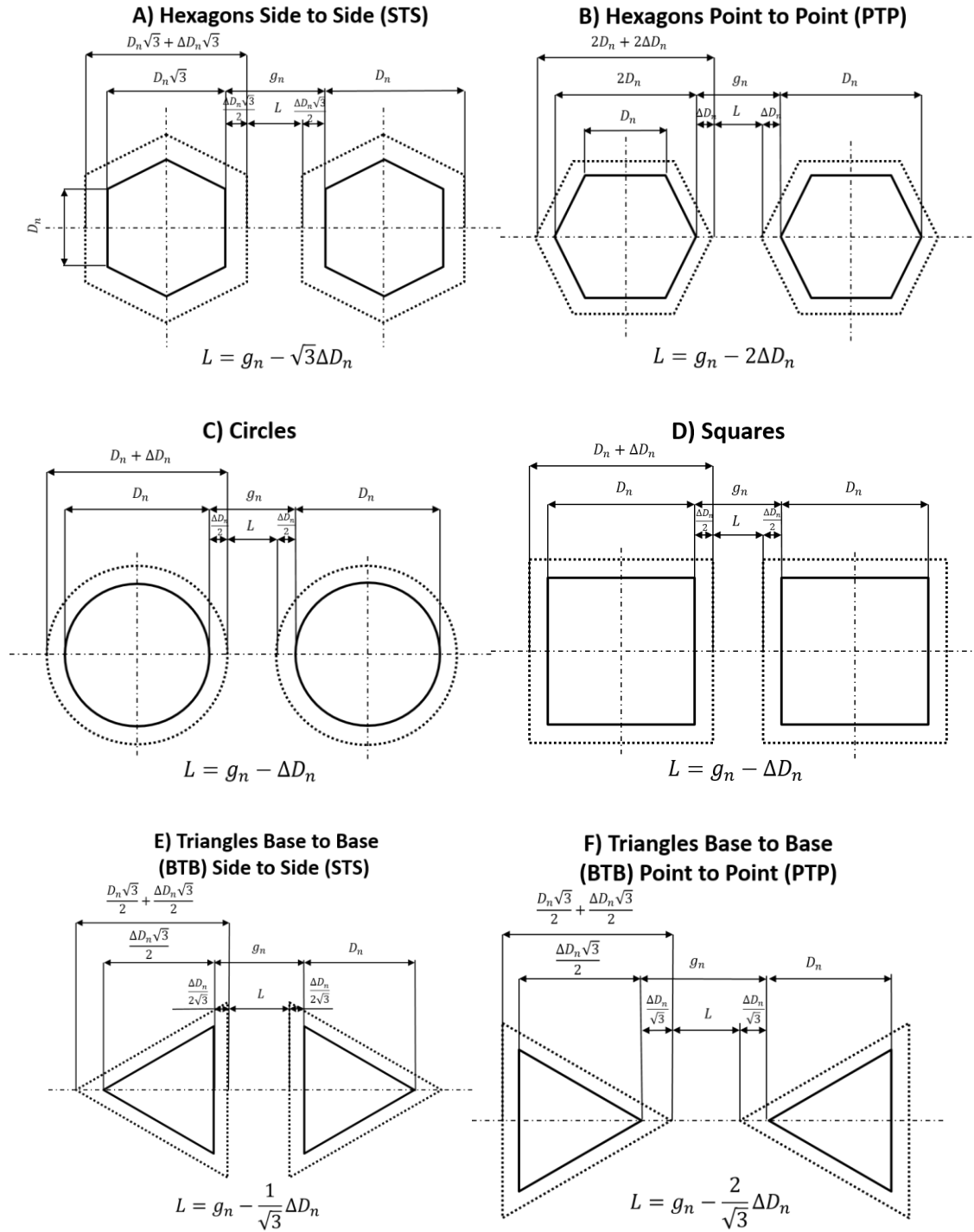


## APPENDICES



## Appendix A

### Types of gap geometry: calculating the shape factor $c_s$









## REFERENCES

- [1] B. R. Eggins, *John Wiley & Sons*, West Sussex, England, (2002).
- [2] N. J. Ronkainen, H. B. Halsallb, & W. R. Heinemanb, *The Royal Society of Chemistry* 2010, **39**, 1747-1763, (2010).
- [3] M. U. Ahmed, M. M. Hossain, E. Tamiya, *Electroanalysis*, **20**, 616-626, (2008).
- [4] D. Erickson, S. Mandal, A. H. J. Yang, B. Cordovez, *Microfluid Nanofluid*, **4**, 33-52 (2008).
- [5] S. Prasad, *Nanobiosensors in Disease Diagnosis*, **3**, 1-10, (2014).
- [6] H. Ju, et al., *NanoBiosensing*, 147-170, (2011).
- [7] C. S. Sharma, H. Katepalli, A. Sharma, M. Madou, *Carbon*, **49**, 1727-1732, (2011).
- [8] A. Qureshi, W. P. Kang, J. L. Davidson, Y. Gurbuz, *Diamond & Related Materials*, **18**, 1401-1420, (2009).
- [9] K. Balasubramanian, M. Burghard, *Analytical and Bioanalytical Chemistry*, **385**, 452–468, (2006).
- [10] J. Wang, *Electroanalysis*, **17**, (2005).
- [11] U. Yogeswaran, & S. Chen, *Sensors 2008*, **8**, 290-313 (2008).
- [12] F. Patolsky, et al., *American Chemical Society*, 4261-4269, (2006).
- [13] P. E. Sheehan, & L. J. Whitman, *Nano Letters*, **5**, 803-807, (2005).
- [14] A. M. Morales, & C. M. Lieber, *Science*, **279**, (1998).
- [15] Vayssieres, B. L., (2003), Growth of Arrayed Nanorods and Nanowires of ZnO from Aqueous Solutions \*\*, (5), 464–466.
- [16] X. Wang, C. J. Summers, & Z. L. Wang, *Nano Letters*, **4**, 423-426 (2004).
- [17] H. G. Craighead, R. E. Howard, L. D. Jackel, & P. M. Mankiewich, *Applied Physics Letters*, **38**, 58–61 (1983).



- [18] R. Martinez-Duarte, *Micromachines*, **5**, 766–782 (2014).
- [19] B. Y. Park, L. Taherabadi, C. Wang, J. Zoval, and M. J. Madou, *J. Electrochem. Soc.*, **152**, J136 (2005).
- [20] S. Ranganathan, R. McCreery, S. M. Majji, and M. Madou, *J. Electrochem. Soc.*, **147**, 277 (2000).
- [21] J. Kim, X. Song, K. Kinoshita, M. Madou, and B. White, *J. Electrochem. Soc.*, **145**, 2314–2319 (1998).
- [22] H. Lorenz, et al., *SU-8: a low cost negative resist for MEMS*, *Journal of Micromechanics and Microengineering*, **7**, p.121-124, (1997).
- [23] D. Mark, S. Haeberle, G. Roth, F. von Stetten, and R. Zengerle, *Chem. Soc. Rev.*, **39**, 1153–82 (2010).
- [24] T. L. Edwards, S. K. Mohanty, R. K. Edwards, C. L. Thomas, and A. B. Frazier, *Sensors Mater.*, **14**, 167–178 (2002).
- [25] P. Abgrall, V. Conedera, H. Camon, A. M. Gue, and N. T. Nguyen, *Electrophoresis*, **28**, 4539–4551 (2007).
- [26] R. Martinez-Duarte, and M. J. Madou, *Microfluidics and Nanofluidics Handbook*, 231-262 (2011).
- [27] B. Y. Park and M. J. Madou, *Electrophoresis*, **26**, 3745–3757 (2005).
- [28] W. Ma et al., *Electrophoresis*, **32**, 494–505 (2011).
- [29] Y. J. Chuang, F. G. Tseng, and W. K. Lin, *Microsyst. Technol.*, **8**, 308–313 (2002).
- [30] R. Yang and W. Wang, *Sensors Actuators, B Chem.*, **110**, 279–288 (2005).



- [31] S. J. Lee, W. Shi, P. Maciel, and S. W. Cha, *Proc. 15th Bienn. Univ. Ind. Microelectron. Symp. (Cat. No.03CH37488)*, 389–390 (2003).
- [32] C. Wang, M. Madou, *Biosensors and Bioelectronics*, **20**, 2181-2187 (2005).
- [33] J. C. Lewis, B. Redfern, & F. C. Cowlard, *Solid State Electronics*, **6**, 251-254 (1963).
- [34] S. Yamada, H. Sato, *Nature*, **193**, 261-262, (1962).
- [35] G. M. Jenkins, K. Kawamura, *Nature*, **231**, (1971).
- [36] A. Oberlin, M. Oberlin, *Journal of Microscopy*, **132**, (1983).
- [37] L. A. Pesin, E. M. Baitlinger, *Journal of Materials Science*, **37**, 1-28, (2002)
- [38] R. Martinez-Duarte, *Label-free Cell Sorting using Carbon Electrode Dielectrophoresis and Centrifugal Microfluidics*, PhD Mechanical & Aerospace Engineering, University of California, Irvine (2010).
- [39] R. Martinez-Duarte, M. Madou, *Microfluidics and Nanofluidics Handbook*, 231-268, (2009).
- [40] P. Abgrall, et al. *Electrophoresis*, **28**, 4539-4551 (2007).
- [41]
- [http://repository.upenn.edu/cgi/viewcontent.cgi?article=1010&context=scn\\_protocols](http://repository.upenn.edu/cgi/viewcontent.cgi?article=1010&context=scn_protocols)